Imperial College London
Consultants

ADMLC-R11

A review of the applicability of Gaussian modelling techniques to near-field dispersion

Huw Woodward, Imperial College London
David Gallacher, University of Surrey
Prof. Alan Robins, University of Surrey
Martin Seaton, CERC
Prof. Helen ApSimon, Imperial College London

This report is the independent opinion of the authors

This study was funded by the UK Atmospheric Dispersion Modelling Liaison Committee.

The views expressed in this report are those of the authors, and do not necessarily represent the views of ADMLC or of any of the organisations represented on it

Contents

1. Introduction

This study aims to determine the strengths and limitations of Gaussian plume and puff models at short time and length scales, particularly in the presence of buildings. Gaussian plume models were initially designed to estimate long term average concentrations from continuous plume releases. Their very short run times and good performance for such problems have led to their widespread use. However, they have limitations at short time and length scales, particularly in the presence of buildings or when modelling short term releases, or puffs. This limits their utility in assessing the risk posed by toxic or flammable releases where outputs such as the likelihood of exceeding threshold concentrations or peak doses are required. In this report we define the dose as the time integral of the concentration at a given location. At the short time (<1h) and length (<100m) scales considered here the impact of buildings on the plume dispersion is likely to be significant, while the building orientation and geometry may also be important. This report focuses on the modelling of both continuous (plume) and short term (puff) releases upwind of a single building. Three methods are used; wind tunnel simulations, Computational Fluid Dynamics (CFD), and a Gaussian plume model.

The application of Gaussian plume models for the evaluation of long term concentration averages is wide ranging and includes the simulation of stack emissions (Stathopoulos et al. 2008), agricultural emissions (Stocker et al, 2017) and radioactive emissions (HPA, 2009). However, there are many situations in which short term fluctuations in concentrations are important. These include releases of flammable or toxic materials, or when the odour of a release is a concern. In the case of a flammable gas, the long term average concentrations are of secondary concern, rather it is the likelihood of exceeding lower and upper threshold flammability limits which is important (e.g. Lilley 1997, 2011). In the case of the release of a toxic cloud, we are concerned with the dose if exposed and the probability of acute exposure events. In this case both the magnitude of the fluctuations in concentrations and the exposure time are relevant, as the dose is calculated from the concentration integrated over the exposure time, in addition to the intermittency of the signal. Further, the toxicity of a hazardous gas often does not increase linearly with concentration, for example the toxicity often increases exponentially with concentration (Griffiths & Megson, 1984, Griffiths 1990). In this case the full time series concentration distribution should ideally be known.

Accounting for the impact of buildings on dispersion poses a considerable challenge for Gaussian plume models. As buildings disrupt the air flow the mean concentration field can no longer be described accurately by a single Gaussian distribution. Nonetheless methods have been developed to account for the impact of buildings using theoretical considerations and empirical relations derived from wind tunnel simulations (Hunt & Robins 1982, Apsley 1988, Robins et al. 1997). These models were primarily designed to simulate the downwash of above roof releases into the building wake, or the behaviour of fully entrained releases, rather than emissions upwind. There are occasions when the effect of the building on dispersion can be considered small enough to ignore, for example when the plume has spread sufficiently to be very large relative to the building size. However, at short length scales the building shape and size, orientation and location relative to the release are likely to be relevant. Further, the impact of the building on dispersion can also be relevant for larger time and length scale problems when the release is near the building as any impact on initial dispersion will affect the downwind plume.

In this report we deliberately push the Gaussian plume model beyond its design purposes in order to evaluate its performance and utility in modelling the dispersion of a release at short time and length scales. This involves investigating its utility in evaluating peak concentrations, the probability of exceeding threshold concentrations and the range of dose for a range of release durations. We focus on a release upwind of a 24 m, cubical building in order to assess both the performance of the building model at these scales and to determine an appropriate strategy to deal with buildings within the context of emergency response. It is of note that the treatment of building effects in Gaussian models has not thus far focused on the impact of buildings on the dispersion from upwind sources. The release of a substance upwind of a building is therefore both a highly relevant case when considering dispersion at these scales and poses a challenge to the current treatment of buildings by Gaussian plume models.

The wind tunnel simulations were performed in the EnFlo wind tunnel at the University of Surrey (EnFlo, 2020). The EnFlo wind tunnel can simulate the release of passive tracer gas within a turbulent flow representative of an urban boundary layer with neutral, stable or unstable conditions, though only the former was used here (i.e. there are no temperature effects). The Large Eddy Simulation (LES) CFD code "Fluidity" was used to simulate equivalent scenarios at full scale, including varying boundary layer stabilities. The LES method allows the larger turbulent features of the flow to be resolved, while assuming turbulence below a certain length scale can be modelled as additional viscosity. LES simulations can output results at higher spatial resolution than within the wind tunnel, where the number of measurement locations is somewhat limited. Here the LES simulations were used to provide a fuller picture of the flow behaviour and tracer dispersion, simulate different atmospheric stabilities, and to explore the challenges of simulating complex, highly time variant urban dispersion. Finally, the Gaussian plume model used was the Atmospheric Dispersion Modelling System (ADMS) developed by Cambridge Environmental Research Consultants (CERC). ADMS is an advanced Gaussian plume model with features such as a building effects module, which simulates the impact of a building on plume dispersion, and a fluctuations module, which allows for the calculation of statistics of the short-term fluctuations in concentrations about the long term mean. The ADMS building module is broadly similar in concept but with significant differences in detail to the building models possessed by other Gaussian plume models such as AERMOD (AERMOD-PRIME) and the simpler ASHRAE and R157 models. In the case of ADMS, the effect of a building on an upwind release can also be simulated although this was not the design purpose of the model. These advanced features and its widespread use make ADMS a useful and relevant tool for the evaluation of Gaussian plume models for the short time and length scale problems considered here.

The inclusion of a building in our simulations provided insight into the additional complexity in air flow and dispersion introduced in urban areas by the presence of buildings. It also allows an assessment of the ADMS building model which is a widely used tool in the UK. A range of puff release times was considered in order to explore the effect on the variance in concentrations and dose. The relevance of the long term mean concentrations calculated by Gaussian plume models to short term statistics was also considered.

An overview of the ADMS Gaussian plume model and its relevant modules such as the Building module and Fluctuations module is given in Section 2. Sections 3 and 4 detail the wind tunnel and LES methodologies used. In Section 5 the time average concentrations from a continuous release

are compared for each method, the effect of varying building geometries and boundary layer stabilities is considered. Section 6 focuses on short term puff releases modelled within the wind tunnel and the use of the ADMS Fluctuations module to simulate puff ensembles. A discussion of the results is given in Section 7 and conclusions in Section 8.

2. Gaussian plume model

2.1. ADMS Gaussian plume model

ADMS models a continuous release, or plume, for a stable or neutral boundary layer using the R91 (Clarke, 1979) formulation as given by equation 1. The model assumes a Gaussian distribution within the boundary layer, with reflections at the ground and, when present, the inversion layer.

$$C = \frac{q_s}{2\pi\sigma_y\sigma_z U}\exp\left(-\frac{y^2}{2\sigma_y}\right)\left\{\exp\left(\frac{-(z-z_s)^2}{2\sigma_z^2}\right) + \exp\left(\frac{-(z+z_s)^2}{2\sigma_z^2}\right) + \exp\left(\frac{-(z-2h+z_s)^2}{2\sigma_z^2}\right) + \exp\left(\frac{-(z+2h-z_s)^2}{2\sigma_z^2}\right) + \exp\left(\frac{-(z-2h-z_s)^2}{2\sigma_z^2}\right)\right\} \quad (1)$$

The first term of the equation, $q_s/2\pi\sigma_y\sigma_z U$, represents the plume centreline concentrations in the absence of reflections, where q_s is the source emission rate, U is the mean wind velocity at source height, and σ_y and σ_z are the horizontal and vertical dispersion parameters, respectively. In this report we refer to the average velocity components as U, V, W and the instantaneous components of the velocity field as u, v, w. The dispersion parameters at any given location x downwind of the source, $\sigma_y(x)$ and $\sigma_z(x)$, are functions of both the flow turbulence parameters, σ_v and σ_w (or $\sqrt{uu}$ and $\sqrt{vv}$), and the time, $t = (x - x_s)/U$, from release.

The horizontal spread of the plume is assumed to be a Gaussian distribution as is represented by the first exponential in equation 1. Larger values of σ_y lead to a wider distribution and therefore a wider plume with lower concentrations. As σ_y increases with time from release, the plume width increases with distance downwind.

The terms within the curly brackets give the vertical distribution of the concentration, the first term represents the concentrations in the plume emitted directly from the source, the second accounts for the reflection of the plume at the ground, while the remaining terms are associated with further reflections either at the ground or at the inversion. Over the short length scales considered in this report the plume does not reach the inversion layer and therefore these last terms can be neglected.

Amongst other things, the vertical dispersion parameter is also dependent on the buoyancy frequency, N, which is a measure of the stability of the fluid. Increasing stability is associated with increasing N, whereas N is equal to zero in perfectly neutral conditions. Stable stratification is associated with reducing turbulence levels and length scales and, as a consequence, reduced plume spread. However, the more unstable the flow, that is the more vertical mixing due to buoyancy effects, the larger the vertical dispersion parameter and the greater the vertical plume spread. The horizontal dispersion parameter contains a term which accounts for large scale variations in the wind direction; for the purposes of this report, this was set to zero. This is so that direct comparisons could be made with the wind tunnel and CFD simulations for which such large-scale changes in wind direction cannot be easily modelled. Including the term would result in increased

lateral plume spread, as would increased horizontal turbulence. Therefore the exclusion of the term does not limit the relevance of the results in this report any more than the limited number of flow conditions considered. As this report considers short time and length scale scenarios, this was seen as an acceptable assumption as large scale changes in wind direction are less relevant over short time scales. The full formulation of the dispersion parameters for neutral and stable boundary conditions can be found in the Appendix 1. Figure 1 shows the vertical and horizontal concentrations given for a plume released under neutral boundary layer conditions at various distances downwind of the source.

For unstable boundary layers ADMS adopts a non-Gaussian distribution for the vertical concentrations (CERC, 2016), based on that of Hunt et al. (1988). This skewed Gaussian plume accounts for the presence of large-scale vertical eddies which exist during unstable conditions, as illustrated in Figure 2 (b), which clearly shows more plume spread and the associated asymmetry relative to neutral conditions.

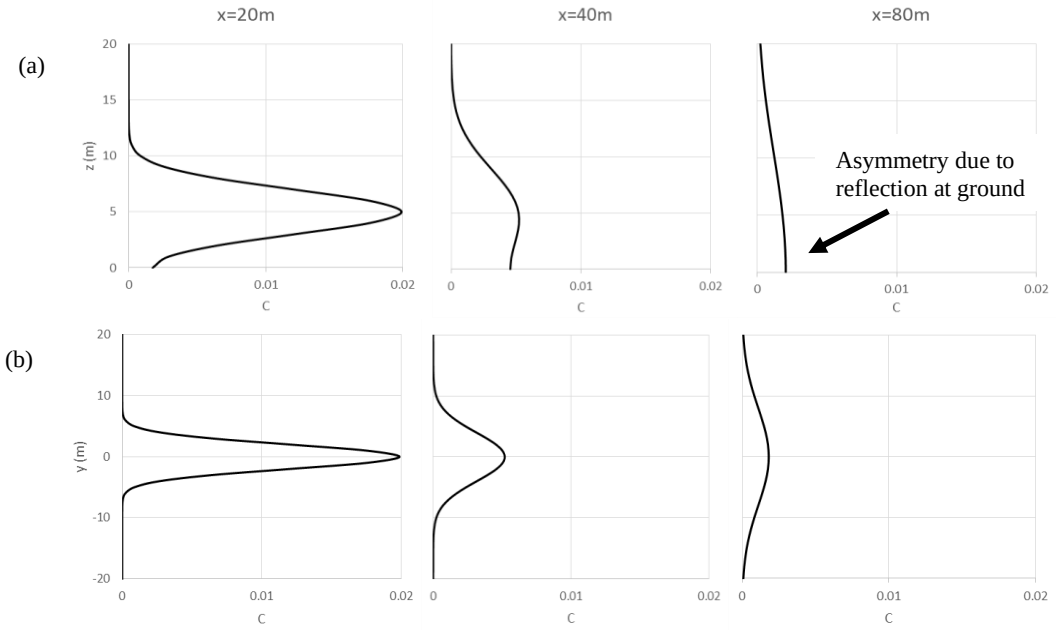

Figure 1: Concentrations given by Gaussian plume models at three locations downwind of source at height Z_s=5m (a) vertical profiles at y=0m, (b) horizontal profiles at $Z = Z_s$.

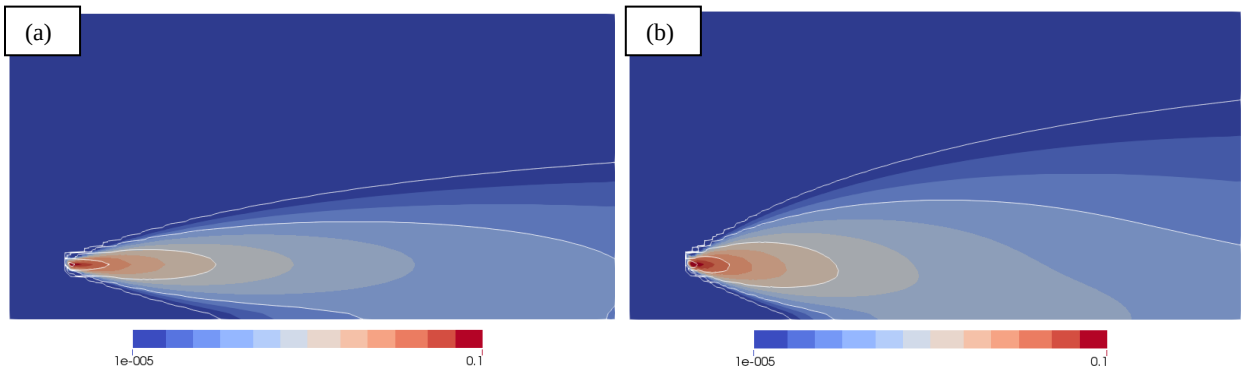

Figure 2: Concentration contours on x-z plane at y=0m for continuous plume under (a) neutral boundary conditions and (b) unstable boundary conditions (Pasquill-Gifford stability B/C).

2.2.ADMS meteorology module

A number of meteorological variables are required in order to calculate plume concentrations using equation 1.

The ADMS meteorology processor determines the boundary layer stability based on a set of user inputs. The minimum required inputs are wind speed and direction and surface heat flux. Alternative inputs can be used when the surface heat flux is not known, for example the user can input the time of day, date and cloud cover, from which the meteorology module will estimate the surface heat flux. The meteorology processor also uses these inputs to calculate the boundary layer height and Monin-Obukhov length (L_{MO}) which are used to classify the stability. Figure 3 shows a schematic of the variation of the Monin-Obukhov length and boundary layer height with atmospheric stability (CERC, 2016). The approximate equivalent Pasquill-Gifford stabilities (A-G) are also shown. The ADMS user guide provides the following guidance relating the Monin-Obukhov length and boundary layer height (h) to boundary layer stability:

Stable	$h/L_{MO} > 1$
Neutral	$-0.3 \leq h/L_{M0} \leq 1$
Unstable	$h/L_{MO} < -0.3$

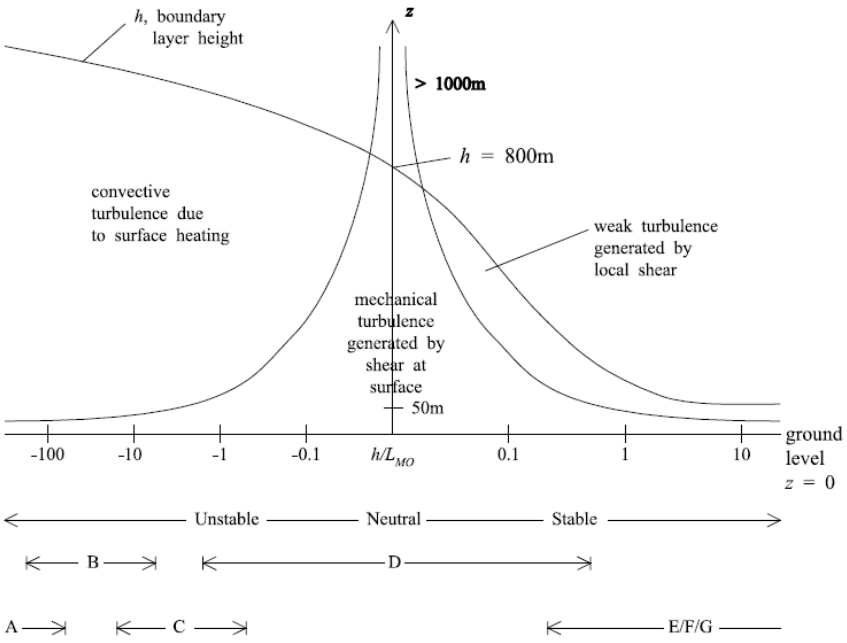

Figure 3: Dimensional schematic representation of variation of Monin-Obukhov length with atmospheric stability (ADMS 5 User Guide, CERC, 2016).

Profiles for the velocity, Reynolds stresses and temperature are then produced based on the stability class derived and the surface roughness length, z_0, which is also provided by the user. The normalised Reynolds stresses are given by $uu/{U_{ref}}^2$, $vv/{U_{ref}}^2$ and $ww/{U_{ref}}^2$ where u, v and w are the x, y and z unsteady components of the velocity and U_{ref} is the average velocity at a reference height which we take as the boundary layer height. The dispersion parameters required for the Gaussian plume model (equation 1) can then be calculated using the flow turbulence and temperature values provided by this parameterisation. Figure 4 shows the normalised velocity and Reynolds stress profiles for three different boundary layer stabilities, B (unstable), D (neutral) and F (stable). The boundary layer stability affects both the velocity profile and the turbulence, with much higher Reynolds stresses present for the unstable boundary layer in particular. It should be noted that the boundary layer height used to normalise the y-axis would be significantly different for each case, with larger values expected for the unstable case and smaller for the stable case.

It is also possible to bypass the ADMS meteorology module by inputting user-defined profiles of velocity and Reynolds stresses. For example, the flow profiles measured in the wind tunnel can be used once appropriately scaled.

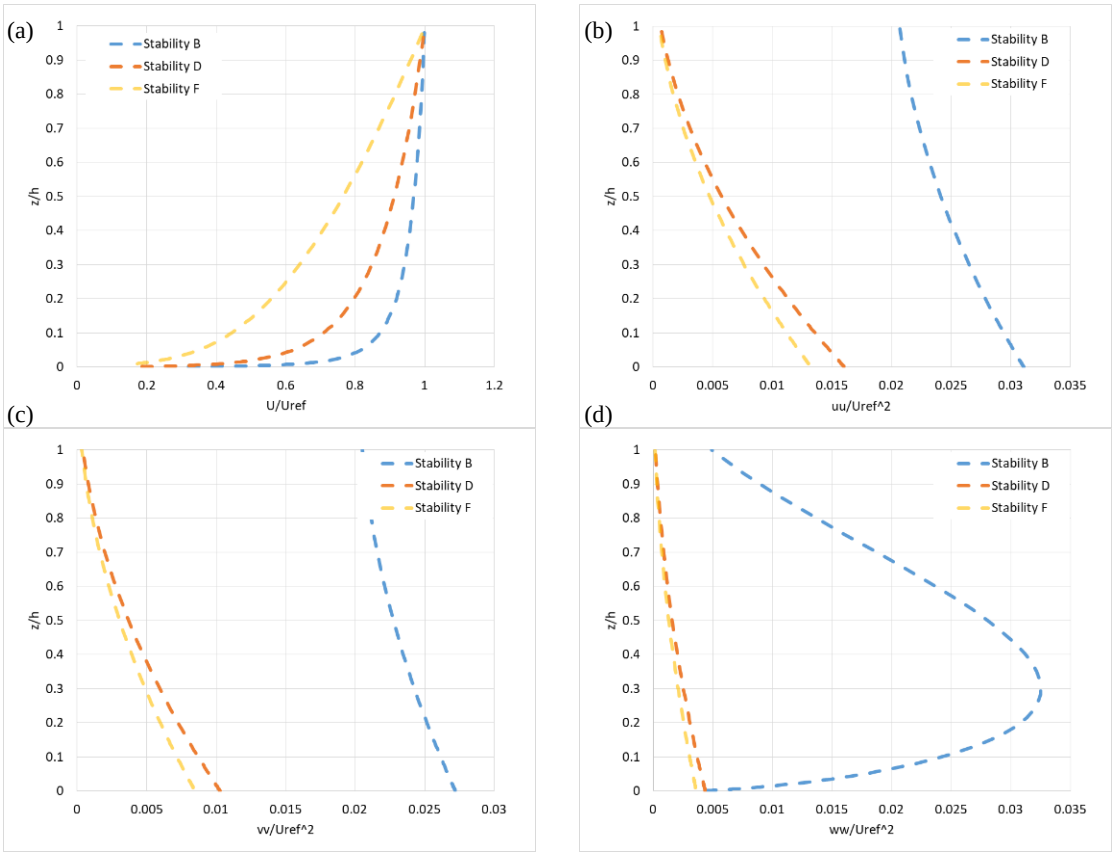

Figure 4: ADMS flow profiles for three different boundary layer stabilities.

2.3. Flow around a building

Figure 5 shows a schematic of the mean flow field around a normal facing, rectangular building. The main features include the separation of the flow at the leading edge of the roof and the reattachment of this flow to the downwind roof surface. This reattachment does not always occur, for example for buildings with roofs which do not extend far downwind. An entrainment of the flow is then seen into the recirculation zone, or cavity, of the building. Near the ground, a horseshoe vortex is seen to extend from the front face of the building, around the sides and downwind past the building. This vortex forms as an interaction with the vorticity in the upwind boundary layer as the flow is forced to deflect around the front face of the building. These features are also seen for oblique facing buildings, although the horseshoe vortex tends to be much broader because of the nature of the flow field around the building. A roof vortex system also occurs in this situation, creating mean downflow over the building and downwind.

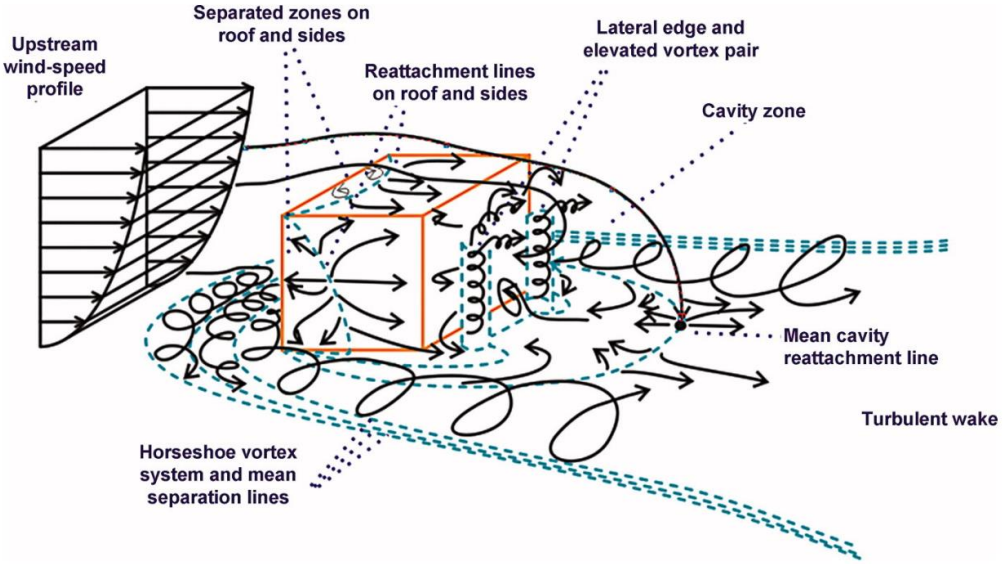

Figure 5: Schematic representation of the mean flow around an isolated rectangular building. From Hosker (1984) and modified by Blocken et al. (2011).

2.4. Overview of the ADMS buildings module

The buildings module within ADMS has the following features:

(1) A complex of rectangular or circular buildings is represented by a single block with 'equivalent' crosswind and vertical dimensions. This process is carried out separately for each source and each set of meteorological inputs.

(2) The disturbed flow field consists of a recirculating flow region in the lee of the building (and perhaps above the roof) and a turbulent wake downwind (the main wake).

(3) There is a uniform concentration within the well-mixed recirculating flow, which is calculated based upon the fraction of material entrained (or emitted directly into the region).

(4) Concentrations in the main wake from an elevated release are the sum of a ground-level plume from the entrained fraction and an elevated plume from the remainder.

(5) Streamline deflection over and in the lee of the building reduces the height of elevated plumes. Plume spread within the wake is increased by the combined effects of the mean velocity deficit and excess turbulence in the wake.

Further details on the building effects module within ADMS can be found in Appendix 2. Note that the buildings module within AERMOD is based on similar concepts, although the specific implementation differs at almost every stage.

2.5. ADMS fluctuations model

ADMS contains a fluctuations model which produces statistics of fluctuations in concentration. This module takes into account variation due to turbulence and in the meandering of the mean wind. For short sampling times, of an hour or less, the boundary layer turbulence is usually the dominant cause of fluctuations, while for longer times, changes in the mean wind direction can become important. Meteorological parameters other than the wind direction are assumed to remain constant over a sampling time of one hour.

The output provided for each hour depends of the type of calculation being carried out and this could fall into one of three possible types:

- For continuous releases the fluctuations module calculates the variance of the fluctuations and the probability that the concentration averaged over the specified averaging time exceeds a particular value. The results are equivalent to those obtained by making many measurements over the averaging time. If the sampling time is much greater than one hour, the meteorological conditions would in general change over the period and the results obtained, which assume steady meteorology, would not generally be relevant to what happens in reality.
- For time-integrated concentrations from finite duration releases, the fluctuations module calculates the variance and the probability that the time-integrated concentration exceeds a particular value**.** The results are equivalent to those that would be obtained by making time-integrated measurements for a large number of identical puff release, under identical average meteorological conditions, but taking account of turbulent fluctuations. Note that in this case an averaging time is not required since time-integrated concentrations are being calculated. If the release duration is much greater than one hour, the meteorological conditions would in general change over the period and the results obtained, which assume constant meteorology, would not generally be relevant to what happens in reality.
- For instantaneous concentrations from finite duration releases, the module calculates the variance and the probability that the instantaneous concentration at a specified time exceeds a particular value. These results are equivalent to those that would be obtained by making instantaneous concentration measurements for a large number of identical puffs released under identical meteorological conditions but taking account of turbulent fluctuations.

The fluctuations module cannot currently be used in conjunction with the building module.

2.6.ADMS puff model

ADMS contains a puff module that can be used for modelling releases lasting a short duration, usually much less than one hour. The module can calculate two types of output. These are time-dependent concentrations, i.e. a "snapshot" of the ensemble-averaged concentration at various times after the release; and time-integrated or dose concentrations. For the time-integrated concentrations the standard plume concentration is multiplied by the length of release to calculate the dose experienced at each location.

For time-dependent output, the release is modelled in terms of up to three separate regions, front, plateau (centre) and rear, as shown in Figure 6. If the release is ongoing there is no rear, likewise if the release is instantaneous there is no plateau region. The size of the plateau region is reduced as the puff travels downstream due to the front and rear spreading.

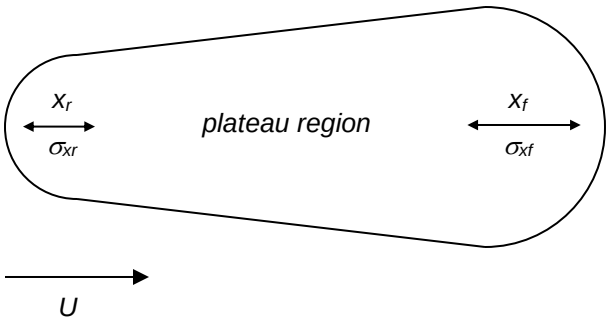

Figure 6: Diagram showing the three regions for an ensemble-averaged puff release in ADMS (CERC, 2016).

The front and rear-end along-wind spreads are calculated from the longitudinal turbulence values, vertical spread and vertical gradient of the velocity. Within the plateau region the spread parameters are calculated using the same algorithms as the plume model.

The puff model can handle releases from instantaneous up to a few hours, although the meteorological conditions are kept constant throughout the release and dispersion so care must be taken with longer release durations. The puff model cannot be used in conjunction with the building module.

3. Wind tunnel experiments

The aim of the wind tunnel experiments was to determine the concentration and velocity fields around the cube-shaped building when pollutant was released upstream, in addition to gaining insight into the behaviour of short-term puff releases in the presence of a building.

In order to achieve this a series of measurements was performed in the EnFlo wind tunnel at the University of Surrey. The flow field was investigated using a two-component Laser Doppler Anemometer (LDA) to determine flow advection velocity components, but also important flow parameters such as the shear stresses and turbulence intensities and their variation with spatial position in the flow field. Secondly, the spatial variation of concentration in the vicinity of the building was determined – upstream, in close proximity and further downstream in the building wake: the concentration values were measured in a series of downstream planes perpendicular to the main direction of flow as shown in Figure 7 and Figure 8. Thirdly, short duration "puff" releases were made and the dose per puff determined by measurement at a range of spatial positions. The puff release measurements of concentration were typically made with in excess of one hundred repeat releases for a given measurement and the dose per puff values were statistically analysed to give estimates of the variation in the dose received for a given short term release event. Measurements of puff releases were performed at the plume centreline (Plume Concentration Maximum, PCM) at each of the measurement planes; additional measurements were taken offset at approximately the Full Width Half Maximum (FWHM) positions along the plume cross sectional profile from the PCM in both vertical and horizontal (crosswind) directions. The FWHM co-ordinates were defined as the positions determined from the mean concentration profile at which the concentration value had fallen to half of the maximum value measured at the PCM.

3.1. Flow field measurements with a Laser Doppler Anemometer (LDA)

A Laser Doppler Anemometer (LDA) was used to measure the flow velocity statistics. A self-levelling laser light sheet system was used both to align the LDA with the wind tunnel co-ordinate system and the source with the approach flow direction. Two orthogonal axes of measurement were possible at any one time. Pairs of velocity component measurements were possible: either (*U*,*V*) or (*U*,*W*) and both of these were made over the flow field for two orientations of the building to the wind. Measurements of (*U*,*V*) or (*U*,*W*) were made and combined into a single data set for analysis, with an analysis of other relevant quantities of the flow field; e.g. the shear stress, uw/U_{ref}^2, where U_{ref} is the velocity at a reference height at a location where the flow is undisturbed by the building. Measurements of the flow field were made at the same downstream co-ordinates used in subsequent measurements of the concentration field, as indicated in Figure 7 and Figure 8.

3.2. Concentration field measurements

Passive releases were selected as being most appropriate for this series of measurements: these involved a horizontal release aligned with the tunnel wind direction and matched to the local streamwise flow velocity. The downstream measurement planes were chosen to intercept the plume and show the effects of plume interaction with the cube out to the plume 'tails', both vertically and horizontally. A single Fast Flame Ionisation Detector (FFID) was used to make the measurements, using a sampling frequency of 400Hz. The emission comprised a trace gas, propane, mixed in a passive carrier, such that the overall density was essentially that of air. The source trace gas concentration was kept in the range 1-2% for the continuous measurement series and a sampling time of 0.5 minutes was used at each sample position. A source diameter of 7.8mm was used, which equates to 0.78m at full scale. During each measurement sequence the FFID detector was periodically recalibrated against variations in signal background and against trace gas calibration mixtures supplied by an inlet nozzle located downstream of the model in the tunnel. Locations in the (*Y*, *Z*) plane were sampled according to an intelligent sensing algorithm; i.e. positions recording below 5% of the Plume Concentration Maximum (PCM) signal were excluded from the measurement when making traverses across the plume. This range of sampling was sufficient to detect the PCM and extend past the Full Width Half Maximum (FWHM) in all cases.

3.3. Release locations, building orientation and release durations

Two building configurations were simulated: a cube building orientated such that the wind is normal to the building face; and an oblique building at an angle of 45 degrees. The cube side dimension, *H*, at wind tunnel scale was 240 mm, equivalent to 24 m at full scale. As both wind tunnel scale and full scale dimensions are considered within the report, dimensions are scaled according to the dimension of the building; e.g. a downstream distance in the *X* co-ordinate of the geometry used is referred to in non-dimensional units of *X/H* as labelled in Figure 7 and Figure 8. Where the dimensions *X*, *Y*, *Z* are referred to directly, the following convention is used: wind tunnel model co-ordinates are stated in mm and equivalent full-scale dimensions in metres. The centre of the coordinate system is taken to be at ground level below the centre of the cube building.

For the wind tunnel experiments two release locations (R2 and R4) were used, both at a distance of 2*H* upwind of the front face of the cube in normal incidence, i.e. at *X/H*=-2.5 with *X=Y=Z=0* taken to be at ground level at the centre of the building. The first of these, R2, was a near-ground release at a height of *H*/4 (60 mm) and the second, R4, was at an "above roof" height of 4*H*/3 (320

mm), both at *Y*=0. Five different release periods were used at each location; 0.05, 0.10, 0.25, 0.5 and 1.0 seconds, with the shortest being equivalent to 5 s at full scale (F/S).

The dimensionless quantity, $U_{ref}T/H$, links model and F/S times, so that:

$$T_{FS} = T_{WT}\frac{H_{FS}}{H_{WT}}\frac{U_{WT}}{U_{FS}}$$

The wind tunnel experiments were conducted at a nominal scale of 1:100 and used a reference speed, U_{ref}, at the boundary layer edge, Z = 1m, of 2ms^{-1}. For a reference wind speed of 2ms^{-1} at Z=100m in the F/S case, a "puff" release of 10 seconds corresponds to 20m travel in relation to a building of H=24m; this is equivalent to 200mm travel in the wind tunnel and a release duration of 0.1 seconds.

The dose received at a given location from a passing puff is a highly variable quantity, particularly for the shorter release durations and reliable statistics can only be obtained from a series of such emissions. Here, typically the number of releases was in excess of 100.

For the wind tunnel experiment the measurement planes downstream of the source were located at *X*/*H*=-2, -1, 0, 1, 2, 5 and these are alternatively referred to as *N2H*, *N1H*, *0H*, *1H*, *2H* and *5H* respectively.

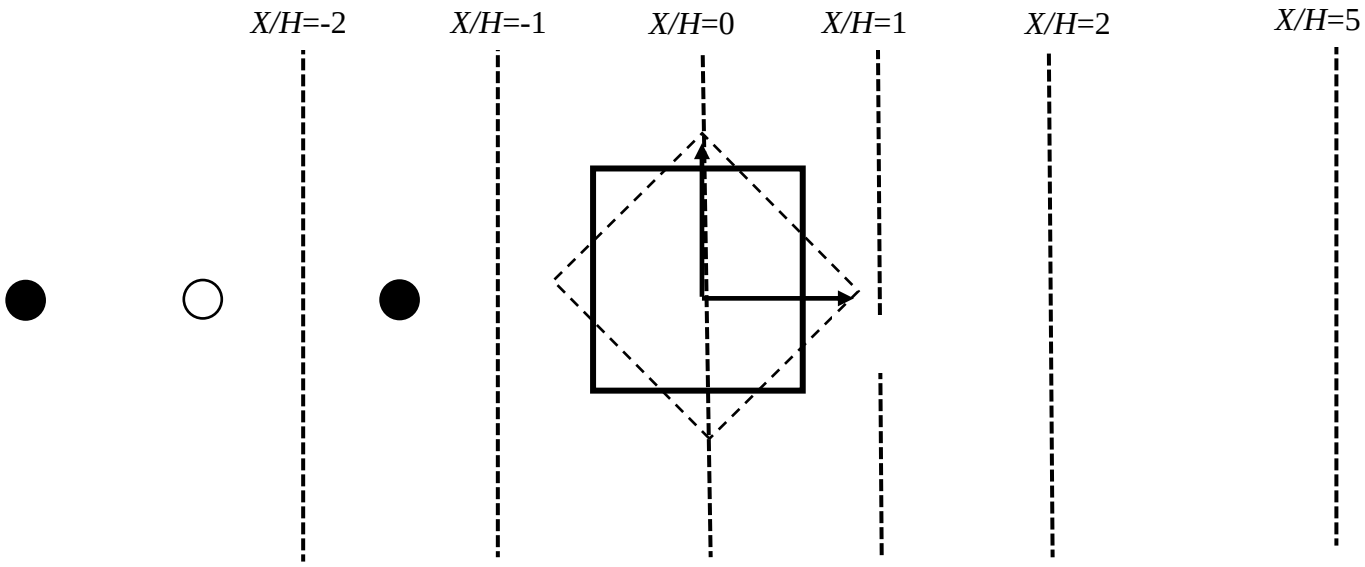

Figure 7: Location of LES releases (filled and hollow) and wind tunnel releases (hollow only) and measurement locations on Z plane.

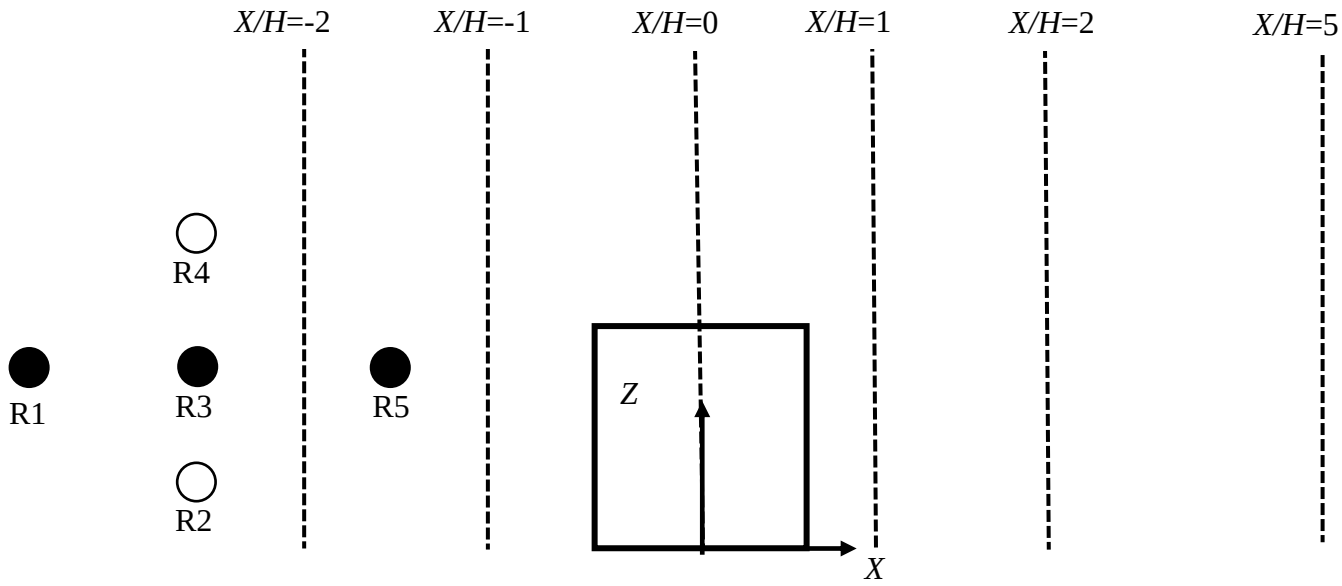

Figure 8: Location of LES releases (filled and hollow) and wind tunnel releases (hollow only) and measurement locations on Y plane.

4. Configuration of large eddy simulations

The CFD model Fluidity is a Large Eddy Simulation (LES) model developed at Imperial College London. The LES method aims to resolve the larger turbulent eddies while sub-grid scale turbulent features are modelled as additional viscosity. A non-isotropic variation of the Smagorinsky sub-grid scale model is used, developed by Bentham (2003). A turbulent boundary layer can be simulated by specifying the desired turbulence and mean flow conditions at the inlet using the Synthetic Eddy Method (Pavlidis, 2010). A plume or puff is modelled as a release of a passive tracer for which an advection-diffusion equation is solved. Previous examples of the use of this method for atmospheric dispersion for flows around buildings include Aristodemou et al. (2009) and Aristodemou et al. (2018).

A domain of dimensions (L x W x H) = (320m x 150m x 120m) was used for the neutral and stable boundary layer simulations. The same horizontal dimensions were used for the unstable boundary layer however a domain height of 200m was used in this case. The building was located at the centre of the domain, over 6H from the inlet, in order to provide enough distance between the upwind release locations and the inlet. These dimensions satisfy the 3% blockage condition recommended by COST Action 732 for CFD simulations of urban environments. No slip boundary conditions were applied at the ground and building surfaces, meaning that the velocity was set to zero at the boundary. Slip boundary conditions were applied at the sides and top of the domain, meaning that the velocity component normal to the surface was set to zero. A spin-up time of 1000s was used for each simulation before the calculation of averages was started. Averages were calculated until deemed suitably converged, with 45 minutes of simulation time being typical. Reynolds stresses for the LES simulations were calculated from the unsteady component of the velocity field by first calculating the time averaged velocity, before subtracting this from the instantaneous velocity field to obtain the unsteady component.

For stable and unstable boundary layer problems a temperature field is solved. This temperature field is then used to calculate a buoyancy force in the momentum equations. It is therefore possible to simulate the effect of temperature gradients on the tracer dispersion. To simulate unstable conditions a positive heat flux was applied at the ground, while a negative heat flux with equal magnitude was applied at the top surface of the domain. At the inlet an average temperature gradient was applied following the method used by Xie et al. (2013). A limitation of this approach is that the largest scale turbulent motions within the boundary layer are not captured. Therefore, it may be expected that vertical mixing is under predicted by the model. However, as shown in Appendix 4, a reasonably good agreement is achieved for concentrations between these simulations and ADMS for an empty domain.

The same approach was used for the stable boundary layer simulations, with a negative heat flux at the ground and equivalent positive heat flux at the top of the domain.

The Fluidity simulation by Pavlidis et al. (2010) of the turbulent flow past a building was used as an initial guide for the mesh configuration as they achieved good agreement between Fluidity and wind tunnel experiments. A mesh size of approximately 1 million nodes was used for the open terrain simulation. For the building case a slightly larger mesh was used, with a total number of nodes of around 1.2 million. Additional nodes were used in the region within 1H surrounding the building faces where the edge length was restricted to no greater than 1m. Figure 9 shows the computational grid at the building surface in addition to a cross section of the grid at Y=0m. As seen in Appendix 3, this mesh configuration was sufficient to achieve reasonably good agreement with the wind tunnel for the flow around a normal facing building.

For the LES simulations, five separate releases were simulated, all of 60 s duration at full scale. The releases were located at (X/H, Y/H, Z/H) = (-3.5, 0, 0.75), (-2.5, 0, 0.25), (-2.5, 0, 0.75), (-2.5, 0, 1.33), (-1.5, 0, 0.75), referred to as R1 to R5 respectively. A diameter of 1m was used for each source in the LES simulations. For consistency the LES analysis also focused on the same downwind planes as those measured in the wind tunnel.

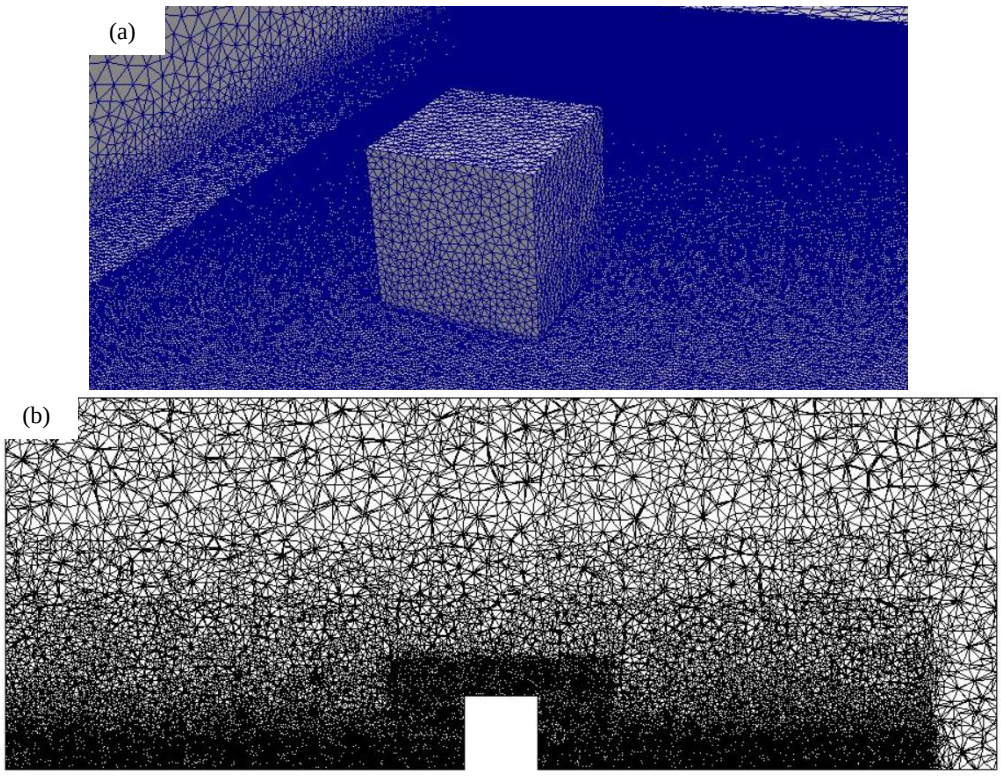

Figure 9: Computational mesh used for LES simulations (a) at the building surface and (b) X-Z plane at Y=0m.

4.1. Challenges to consider when simulating puff releases with LES

The approach taken in this study was to find a mesh configuration sufficient to simulate a statistically steady turbulent flow along the domain length (for the open terrain case), while also capturing the flow behaviour around the building. This resulted in a mesh of 1 to 1.2 million nodes and time steps of around 0.5s. This meant that storing the output for each grid point at each time step was impractical, output storage was therefore restricted to a grid of receptors created in the area of the geometry downstream of the release. For the empty domain problem this grid extended from X/H=-1.67 to 5, Y/H=-1.67 to 1.67 and Z/H=0 to 1.67, with a distance of 0.167H between each receptor in the downstream direction and 0.083H in the vertical and crosswind directions. While this receptor grid reduced the hard drive space required, it also further increased the run time of the simulation as the concentration at each point must be calculated at each time step.

The LES puff simulations were run in parallel on 18 to 24 cores on a HP Z840 workstation. Typically, simulating the dispersion of a single puff past the building took 24 hours of simulation time. As up to a hundred or more puffs are required to obtain meaningful statistics, this simulation time did not allow for a sufficient number of puffs to be simulated within the time constraints of the project. The LES simulation results within this report therefore focus on continuous release simulations only.

A comparison of the ADMS, LES and wind tunnel flow profiles is given in Appendix 3.

5. Continuous releases

While Gaussian plume models are designed to replicate the mean concentrations from continuous and short duration releases, this is usually over distances of hundreds or thousands of metres. For this reason the R91 model contains terms to account for the reflection of the plume at the boundary layer inversion (equation 1). ADMS accounts for the impact of large scale changes in wind direction through an additional term in the horizontal spread of the plume. For the scenarios considered within this study the downwind distances under consideration are less than 200m and the plume does not reach the inversion, even in stable conditions. Further, over the relatively short time scales considered (<1h), it was assumed that no large-scale changes in wind direction occur. This facilitated the comparison of the Gaussian plume model with the wind tunnel and LES results, neither of which attempted to simulate varying wind direction. However, it should be noted that in reality the effective wind direction can change considerably over the time scales considered. A source diameter of 1m was used in ADMS for all cases in this report.

5.1. Open terrain

Before considering the impact of the building on the flow and dispersion, we compare the models for the open terrain case in order to identify any differences in their estimates of free flow dispersion. While ADMS is able to generate boundary layer flow profiles given a set of inputs from the user (see Section 2.2), it is also possible to provide user defined profiles of the flow velocity, turbulence parameters and temperature. In order to compare the three models, the wind tunnel flow profiles shown in Figure 50 in Appendix 3 were used as inputs to ADMS. All concentrations given in this report are normalised using the following equation:

$$C^* = \frac{U_{ref}H^2}{q_s}\frac{1}{t_E}\int_0^{t_E} C(t)\,dt \qquad (2)$$

where, q_s is the mass flow rate of the source, t_E is the time over which the concentration is averaged and $C(t)$ is the time-dependent mass concentration.

Figure 10 shows the time averaged concentrations on the *X*-*Y* plane at a height of 6m for (a) LES, (b) ADMS with the wind tunnel profiles as input and (c) ADMS with parameterised meteorology and assuming a surface roughness of $z_0 = 0.3m$. It should be noted that a log colour scale is used here in order to clearly visualise the large range of concentrations present. The LES plume is clearly narrower than that predicted by ADMS, mainly because of the lower turbulence levels in the LES simulations, as seen in Figure 52 in Appendix 3. The ADMS plume was also found to be wider than that within the wind tunnel when using the wind tunnel flow profiles despite setting large scale variations in wind direction to zero.

Using a surface roughness of 0.3m (equivalent to that used for the wind tunnel approach flow) and the ADMS boundary layer parameterisation leads to a wider plume than that given by ADMS using the wind tunnel flow profiles. Figure 11 shows the equivalent concentrations on the *X*-*Z* plane at *Y*=0m. A closer agreement is seen for the plume depth between each case; however, differences exist in concentration magnitudes.

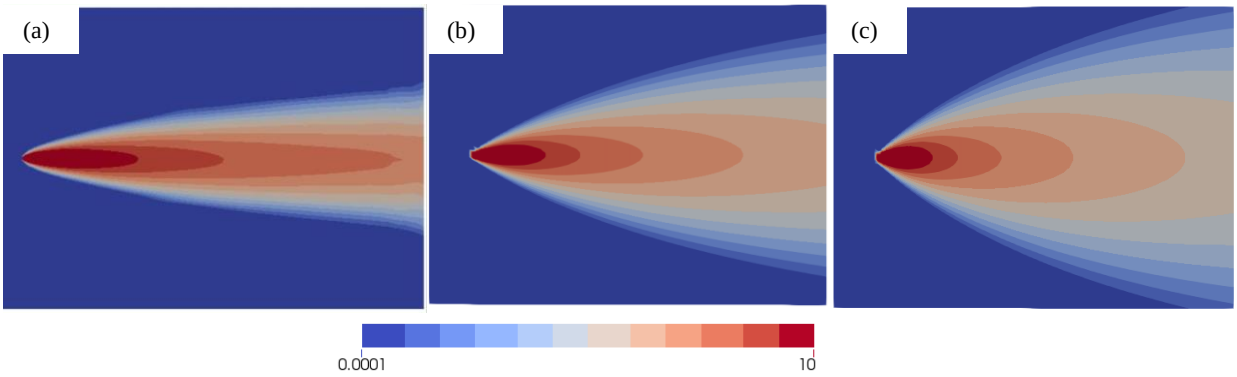

Figure 10: Neutral boundary layer concentrations at Z=6m for (a) LES, (b) ADMS with wind tunnel flow profiles and (c) ADMS with paramaterised meteorology with surface roughness $z_0 = 0.3m$. Release height $Z_s = H/4$. Note: a log colour scale is used here.

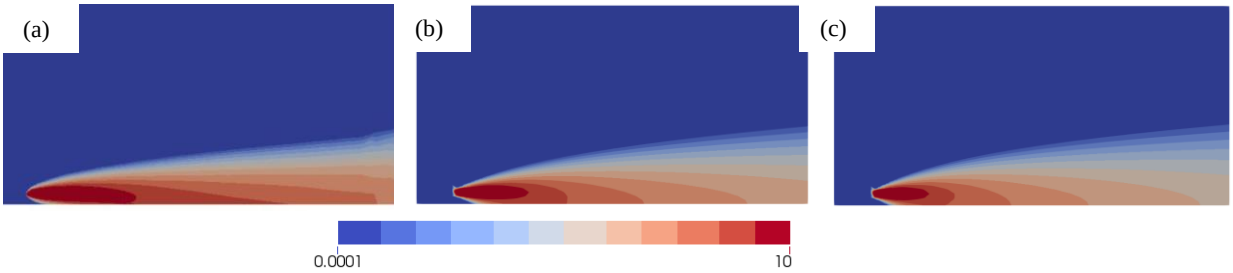

Figure 11: Neutral boundary layer concentrations at Y=0m for (a) LES, (b) ADMS with wind tunnel flow profiles and (c) ADMS with paramaterised meteorology with surface roughness z_0=0.3m. Release height $Z_s = H/4$. Note: a log colour scale is used here.

Measurements were taken in the wind tunnel at each of the downwind locations shown in Figure 7 and Figure 8. Figure 12 shows a scatter plot of the concentrations measured in the wind tunnel and those predicted by ADMS (assuming wind tunnel flow profiles) at a distance of 60m (2.5*H*) downwind of the release. The wider ADMS plume is reflected in the scatter plot as ADMS gives lower maximum concentrations and higher minimum concentrations. This is perhaps unsurprising as the term for plume spread of a Gaussian plume model is derived from real world atmospheric observations. This result is consistent with Higson and Griffiths (1994) who found that their wind tunnel experiments gave higher concentrations at the plume centreline compared to their full scale field experiments, despite the averaging times being short enough to neglect large scale variations in the wind direction. The hypothesised explanation given is that the larger eddies in the atmosphere are not modelled in the wind tunnel. This may also explain the difference between the two models here. Table 1 gives the centreline concentrations at each downwind distance for ADMS and the wind tunnel. Generally the comparison is in line with what would be expected, i.e. within a factor of two.

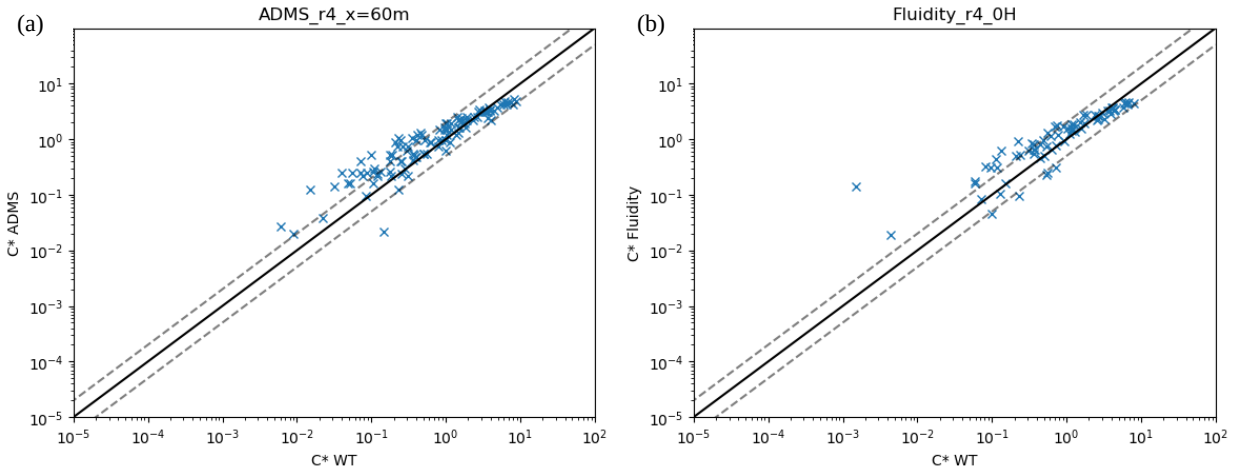

Figure 12: Scatter plot of concentrations at the Y-Z plane and X=60m downwind of release for (a) ADMS with wind tunnel profiles and (b) LES against wind tunnel values. Here the source release height, $Z_s = 4H/3$.

Table 1: Normalised plume centreline concentrations at each downwind distance for wind tunnel and ADMS.

	-1H	0H	1H	2H	5H
C* WT	12.80	8.03	4.17	2.55	1.09
C* ADMS	13.77	5.17	2.71	1.68	0.64
ADMS/WT	1.08	0.64	0.65	0.66	0.59

5.2.Release upwind of a normal facing building

5.2.1. Qualitative comparison between ADMS and LES

The presence of buildings can alter the dispersion pattern of a release by both forcing the plume to take an alternative path to pass around the building, and by increasing the mixing of the plume by generating additional turbulence as the air flows over the building. The ADMS building model used to simulate the effect of the building on plume dispersion is described in Section 2.4.

It should be noted that the approach flow turbulence levels were not equivalent for the two models here, with the LES turbulence around 40% lower than that assumed for ADMS. Therefore, direct comparisons of absolute concentration values will reflect this difference; those for the LES are likely to be higher due to less mixing. However, it was found that increasing the turbulence levels for the LES to be greater than those assumed here for ADMS did not change the flow patterns seen around the building (Appendix 3) and similar dispersion patterns were also observed. Therefore, a qualitative comparison of the dispersion patterns can be made between the two models.

Releases R2 and R4

Figure 13 and Figure 14 show the dispersion of the plume release at $Z_s = H/4$ and $2H$ upwind of the building centrepoint as given by (a) LES and (b) ADMS using wind tunnel flow profiles. The no building case is shown in Figure 10 and Figure 11. The presence of the building clearly has a significant effect on the LES mean concentrations, with a much wider plume seen downwind of the building. In fact this widening of the plume begins roughly half a building length upwind of

the windward face of the building. Similarly, the plume depth is also increased, showing that some of the release travels up and over the building as well as around the sides.

The location of the release lies within the region denoted by **U** in Figure 48. A summary of the flow features assumed by the ADMS building model for a release within this region is given in Table 9. The recirculation region is clearly visible in both Figure 13(b) and Figure 14(b). The building model also considers an elevated plume from above roof height for upwind releases. However, no elevated plume is seen in this case as the plume does not quite reach the height of the building at its leading face. No upwind distortion of the plume is considered within ADMS such as that seen for LES. Due to the absence of the elevated plume, the downwind plume consists of the recirculation region and ground-level plume only.

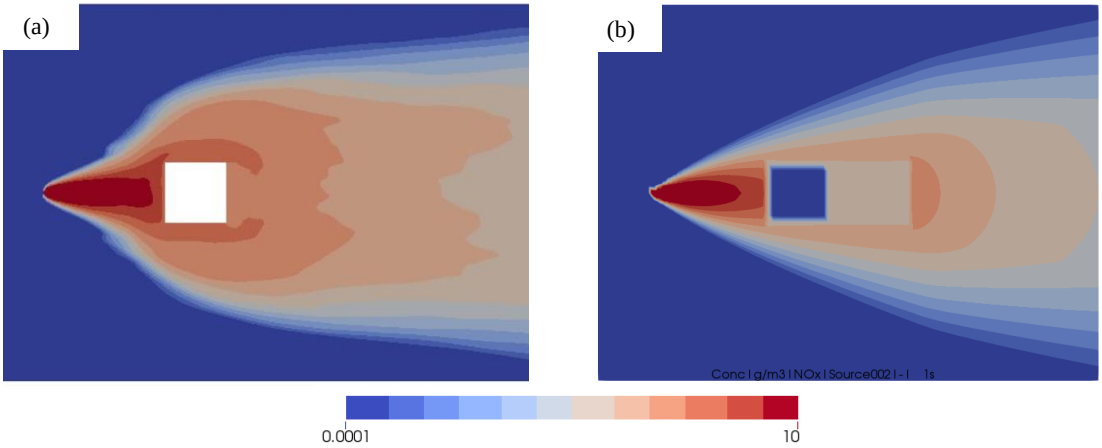

Figure 13: Neutral boundary layer concentrations at Z=6m for (a) LES and (b) ADMS with wind tunnel flow profiles. Release location R2, release height $Z_s = H/4$. Note: a log colour scale is used here.

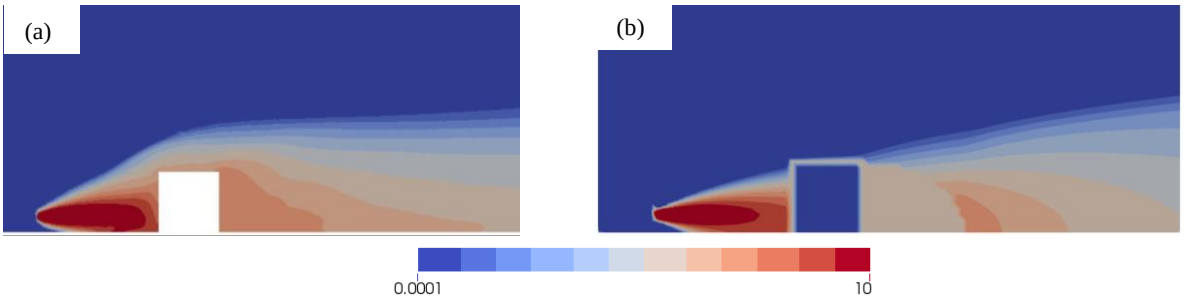

Figure 14: Neutral boundary layer concentrations at Y=0m for (a) LES and (b) ADMS with wind tunnel flow profiles. Release location R2, release height $Z_s = H/4$. Note: a log colour scale is used here.

Figure 15 shows the concentrations of a release upwind of the building at a height of $4H/3$ as predicted by the (a) LES and (b) ADMS building module. Here both the elevated and ground-level plumes are present, with the ADMS module capturing the effect of the entrainment of the plume into the wake region of the building.

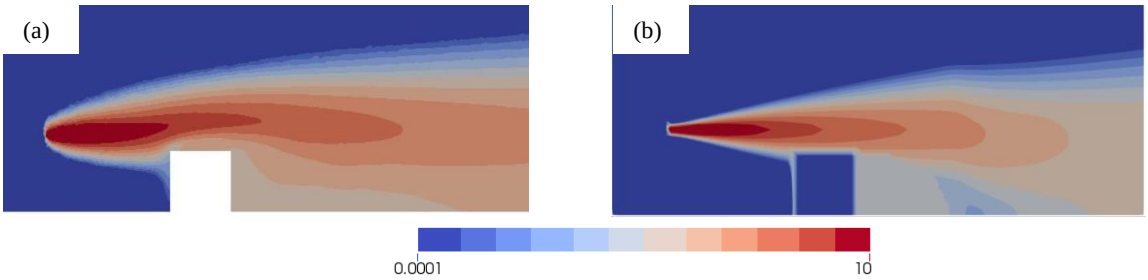

Figure 15: Neutral boundary layer concentrations at Y=0m for (a) LES and (b) ADMS with wind tunnel flow profiles. Release location R4, release height $Z_s = 4H/3$. Note: a log colour scale is used here.

Releases R1, R3 and R5

Figure 16 and Figure 17 show the concentrations for the R1, R3 and R5 release locations. These are all at a height of 18m ($Z_s/H = 3/4$). Downwind of the building the plume is similar in each case and there is good agreement between the LES and ADMS.

As for the lower release, R2, the effect of the building leads to a widening of the R3 and R5 plumes which is not directly accounted for by the ADMS Building module. This widening is particularly prominent for R5 which is the nearest to the building as the plume is narrower when it arrives at the building. However, this widening is not as prominent as that for R2 (Figure 13) and is not accompanied by the elevated concentrations on each side of the building. Rather, the maximum mean concentrations around the building are to be found above the roof, indicating that the main path of the plume is up and over the building. This allows the ADMS building module to provide a good representation of the plume downwind of the building as it is able to capture the downwash and two-plume behaviour. The presence of the building leads to an increase in the depth of the plume from the two nearest sources.

In the case of the LES, the plume is dispersed some distance upwind at the base of the leading edge of the building. This is likely due to the deflection of some of the plume downwards towards the vortex which forms at the building base. The plume is then recirculated within this vortex leading to a degree of upwind dispersion. This is not considered by the ADMS Building module.

The plume from R1 is particularly well represented by ADMS. This is the release location furthest upwind of the building. The discrepancies seen for the closer release locations that are not seen in this case highlights the need to investigate the limitations of the model at these small length scales.

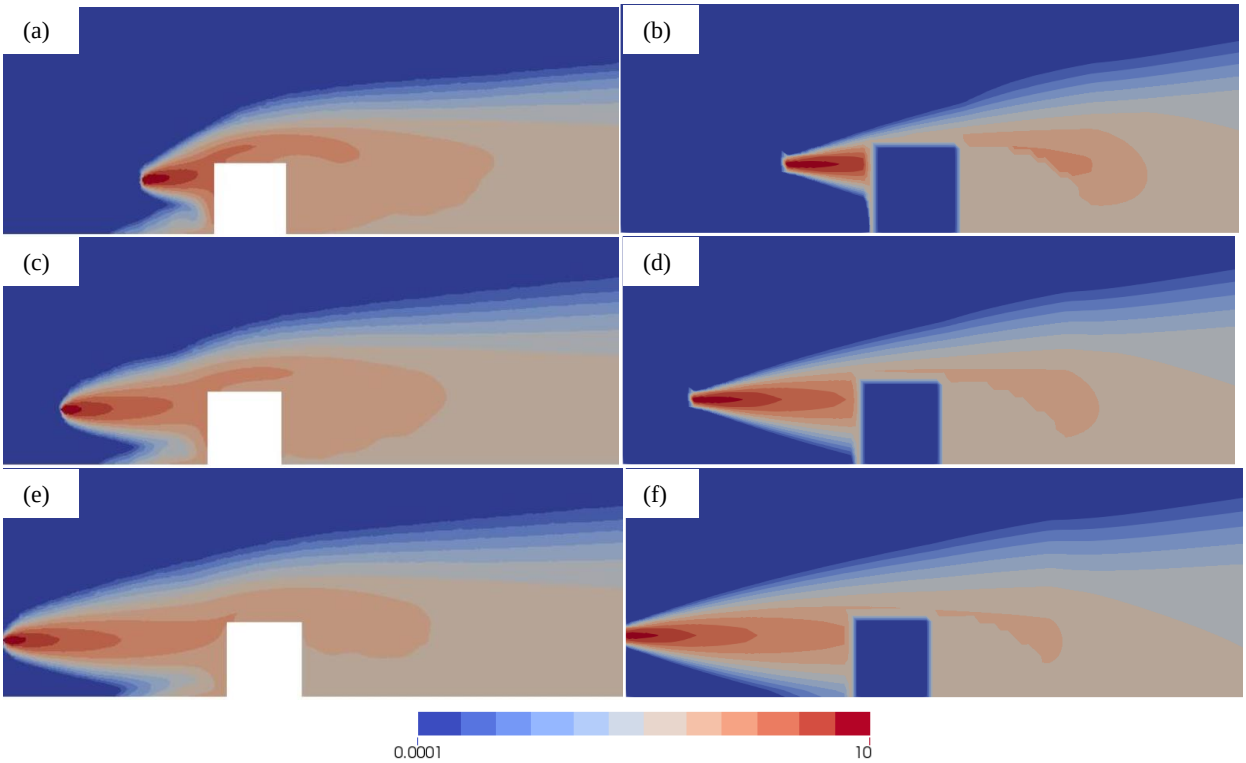

Figure 16: Neutral boundary layer concentrations at Y=0m for (a, c, e) LES and (b, d, f) ADMS with wind tunnel flow profiles. Release locations R1 (X_s/H=-3.5), R3 (X_s/H=-2.5) and R5 (X_s/H=-1.5) with source height $Z_s/H = 3/4$. Note: a log colour scale is used here.

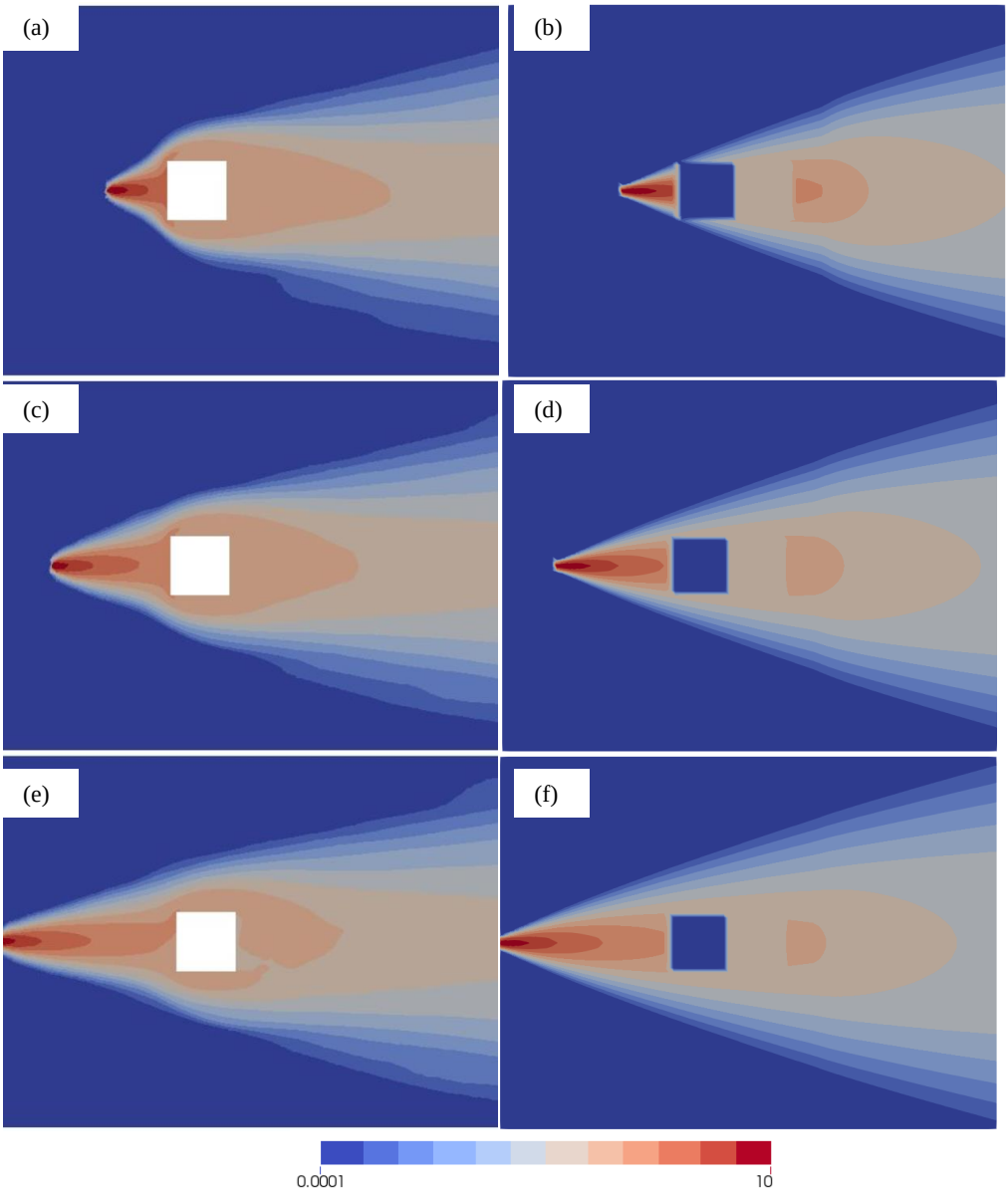

Figure 17: Neutral boundary layer concentrations at Z=18m for (a, c, e) LES and (b, d, f) ADMS with wind tunnel flow profiles. Release locations R1 (X_S/H=-3.5), R3 (X_S/H=-2.5) and R5 (X_S/H=-1.5) with source height Z_S/H=3/4. Note: a log colour scale is used here.

5.2.2. Comparison to wind tunnel measurements

The widening of the plume from release R2 due to the presence of the building was also seen within the wind tunnel. This can be seen from Figure 18 (a) which shows a *Y-Z* plane cross section of the plume at 1*H* and 5*H*. Note that these plots use a linear colour scale. The equivalent plots for ADMS and LES are also shown. The plume divides into two downwind of the building, with two distinct concentration maxima seen as far as 5*H*. ADMS gives significantly lower maximum concentrations downwind of the building and does not include this splitting of the plume into two distinct parts. This is reinforced by the scatter plot shown in Figure 19 (a), which shows that ADMS also gives lower values at most measured points away from the two plume centrelines. A closer

agreement is seen for LES despite the lower upwind turbulence as it is able to simulate the splitting of the plume (Figure 19 (b)).

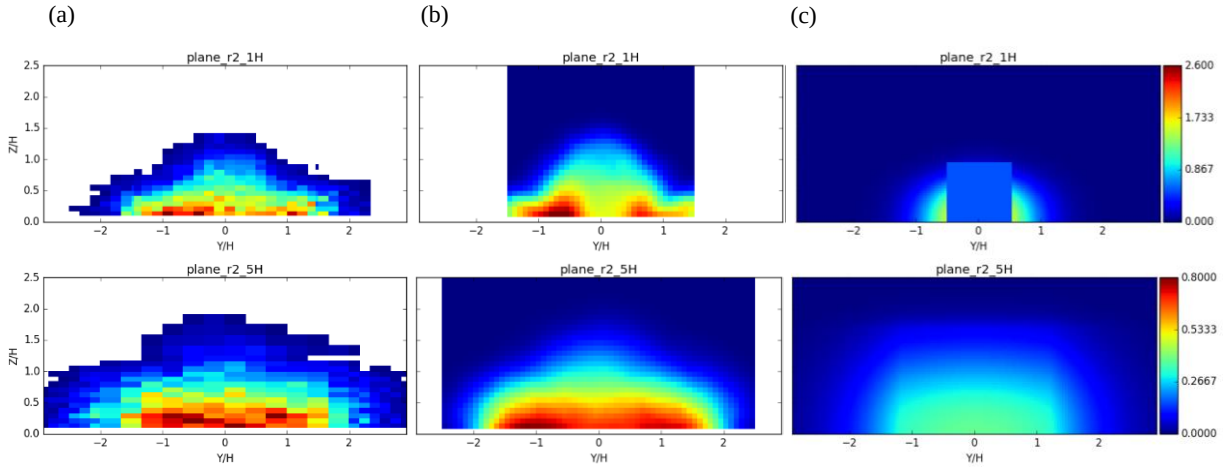

Figure 18: Normalised mean concentrations at locations 1H and 5H for (a) the wind tunnel, (b) LES and (c) ADMS for R2 (Z_s/H=1/4) upwind of normal facing building.

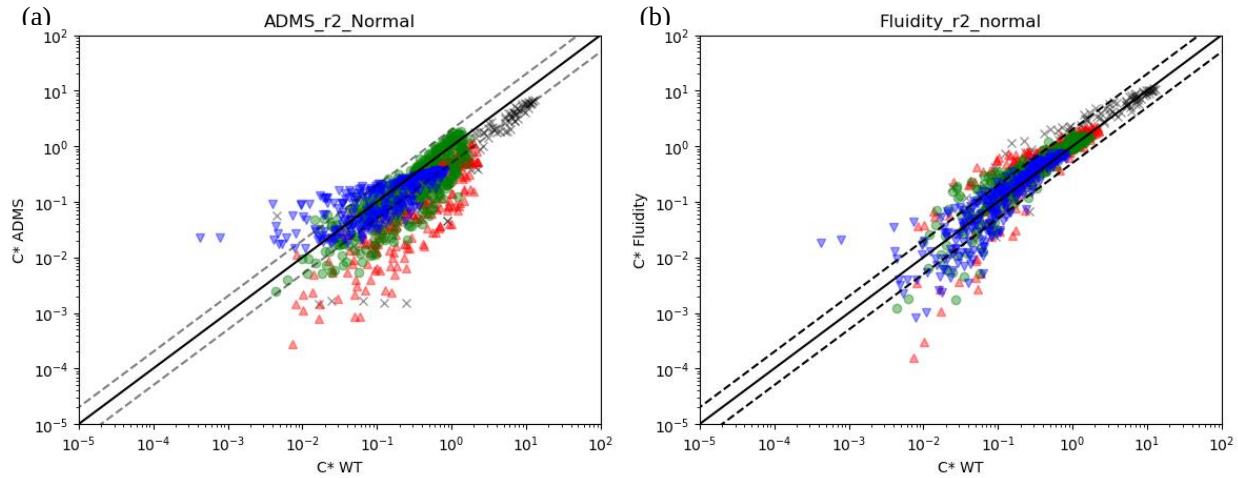

Figure 19: Scatter plot of mean concentrations for release R2 for (a) ADMS against the wind tunnel and (b) LES against the wind tunnel for the Y-Z plane at N1H (black crosses), 1H (red triangles), 2H (green circles) and 5H (blue downward triangles) for normal facing building.

A closer agreement between ADMS and the wind tunnel is seen downwind of the building for release R4. The presence of the building is not immediately evident at *1H* for any of the three representations (Figure 20). However, the plume centreline is more elevated for the wind tunnel and LES ((a) and (b) respectively). Further downwind at *5H* it is no longer possible to distinguish the elevated plume and ground-level plume for ADMS, while in the case of the wind tunnel and LES the elevated plume is dominant. This is reflected in the scatter plot given in Figure 21, where at 5*H* ADMS gives significantly lower maximum concentrations while predicting higher values for the lower concentrations on this plane.

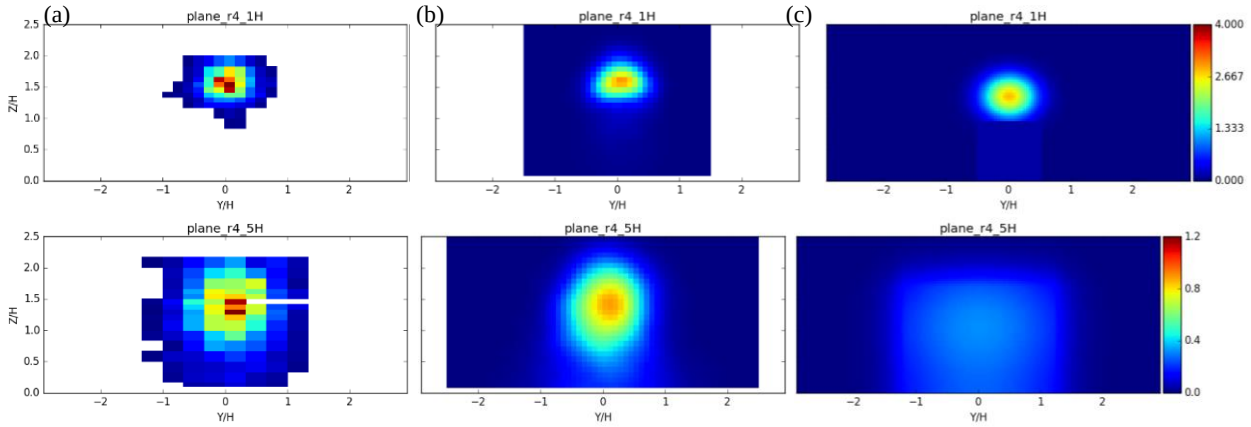

Figure 20: Normalised mean concentrations at locations 1H and 5H for (a) the wind tunnel, (b) LES and (c) ADMS for R4 (Z_s/H=4/3) upwind of normal facing building.

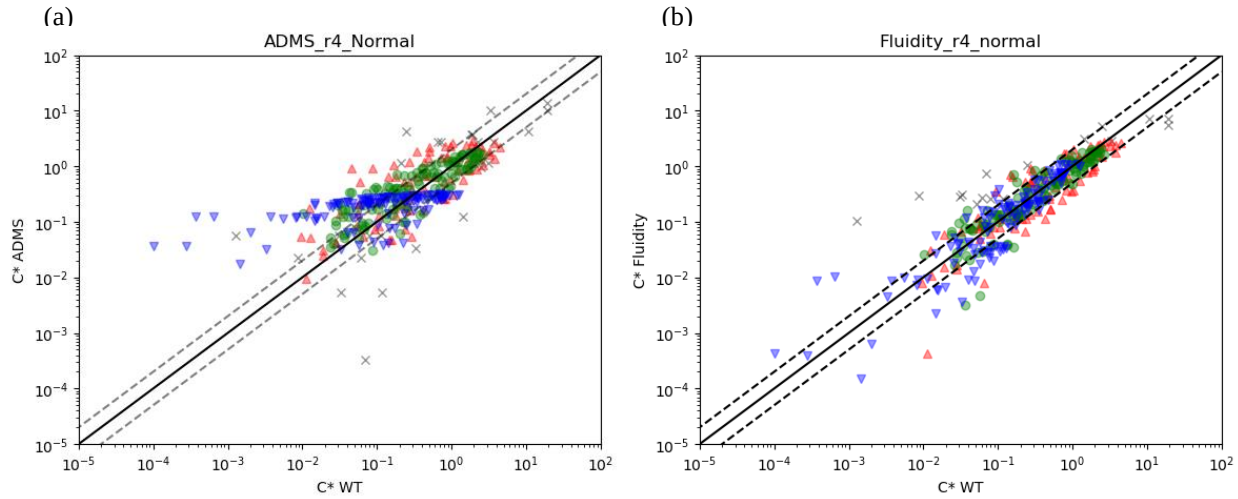

Figure 21: Scatter plot of R4 mean concentrations for (a) ADMS against the wind tunnel and (b) LES against the wind tunnel for the Y-Z plane at N1H (black crosses), 1H (red triangles), 2H (green circles) and 5H (blue downward triangles) for normal facing building.

Table 2 below gives the maximum mean concentrations at the measured plume centreline in the wind tunnel for R2, in addition to the maximum mean concentrations at each downwind location for ADMS. The maximum mean concentration is the maximum of the time averaged mean concentration at any given downwind distance. The wind tunnel concentrations given here are the average for the two plume centrelines either side of the building. The locations of the maxima do not coincide between the two models as is evident from Figure 18. The maximum mean concentrations in ADMS are 30-52% lower than those seen in the wind tunnel. An exception is 2*H* where ADMS gives higher concentrations than the wind tunnel. This region of higher concentrations is directly downwind of the near wake of the building and is visible in Figure 13 (b). Also shown in the table are the maximum mean concentrations at each downwind distance given by ADMS when no building is considered (i.e. an undisturbed plume). It is seen that these concentrations provide good estimates of the maximum mean wind tunnel concentrations either side of the building.

A plot of these concentrations is given in Figure 22 (a) against downwind distance from the source, $X'/H = X/H + 2.5H$. Also shown are the ADMS concentrations at the location of the wind tunnel plume centrelines. These are much lower than the wind tunnel values. Figure 22 (b) shows that good agreement was achieved between the wind tunnel and LES for these concentrations.

Table 2: Maximum mean concentrations for release R2 at wind tunnel centrelines for the wind tunnel (WT), the maximum mean ADMS concentrations at each downwind distance with normal facing building (ADMS max), mean ADMS concentrations in the presence of a normal facing building at the location of the wind tunnel plume centrelines (ADMS WT) and equivalent maximum mean concentrations with no building (ADMS no building).

	N1H	***0H***	***1H***	***2H***	***5H***
WT	12.60	3.49	2.46	1.63	0.765
ADMS max	7.27	1.69	1.63	1.92	0.46
Ratio	0.58	0.48	0.66	1.18	0.60
ADMS WT	7.27	0.29	0.55	0.94	0.46
Ratio	0.58	0.08	0.22	0.58	0.60
ADMS no building	7.39	3.36	2.16	1.58	0.82
Ratio	0.59	0.96	0.88	0.97	1.07

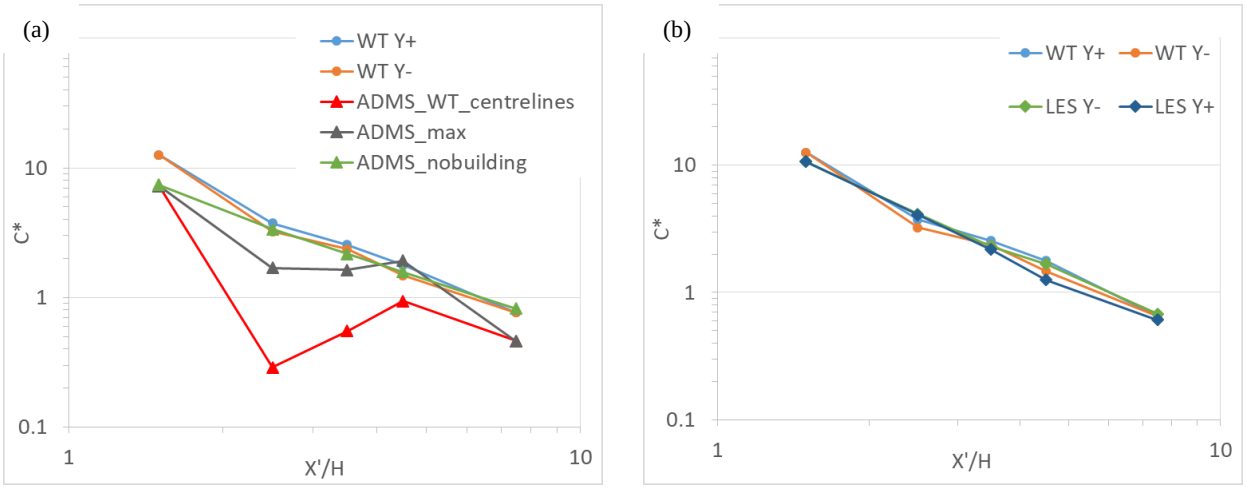

Figure 22: Maximum mean concentrations at dimensionless distances X'/H downwind of the source for release R2, comparing (a) wind tunnel and ADMS, and (b) wind tunnel and LES.

Figure 23 (a) shows the equivalent plots for the higher release, R4. A much closer agreement is seen in this case between the wind tunnel and ADMS. The LES is seen to underestimate the maximum mean concentrations near the source. This is likely due to an insufficiently fine mesh at this height. Figure 23 (b) shows the concentrations downwind of the building near the ground at $Z/H = 1/4$. Wind tunnel measurements were not available for these locations. The importance of accounting for the entrainment of the plume into the building wake is evident as much greater concentrations are seen near the ground when the building is present.

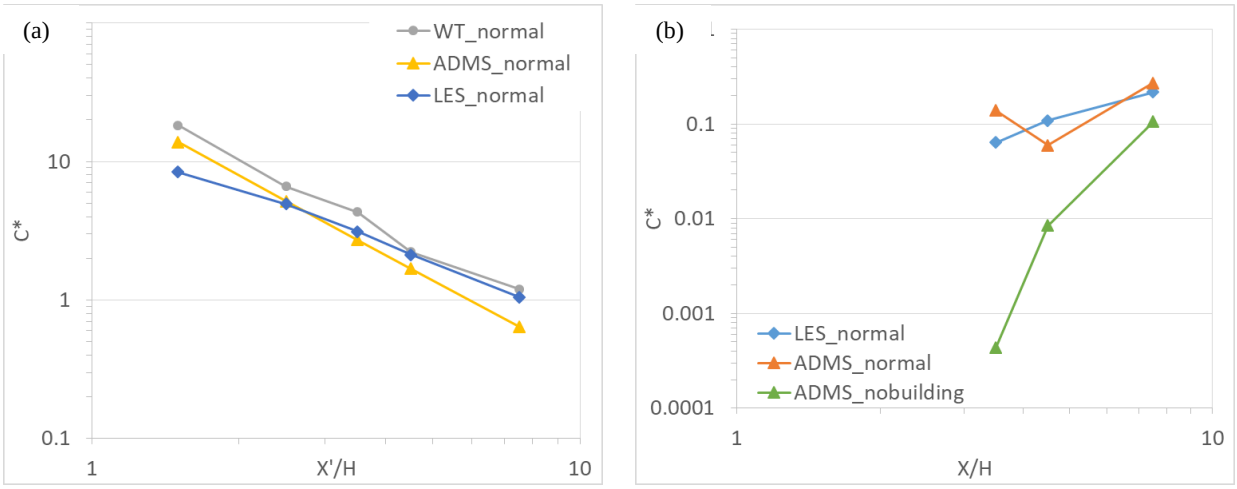

Figure 23: (a) Maximum mean concentrations at dimensionless distances X'/H downwind for higher release R4 and (b) mean concentrations at Y/H=0, Z/H=1/4 for ADMS and LES at locations downwind of building.

5.3. Uncertainties and sensitivities

It is important to establish the sensitivity of the concentrations around and downwind of the building to its orientation and geometry and the upstream flow statistics. As described in Section 2.4, the ADMS building module approximates all building geometries as a normal facing building with an equivalent frontal area. This method has been shown to give sufficiently representative results for rooftop stacks, however it is unclear how sensitive the concentrations from upwind releases are to different building configurations. A further case is also considered in which an additional building is placed upwind.

5.3.1. Oblique building

ADMS treats the oblique facing building as a normal facing building with an equivalent frontal area (see Appendix 2). The building used is of height and width $H = 24m$ at an angle of 45°. Therefore the equivalent building used by ADMS has an effective frontal area of approximately $34m^2$. This larger frontal surface area leads to a larger wake behind the building which in turn leads to an elongation of the recirculation region downwind (i.e. length L_R is increased in Figure 48 and Figure 49).

The mean concentrations at $2H$ for R2 for each model are given in Figure 24 for both the normal building (a-c) and oblique building (d-f). The two plumes seen in the wind tunnel and LES are more pronounced for the oblique building case, suggesting a stronger horseshoe vortex is present. ADMS is clearly seen to underestimate the concentrations relative to these models. The longer recirculation region behind the oblique building, that is evident by constant concentrations within this region, is still visible for the oblique building case (Figure 24 (f)), but is not visible for the normal building case (Figure 24 (c)).

For R4, Figure 25, higher concentrations are seen within the building wake for the wind tunnel and LES. ADMS also gives higher concentrations within the building wake relative to the normal building case as the larger frontal area assumed by the model gives a larger recirculation region and therefore an increase in plume entrainment. However, the impact of the building orientation is

much less significant in the case of the higher release, and a similar comparison is seen between the three models as seen for the normal building in Figure 20.

Figure 26 shows the scatter plot of the ADMS concentrations against those measured in the wind tunnel for the oblique building case.

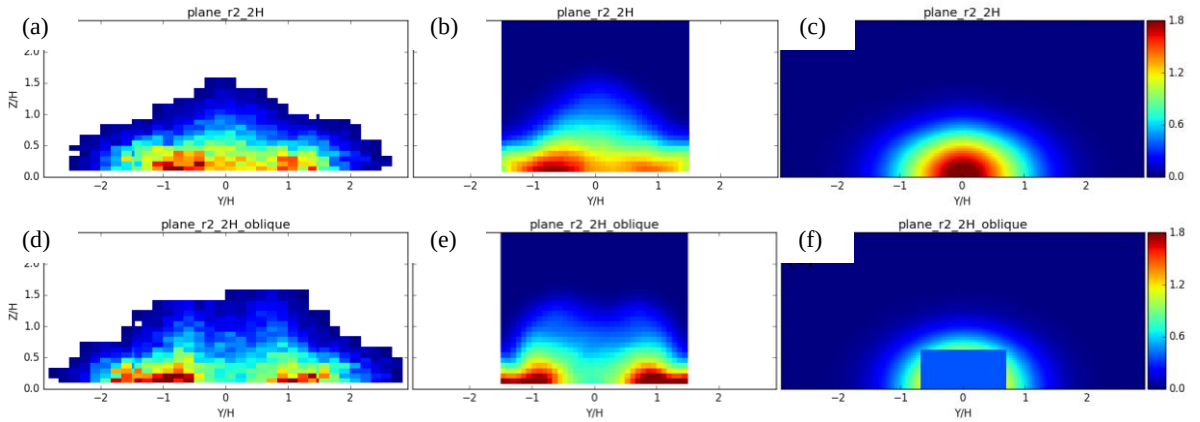

Figure 24: Normalised mean concentrations at locations 2H for the wind tunnel, LES medium turbulence and ADMS for R2 (Z_S/H=1/4) upwind of normal facing building (a, b c) and the oblique building (d, e, f).

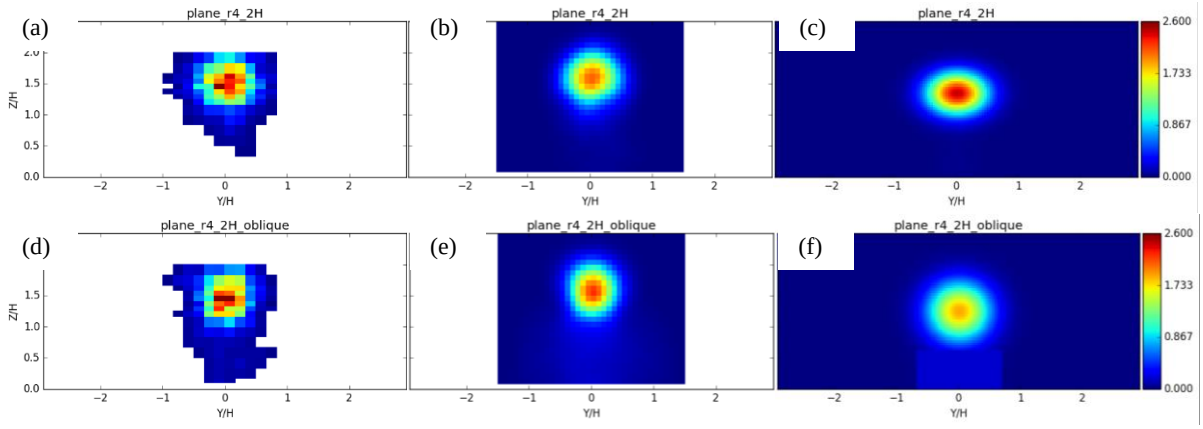

Figure 25: Normalised mean concentrations at locations 2H for the wind tunnel, LES and ADMS for R4 ($Z_S/H = 4/3$) upwind of normal facing building (a, b c) and the oblique building (d, e, f).

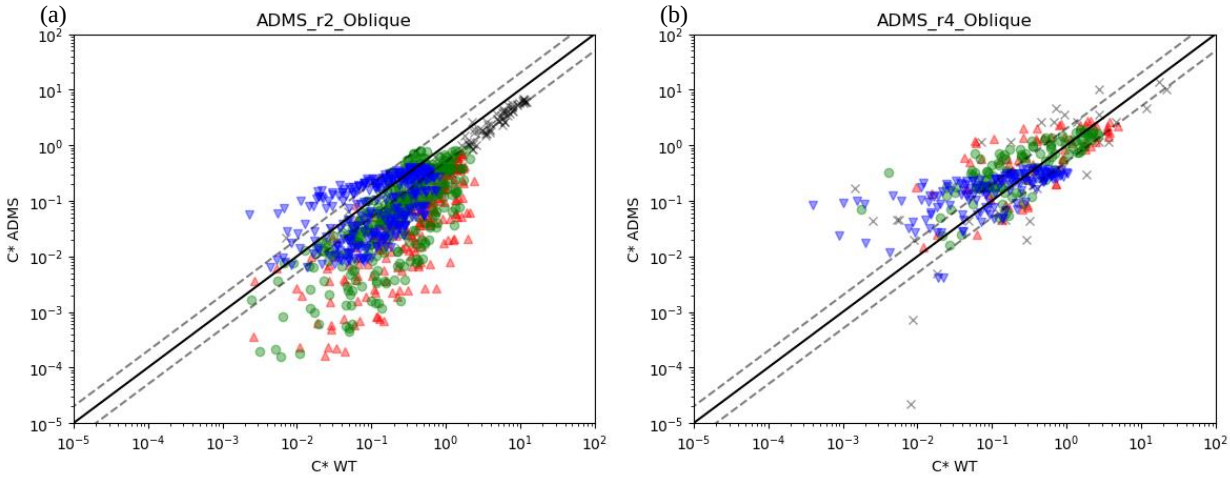

Figure 26: Scatter plot of (a) R2 and (b) R4 mean concentrations for ADMS against the wind tunnel for the Y-Z plane at N1H (black crosses), 1H (red triangles), 2H (green circles) and 5H (blue downward triangles) for oblique facing building.

5.3.2. Asymmetrical orientations and geometries

Some of the factors not accounted for within the ADMS building model include roof shapes, asymmetry in the building geometry relative to the approach flow, the presence of upwind buildings or asymmetry in the approaching flow, all of which would be expected in most urban scenarios. The presence of upwind buildings can be accounted for to some extent within ADMS by using a spatially varying surface roughness, however the impact of individual buildings is not resolved. Three scenarios were simulated using LES to explore these effects. These include a cube building at 30 degrees to the approaching flow, a building at 45 degrees with a pitched roof and a normal facing building with a building upwind at a distance of $5H$. Figure 27 shows the configuration for each case. For the pitched roof case, a height of 18m and 30m was used for the roof base and roof peak, respectively, giving a mean height equivalent to the other buildings of 24m.

Two releases were considered, one at R2 ($X_s = -2.5H, Z_s = H/4$) and one at R4 ($X_s = -2.5H, Z_s = 4H/3$).

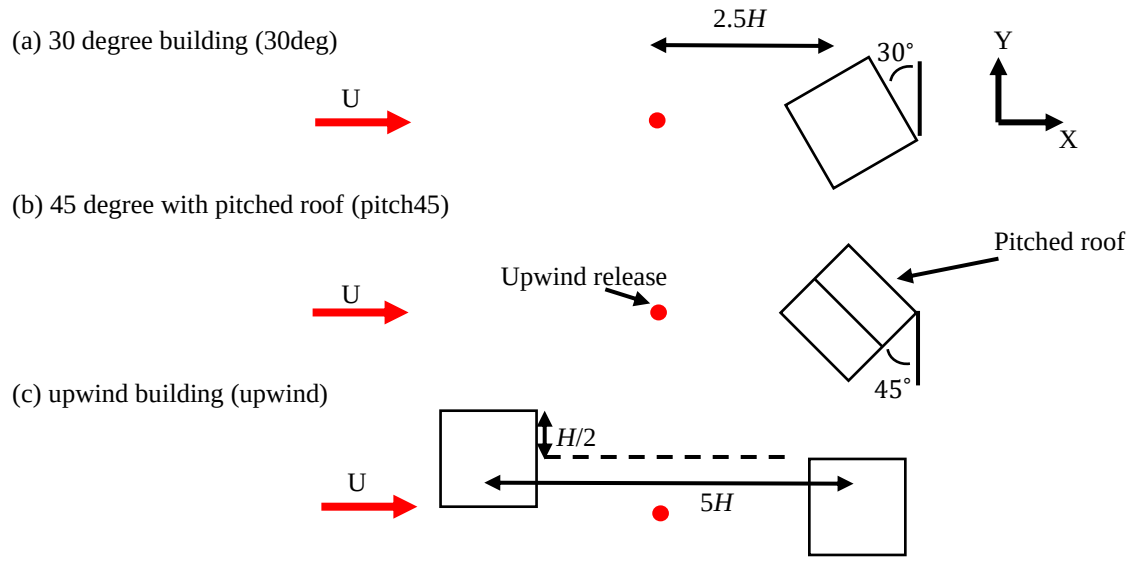

Figure 27: Schematic showing bird's eye view of asymmetric geometries used for LES simulations.

Figure 28 shows the mean concentrations at 2*H* and 5*H* for each of the sensitivity test cases and the lower release height, R2. As expected in this case the orientation of the building plays a significant role. For the 30 degree case, higher concentrations are seen downwind of the side of the building with the larger surface area facing the prevailing wind direction (i.e. Y<0, see Figure 27). In this case the source is not on the stagnation streamline (where stagnation occurs at the leading corner of the building). Rather, the source is to one side of the stagnation streamline and therefore the plume is more likely to arrive at one side than the other, in this case the side with the larger projected surface area.

The impact of the pitch45 case on the lower release mean concentrations relative to the oblique case is less obvious. However, lower concentrations are found within the recirculation region of the building compared to the oblique case (Figure 24).

For the upwind building case the concentrations are much lower due to the increased mixing upwind of the main building due to the impact of the building at -5*H*. However, the asymmetry introduced by the building at -5*H* has a clear impact, with an asymmetrical plume downwind of the main building.

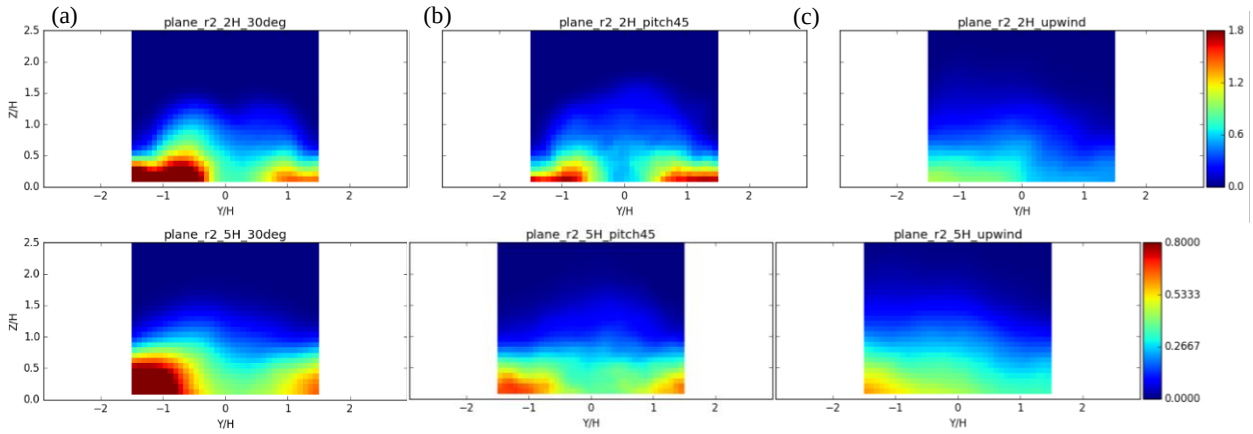

Figure 28: Normalised mean LES concentrations at location 2H and 5H for sensitivity cases for release R2 upwind of (a) 30 degree building, (b) pitch45 building and (c) upwind building.

Figure 29 shows the mean concentrations at 1*H* and 5*H* for each of the sensitivity test cases for the higher release location. While the impact of the building geometries is less in this case, clear differences can still be seen. The shape of the plume is clearly affected by the pitched roof and lower concentrations are seen in this case at the plume centreline. There is also a decrease in the plume entrainment into the recirculation region behind the building in this case, which is evident at 5*H*. The mean concentrations for the upwind case are again much lower than the other cases. This is again due to the increased dispersion of the release upwind of the building. The mean plume height is also significantly lower for the upwind case as the release is entrained into the far wake of the upwind building.

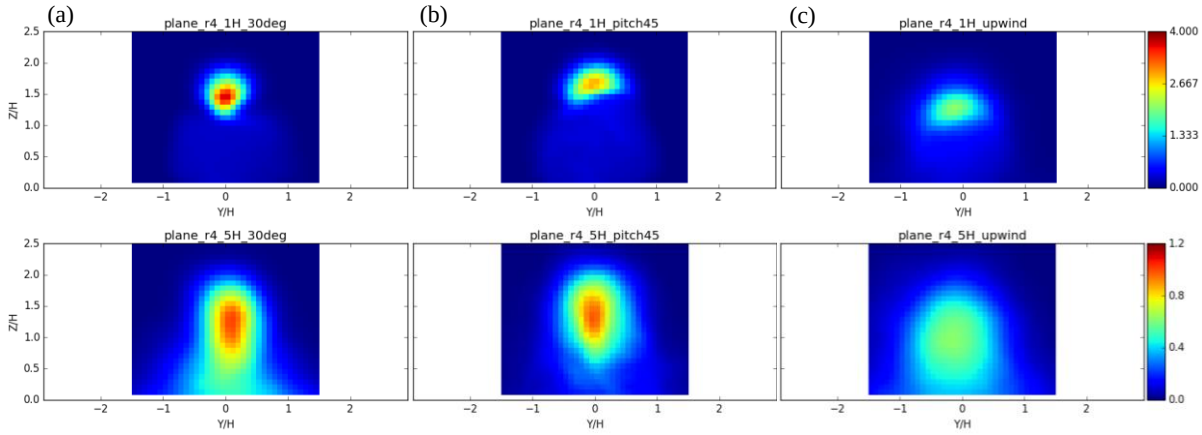

Figure 29: Normalised mean LES concentrations at location 1H and 5H for sensitivity cases for release R4 upwind of (a) 30 degree building, (b) pitch45 building and (c) upwind building.

Table 3 and Table 4 provide the maximum mean concentrations and 95th percentile concentrations evaluated over the LES time step (0.5 seconds) at each downwind location for each building scenario for the R2 and R4 release, respectively. The mean and normalised standard deviation between each building configuration other than the upwind scenario is also given. The upwind

scenario is excluded from these calculations in order to investigate the impact of the configuration of the main building only.

A variation in mean concentrations of up to 58% is seen for the maximum mean concentration at the considered downwind locations. This maximum difference is seen at 1*H* between the normal facing building and the 30 degree building. The cause of the difference is the higher concentrations seen at one side of the 30 degree building due to its asymmetric orientation to the approach flow which results in the source lying to one side of the stagnation streamline. A lower variation is seen for the maximum 95th percentile concentrations of up to around 30%. A smaller variation is seen for the higher release than the lower release where the building orientation and geometry has a greater impact. The concentrations for the upwind building case are up to a factor of 2 lower than the other cases.

Table 3: Maximum mean and 95th percentile values for release 2 at downwind locations for different building configurations.

		Normal	Oblique	30deg	Pitch45	Mean	StdDev/Mean	Upwind
Mean	***1H***	2.60	2.87	4.11	2.81	3.10	0.22	1.23
	2H	1.70	2.16	2.84	1.74	2.11	0.25	1.00
	5H	0.81	0.92	1.12	0.68	0.88	0.21	0.60
95th percentile	***1H***	5.71	6.86	8.74	7.67	7.25	0.18	3.78
	2H	3.66	4.60	5.63	4.54	4.61	0.17	2.61
	5H	1.50	1.77	2.11	1.67	1.76	0.15	1.34
95th/Mean	***1H***	2.20	2.39	2.12	2.72	2.36	0.11	3.07
	2H	2.15	2.13	1.98	2.60	2.22	0.12	2.61
	5H	1.85	1.92	1.89	2.44	2.02	0.14	2.25

Table 4: Maximum mean and 95th percentile values for release 4 at downwind locations for different building configurations.

		Normal	Oblique	30deg	Pitch45	Mean	StdDev/Mean	Upwind
Mean	**1H**	2.87	3.08	3.64	2.87	3.11	0.12	2.08
	2H	2.09	2.25	2.48	1.99	2.20	0.10	1.41
	5H	1.11	1.12	1.01	0.98	1.05	0.07	0.62
95th percentile	**1H**	4.71	5.54	6.63	4.74	5.41	0.17	4.63
	2H	3.46	3.85	4.59	3.18	3.77	0.16	2.88
	5H	1.95	1.99	2.04	1.87	1.96	0.04	1.25
95th/Mean	**1H**	1.64	1.80	1.82	1.66	1.73	0.05	2.23
	2H	1.65	1.71	1.85	1.60	1.70	0.06	2.05
	5H	1.76	1.78	2.02	1.91	1.87	0.07	2.01

5.4. Boundary layer stability

So far the analysis has been limited to neutral boundary layers only. LES was also used to simulate the dispersion of a continuous release within a stable and unstable boundary layer.

A similar approach was used to configure the simulations as for the neutral simulations. The synthetic eddy method was used to apply a turbulent flow at the inlet. A potential temperature profile was also applied at the inlet, along with a heat flux at the ground to simulate the heating or

cooling of the air by the ground. Details of the configuration of the simulations can be found in Appendix 4. ADMS flow profiles were used as inlet boundary conditions, however the resulting flow statistics of the LES simulation at the location of the release differed somewhat from these. Nonetheless, flow profiles representative of the considered stability class were achieved. It should be noted that large scale motions in the atmosphere are not accounted for here as these are limited by the domain size used. In this case a height of 200m was used for the domain, whereas a boundary layer height of 800m was assumed when generating the boundary conditions using ADMS. Therefore only the lower quarter of the boundary layer is simulated and air flow is capped at 200m. This is a particular problem for unstable boundary layer simulations as large scale vertical motions are present under these conditions. However, despite this limitation a comparison of LES and ADMS concentrations for a release at z = 6m showed reasonably good agreement for the open terrain case (Appendix 4).

The meteorology parameters used for the stable and unstable boundary layer simulations are given in Table 5, along with the corresponding stability defined both by the Pasquill-Gifford stability class and the Monin-Obukhov length (L_{MO}). The reader is referred to Figure 3. While a low heat flux of $5W/m^2$ is used for the unstable case, the boundary layer lies between the Pasquill-Gifford stability classes B and C due to the low wind speed used of $1.25m/s$. As an example, this is equivalent to a heat flux of $20W/m^2$ and a wind speed of $2m/s$, or a heat flux of $45W/m^2$ and a wind speed of $2.5m/s$.

Table 5: Meteorology parameters used for unstable and stable boundary layer simulations and corresponding stability class.

	z_0 (m)	Wind speed at 10m (m/s)	Surface heat flux (W/m^2)	Boundary layer height (m)	Pasquill-Gifford stability	h/L_{MO}
Unstable	0.3	1.25	5	800	B/C	-12
Stable	0.3	2	-6	120	F	1

A comparison of the LES and ADMS concentrations at 1*H*, 2*H* and 5*H* for a release at R2 for the stable boundary layer is shown in Figure 30. The concentration distributions are similar to those seen for the neutral boundary layer (Figure 18 and Figure 24 (b,c)). The two maxima either side of the building at ground level are once again present for the LES simulations. Increased concentrations at ground level are expected for stable boundary layer profiles due to a suppression of vertical mixing by the negative buoyancy of the air.

Figure 31 shows the equivalent plot for the unstable case. Note that the colour scales used differ to those in Figure 30. The downwind plume is clearly asymmetrical for the LES simulation. This is due to a lack of convergence. A much longer time was needed to reach a well-converged mean concentration for the unstable case. This is due to the increased mixing for this case in addition to the longer time scales of the turbulent eddies which are larger than those of the neutral and stable cases. The simulation was stopped after the "real time" of the calculation for the mean concentration reached 1 hour and 30 minutes. Despite the increased vertical mixing for the unstable case, two distinct maxima are still seen at 1*H*. At 2*H* only one maximum is seen, however this maximum is located away from the building centreline, indicating that the effect of the horseshoe vortex prevails. By 5*H* the plume centreline is aligned again at the building centreline and two distinct plumes are no longer visible.

Equivalent figures for the elevated release R4 can be found in Appendix 4.

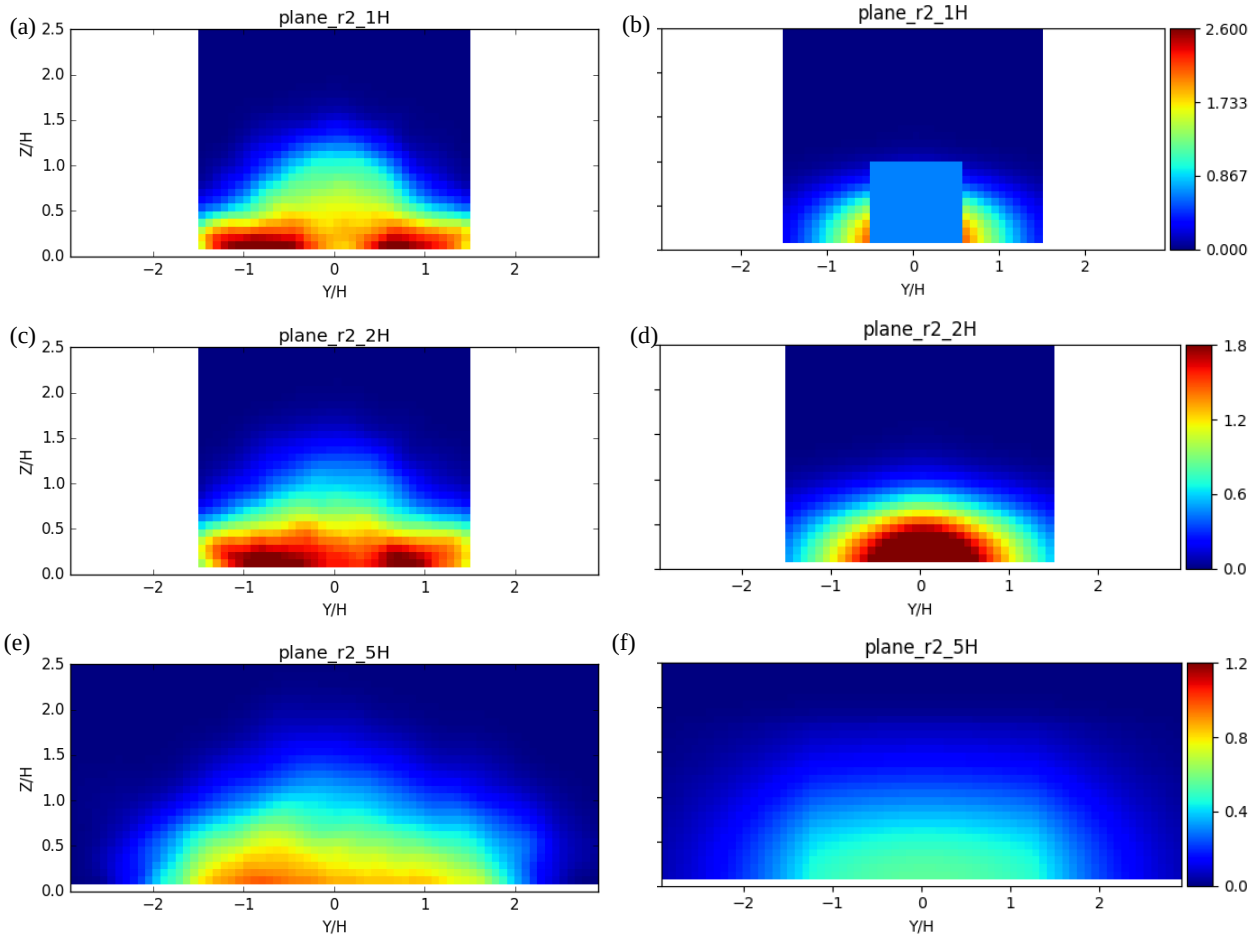

Figure 30: Stable boundary layer normalised mean concentrations at location 1H, 2H and 5H for R2 upwind of a normal facing building for LES (a, c, e) and ADMS (b, d, f).

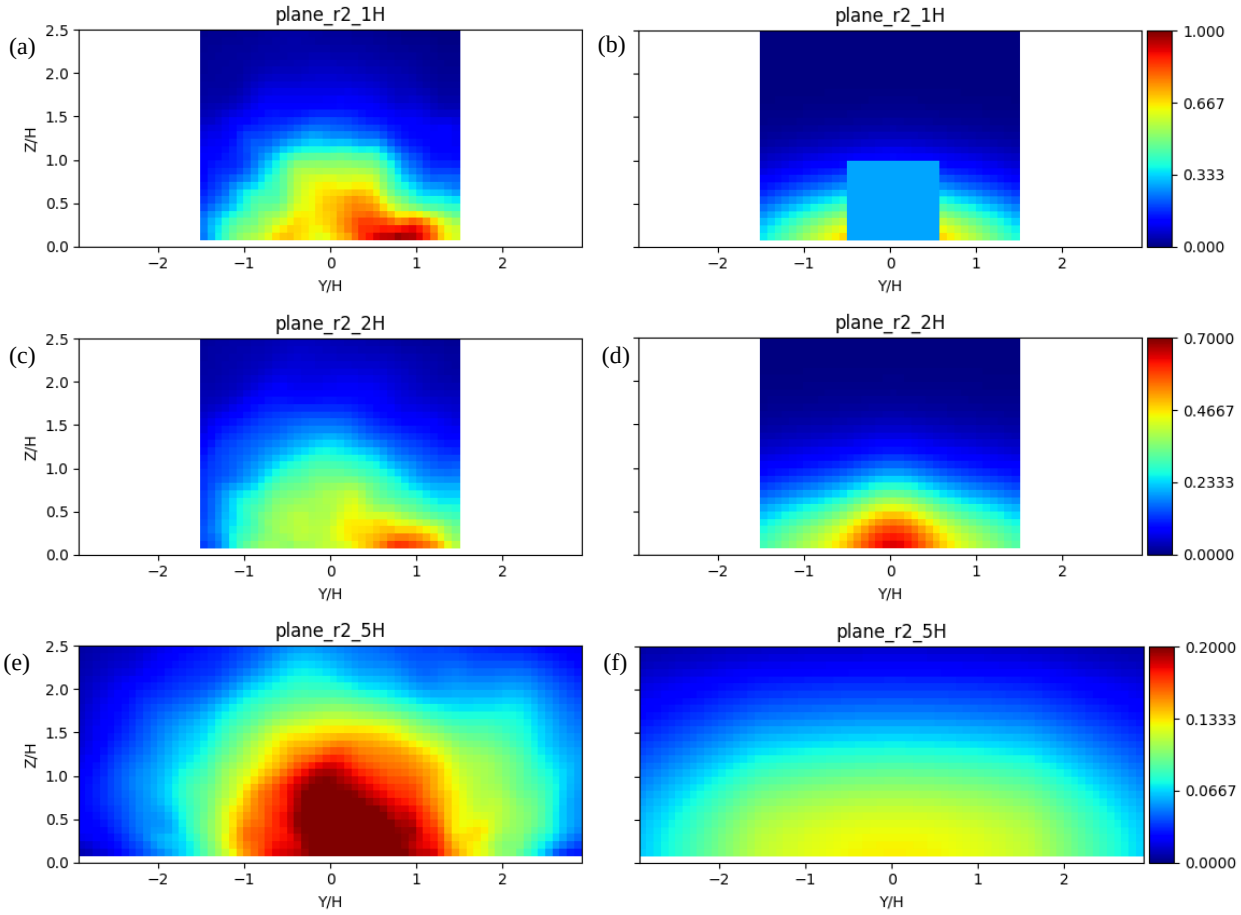

Figure 31: Unstable boundary layer normalised mean concentrations at location 1H, 2H and 5H for R2 upwind of a normal facing building for LES (a, c, e) and ADMS (b, d, f).

6. Fluctuations and puff releases

Short duration releases, or puffs, are inherently difficult to simulate due to the short time scales involved and the highly unsteady nature of their dispersion within atmospheric flows. Similarly, the evaluation of average concentrations over short time periods from both plume and puff releases are a challenge to resolve. While for the evaluation of long term exposure the time averaged concentration is usually the most relevant and useful output, over shorter time periods or when considering short puff releases, it is often the maximum feasible concentration or dose over a short exposure time which is of concern. In this case a time averaged concentration field estimated by a Gaussian plume model can be used to estimate the likely direction of the dispersion of the puff, but does not provide an expected range of dose at any given location.

6.1. Puff time series and exposure time

When a release should be considered a puff rather than a plume depends on the travel time of the release relative to the release time, Δt. When the release time is much longer than the travel time the release can be considered a plume, while when the travel time is less than the release time it can be considered a puff.

Here we define the normalised dose, χ, from a puff release as:

$$\chi = \frac{U_{ref}H^2}{q_s \Delta t} \int_0^{t_E} C(t)\, dt, \qquad (3)$$

where $q_s\Delta t$ is the total release. This is equivalent to the normalised concentration given by equation 2 when $\Delta t = t_E$. For a continuous release the normalised dose and normalised concentrations are equivalent, as the total release during the exposure period is $q_s \Delta t = q_s t_E$. For the dose calculated in this section we ensure that the exposure time t_E is greater than the passing time of the puff such that the "total" puff dose is obtained.

The highly variable nature of puff dispersion can be seen from the time series plots in Figure 32. Here we see concentration measurements in the wind tunnel at *1H* for three puffs of 0.5 s release duration. We see periods of very low concentrations interrupted by very high, very short concentration peaks; i.e. pronounced intermittency, and great case-to-case variability.

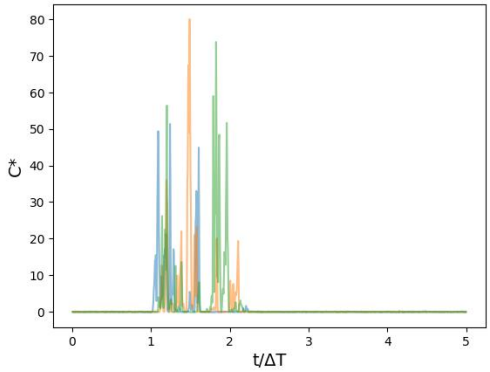

Figure 32: Time series of normalised concentrations for three overlaying 0.5 s emission, R4 puffs at 1H in the wind tunnel.

6.2.Convergence

In the case of the continuous release the concentrations were measured at each location for 30 seconds in the wind tunnel, equivalent to 50 minutes at full scale. Figure 33 shows the convergence of the mean plume concentration and the 95th percentile/mean at $N1H$ for the R4 release. In both cases it seems that the values have converged sufficiently to give a reasonable estimate of the true value. These plots are typical for the plume concentration measurements at all locations.

These convergence plots give an indication of the timescale at which the mean concentrations calculated by a Gaussian plume model become representative of the real mean for a neutral boundary layer. After around 15 seconds the mean value seen in Figure 33 (a) remains relatively constant. At full scale this is equivalent to 25 minutes. Therefore mean concentrations calculated over periods longer than 25 minutes real-time would be expected to remain broadly unchanged, while for periods shorter than 25 minutes the mean concentration could vary, with increasing variation as the averaging period is decreased. Gaussian plume models are often used to calculate hourly averaged concentrations. These wind tunnel results suggest that the calculated mean concentrations remain representative down to a time period of around 25 minutes for this particular test case under neutral conditions.

Similar convergence times may be expected under stable atmospheric conditions as mixing is again dominated by turbulence generated by the flow of air over buildings and other objects. However, in the case of an unstable boundary layer, a longer time to reach converged mean concentrations may be expected. This is due to the increased variability seen in these conditions where much larger mixing scales are involved due to convectively driven motions in the atmosphere. This is reflected in the mean plots shown for the unstable LES simulation (Figure 31), where the concentrations are far from well-converged even after 1 hour and 30 minutes of simulation time.

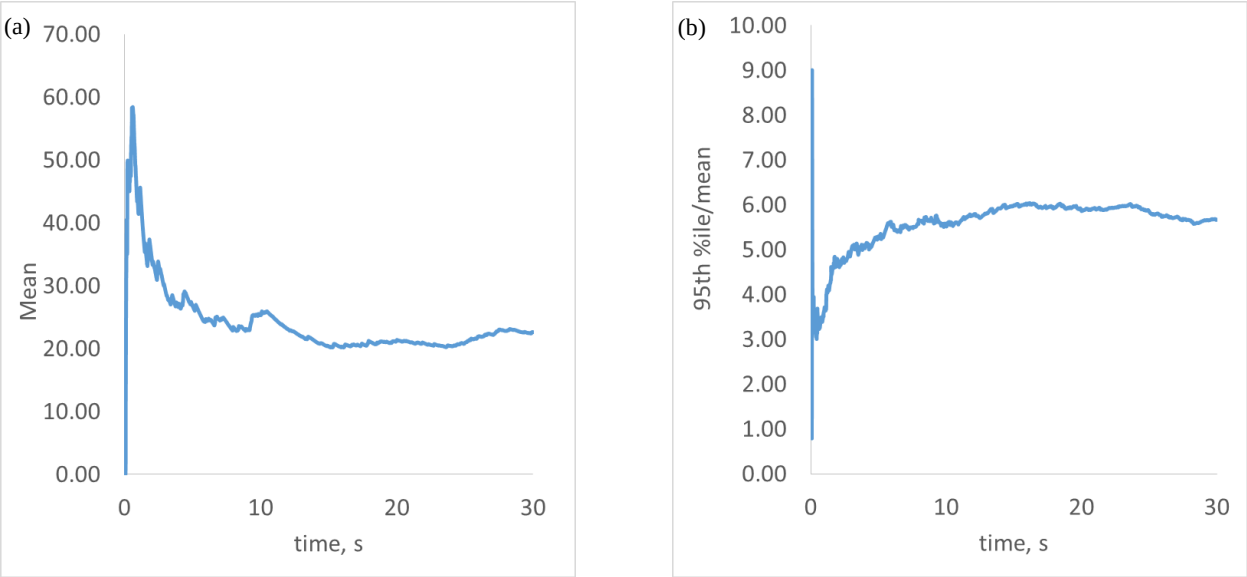

Figure 33: Convergence of (a) normalised mean dose and (b) 95th percentile/mean at X/H=-1 for a continuous release at R4.

It was unclear before undertaking the wind tunnel experiments how many puffs would be needed to obtain a statistically meaningful distribution for puff dose, though previous work suggested numbers in excess of 50. It was also expected that the longer duration puffs would reach convergence within fewer instances than shorter releases. For the longest puff release time of 1s, 90 puffs were released in total, while for the shortest puff release time of 0.05s, around 190 puffs were released.

Figure 34 shows the convergence to the normalised mean dose χ (according to equation 3) and the 95th percentile/mean of χ for the different puff release times at $N1H$. The normalised mean dose, given by equation 3, is expected to be equal for all puff release times. It is therefore clear from Figure 34 (a) that full convergence has not been achieved for the puff releases at this location, for which the normalised mean varies by up to 40% between puff release times. This is also the case for the 95th percentile/mean shown in Figure 34 (b). Here the ratio is expected to be highest for the shortest release, $\Delta t = 0.05s$, however a higher value is seen for $\Delta t = 0.1s$. This is likely due to the higher mean seen for $\Delta t = 0.05s$ in Figure 34 (a). The variation of the 95th percentile dose and how this varies with puff duration is explored further later in this report: it should be noted from Figure 34 (b) and Figure 35 (b) that the longer duration puff releases showed a marked reduction compared to the shorter duration puff releases.

Better convergence was achieved for the puff releases at the measurement points further downwind. Figure 35 shows the convergence of the puff statistics at $1H$. Here the normalised mean

is in agreement between each puff release time within 12%. The 95th percentile/mean plots also reflect the expected behaviour, with a higher peak-to-mean ratio for shorter puff releases.

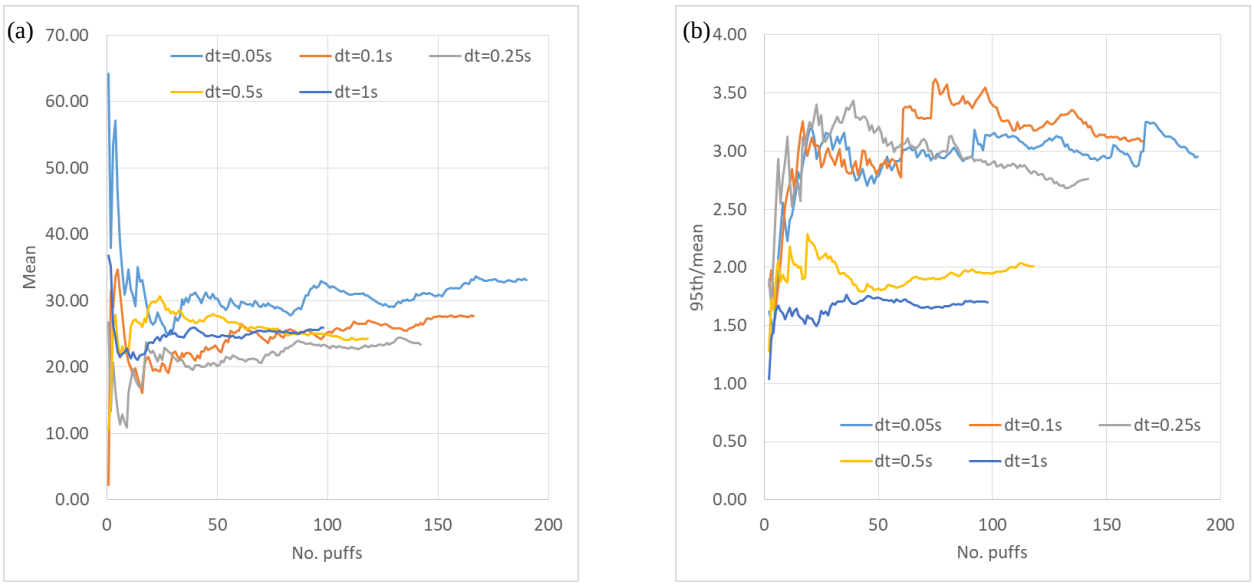

Figure 34: Convergence of (a) normalised mean and (b) 95th percentile/mean at X/H=-1 for puffs released at R4.

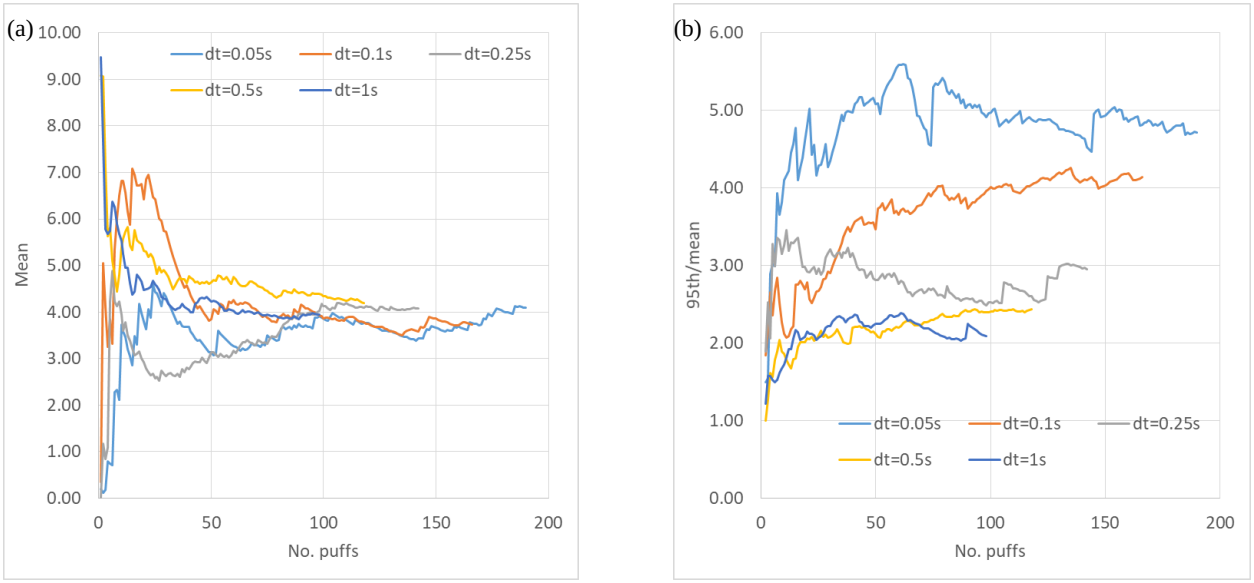

Figure 35: Convergence of (a) normalised mean and (b) 95th percentile/mean at X/H=1 for puffs released at R4.

6.3. Probability density functions

Probability density functions (PDFs) for the puff dose of the R4 release with $\Delta t = 0.5s$ at each downwind location are shown in Figure 36. The lack of convergence to a smooth distribution is evident at each location. However, sufficient puffs were simulated to show the general shape of the distributions, which appear to be log normal. The distributions are much shallower and broader at points closest to the release. This is expected as here the puff has had less time to mix and is

therefore smaller in size with high concentrations. This means that the puff is more likely to miss the measurement point completely, leading to a higher proportion of zero dose puffs. While in the case that the puff does pass through the measurement point, a high dose is more likely. For points further from the release location the distributions are much narrower, indicating a smaller range in dose values with a much lower maximum normalised dose. In this case the puff has had time to mix and increase in size before reaching the measurement point.

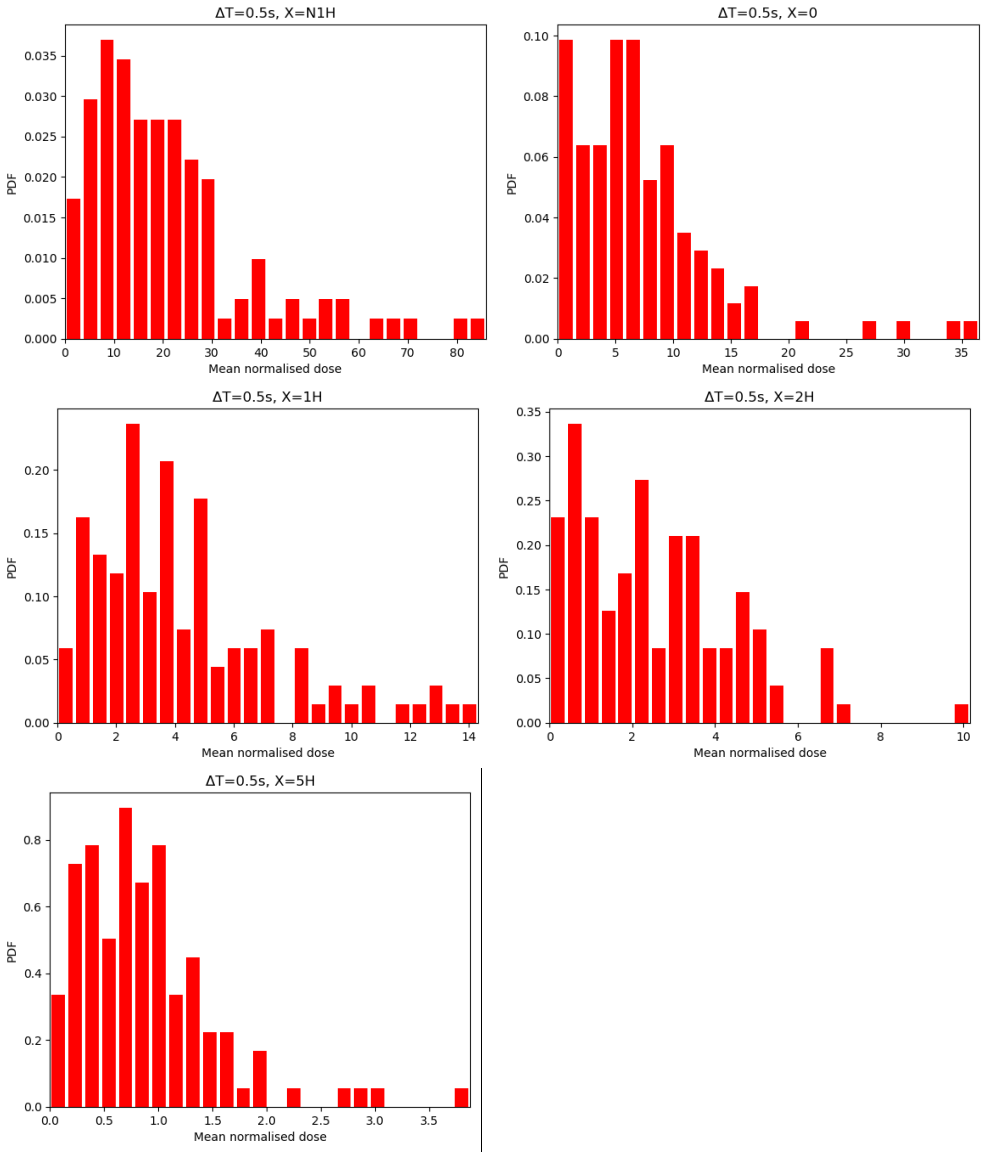

Figure 36: Probability density function for mean dose from release R4 puffs at different downwind locations.

The effect of changing the puff release time is shown in Figure 37 which shows the PDFs of normalised dose at $1H$. A zero or very low dose is much more likely for shorter puff release times as the puff themselves are smaller. A much larger range in normalised dose values is also seen for the shorter puff releases. It should be noted that these values are normalised by the puff release time, Δt (see equation 3). Therefore, the range in absolute dose values is not greater for short dose releases, rather it is the extent of the range relative to the mean that is greater. For longer puff

release times the PDF is much narrower reflecting a much smaller range in possible normalised dose.

These distributions highlight the difficulty in modelling puff releases at these scales; the shorter the release time, or the closer to the release, the greater the uncertainty.

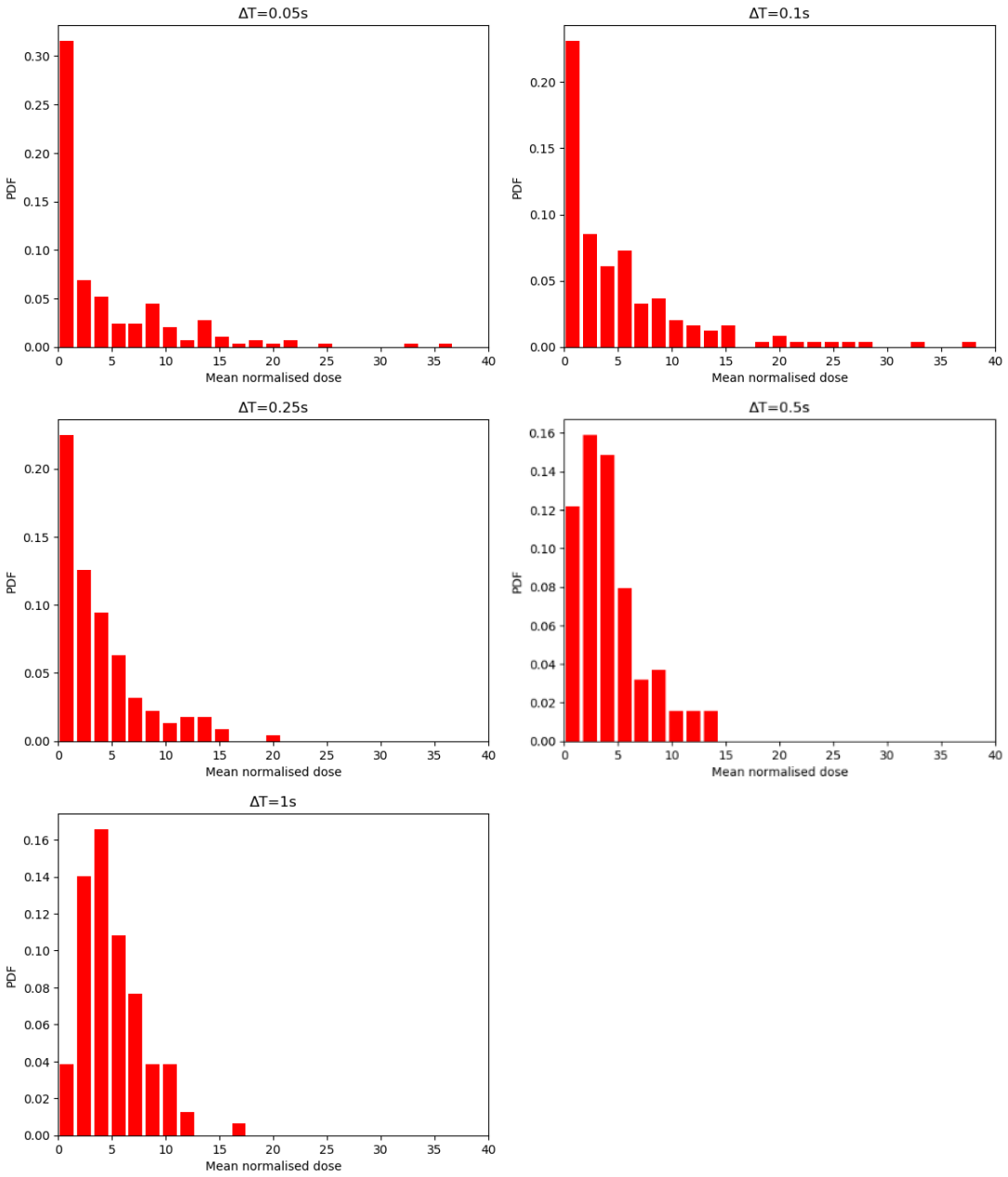

Figure 37: Probability density function for mean dose from all Z_s/H=4/3 wind tunnel puffs at$X/H = 1$ for different puff release times, Δt.

6.4. Mean dose and mean concentrations

Normalising the mean dose for the different puff ensembles using equation 3 leads to a value that is independent of release time. This is evident from the distributions shown in Figure 37, where the shape and range varies about a mean that is roughly constant for varying release times. In Table 6 the values of normalised mean dose are presented for different puff durations in the wind tunnel. The mean value of χ was 1.91 with a coefficient of variation of 2.9%, which indicated that the dose per puff scaled linearly with puff release duration.

Table 6: Normalised dimensionless concentration, χ, at plume centreline location with puff duration Δt for release R2, normal incidence to cube, X/H=1.

Δt (s)	0.05	0.1	0.25	0.5	1.0
χ	1.97	1.95	1.83	1.93	1.87

Further, the normalised mean dose was seen to be equal to the normalised mean concentration (equation 2) for a continuous release when an equivalent mass flow rate, q_s, is assumed. Figure 38 shows the normalised mean dose at various downwind locations and puff release times against the normalised mean concentration for a continuous release. The mean dose for puff ensembles can therefore be approximated from the mean concentration from a continuous release with equivalent q_s. What follows is that the expected variation from the mean value of χ can be described statistically.

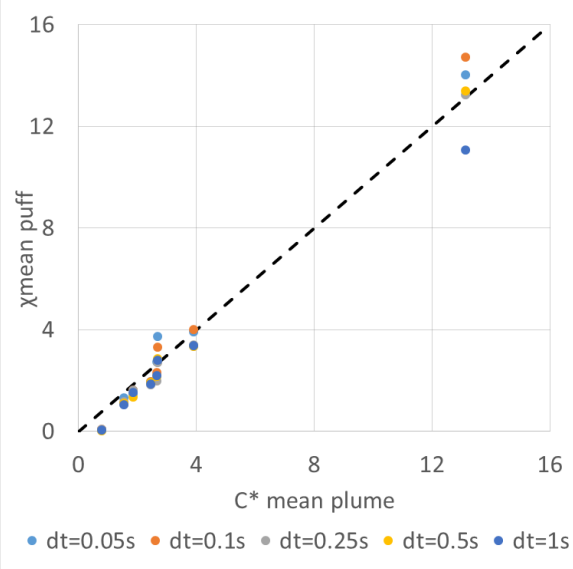

Figure 38: Normalised mean puff dose against normalised mean plume concentration for release R2. The black line indicates the x=y line.

6.5. Peak-to-mean ratios

Where reasonable estimates of the mean dose or mean concentrations are available, peak-to-mean ratios can be used to provide quick estimates of the peak dose or concentrations for given puff release times (e.g. Singer 1961, Santos et al. 2009). Here we use the 95th percentile to represent the "peak" dose or concentrations. Similarly the ratio of the standard deviation to the mean, or the

Coefficient of Variance (CV), can be applied to estimate the variance in dose about the mean. The CV and peak-to-mean ratios were seen to be dependent on release height, building orientation and, to some degree, the downwind measurement location. However, despite the complexity of the behaviour of puff ensembles, the variance in the CV and peak-to-mean ratios was seen to be sufficiently small that "rule-of-thumb" curves could be fitted to the data. Such curves could be used to provide quick, crude estimates of the variation in dose or concentrations expected about the mean for a neutral boundary layer case. However, it should be noted that additional factors not accounted for in this report, such as release diameter, could have a considerable effect on these ratios.

Figure 39 shows the coefficient of variation against the ratio of puff length scale to building height (*PLS/H*) for building orientations for (a) the lower release R2 and (b) the higher release R4 for each downwind location. The *PLS/H* is used as a non-dimensional puff release time and is given by:

$$\frac{PLS}{H} = \frac{U_{ref}\Delta t}{H}. \qquad (4)$$

The PLS represents to the initial length of the puff at the end of the release time release time Δt at a given reference height (1m in the wind tunnel, corresponding to a distance of 100m in these simulations). Expressed in this way *PLS/H* represents a dimensionless length scale for a puff release that may be generalised.

Generally, lower variance about the mean was seen for the lower release as compared to the higher release. This is likely partly due to the smaller turbulent length scales near the ground. Smaller eddies lead to a mixing of the puff with the surrounding air, whereas larger eddies advect the entire puff along a meandering path. The greater influence of the building on the lower release also results in increased mixing of the puff or plume.

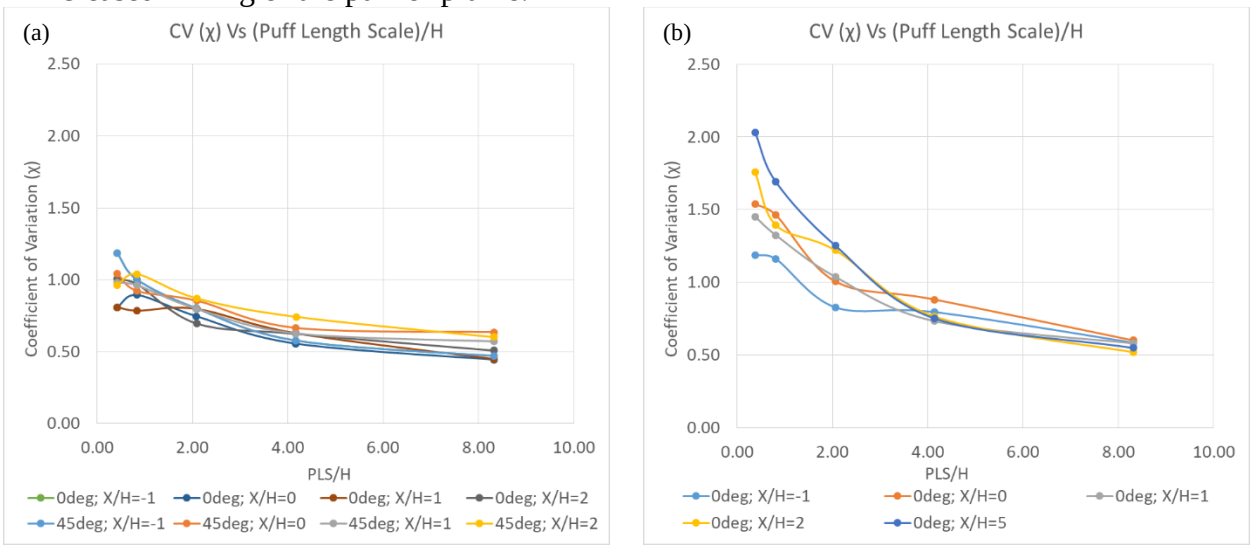

Figure 39: Coefficient of variation against PLS/H for different building orientations and downwind locations for (a) R2 release ($Z_s/H = 1/4$) and (b) R4 release ($Z_s/H = 4/3$).

Figure 40 (a) shows the coefficient of variation against puff length scale over building height for both release locations and building orientations. These curves represent the average CV values

across each downwind location (-1*H*, 0*H*, 1*H*, 2*H*, 5*H*). The difference between the two release positions is particularly pronounced for the shorter puff release times (or *PLS/H*). However, for the 45 degree case around the *Y*+ side of the building a higher variance was seen relative to the other lower release paths. This is likely due to a small asymmetry in the wind tunnel setup leading to the lower mean concentration path around the *Y*+ side of the building and therefore higher CV values (as CV=standard deviation/mean).

The higher release, R4, which is dispersed above the roof of the building, showed similar behaviour to the no building case which is also shown.

Figure 40 (b) shows the best fit curves for the CV and 95th percentile/mean ratio for all release locations, building orientations and measured locations. The error bars represent the standard deviation. These "rule-of-thumb" curves can be used to provide a quick estimate of peak dose given the mean dose of an ensemble of puff releases.

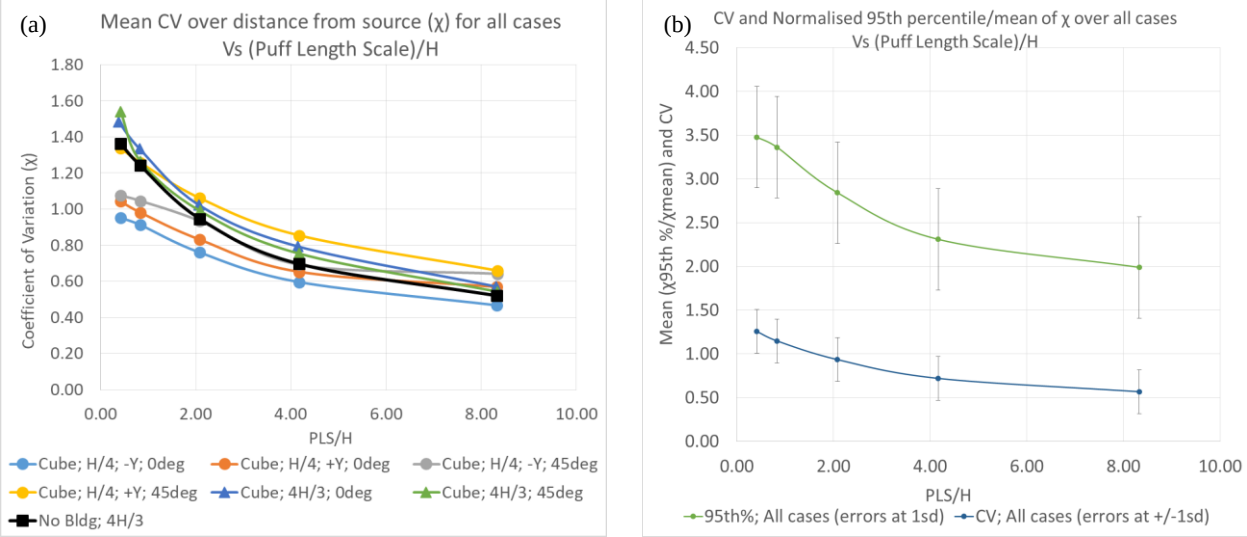

Figure 40: (a) Average coefficient of variation for all downwind locations against PLS/H for different building orientations and release locations and (b) "rule of thumb" best-fit curves for the 95th percentile/mean and CV/mean ratios against PLS/H. Error bars indicate the standard deviation across all cases and all downwind locations.

6.6.ADMS Fluctuations module

6.6.1. Continuous releases

For continuous releases the ADMS fluctuations module calculates the fluctuations of concentration within a plume over timescales shorter than the main averaging time. In addition to calculating a sigma value, percentiles or exceedances of specific values can be output allowing for a probability distribution of the concentrations to be determined. For the wind tunnel, measurements were made at a high sampling rate (a sampling interval of 0.0025s) over a longer period. The overall average of these measurements is taken to be the mean concentration, however we can use these raw measurements to determine a probability distribution for the concentrations over any shorter timescale.

For a continuous release we have two time series measurements from the wind tunnel. For these the source and measurement height is $Z/H = 4/3$ (i.e. source R4) and the downstream measurements are equivalent to the -1*H* and 1*H* locations when a building is included. This setup was replicated within ADMS accounting for the change in scale. The normalised mean concentration for the two cases for each of the wind tunnel and ADMS are given in the table.

Table 7: Comparison of mean concentration values for ADMS and wind tunnel results in the undisturbed boundary layer.

	Wind Tunnel	ADMS
-1*H*	22.6	19.2
1*H*	4.2	3.7

To calculate a PDF from the wind tunnel data, the raw data was taken (0.0025 s sampling interval giving 12,000 measurements) and sorted into order from lowest to highest. This was then plotted against position in the list, with the lowest value representing the 0th percentile and the highest representing the 100th percentile. With a large number of measurements this gives a good indication of the probability distribution. The fluctuations module in ADMS was used with an averaging time of 0.25 s to output data to compare against these results. Each of the percentiles from the 5th to the 100th is output in intervals of 5. To allow for comparison of the shape of the distribution between the different downwind distances the percentile values are normalised by the mean concentration at that location.

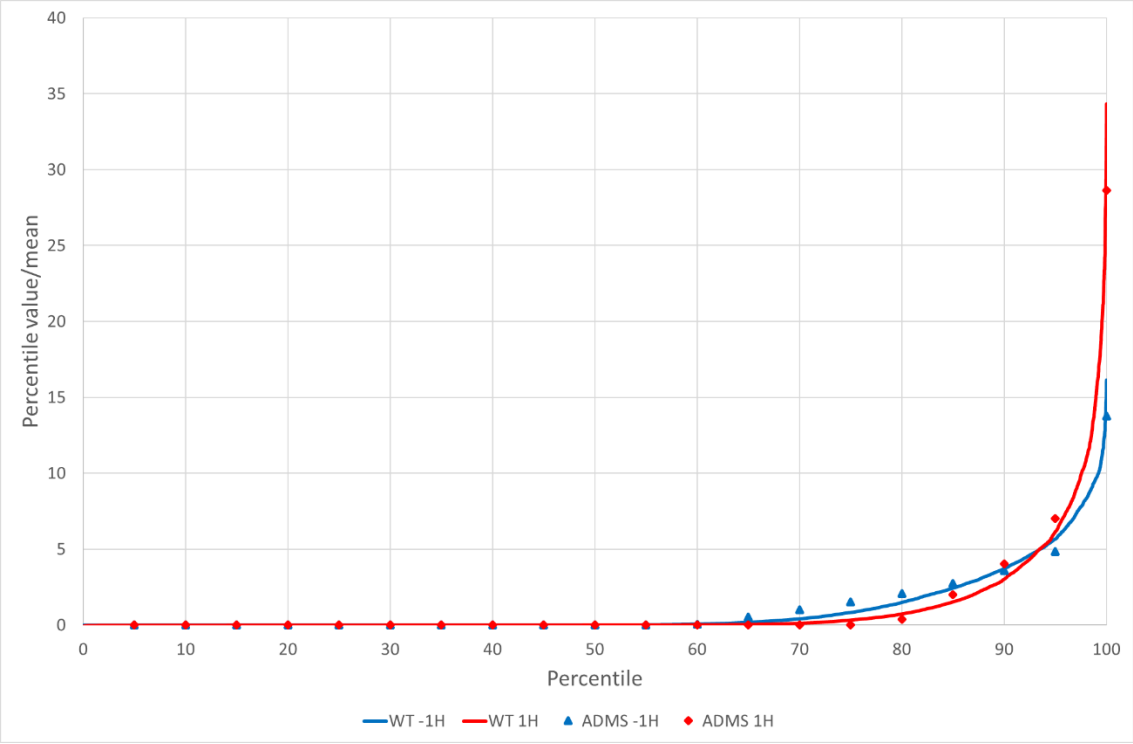

Figure 41: Percentile values for ADMS (symbols) and wind tunnel (solid lines) at downstream locations -1H (blue) and 1H (red).

Figure 41 shows the wind tunnel and ADMS results. The wind tunnel results are represented by the solid lines and the ADMS results by the symbols. The different colours represent the different distances downstream. We can see from the plot that there is a good agreement between ADMS and the wind tunnel results. For both downstream distances near zero concentrations are seen for

over half of the distribution with a rapid climb to the peak at the 100th percentile. The further downstream output point has a higher peak-to-mean ratio than the closer point indicating that the effects of plume meander are more important than plume spread for this case.

The raw data from the wind tunnel can also be used to calculate the probability distribution for longer time periods by averaging over several consecutive data points from the raw data. This can be done in two ways, either using a rolling average or using discrete windows within the data set. A rolling average gives more data points but they are not independent of each other. Two further averaging times are considered here, 0.025 s and 0.25 s. The table shows the number of data points in each measurement set.

Table 8: Number of data points for the different averaging times.

Averaging time (s)	Averaging type	Number of data points
0.0025	Raw	12,000
0.025	Rolling	11,991
0.025	Discrete windows	1,200
0.25	Rolling	11,901
0.25	Discrete windows	120

Figure 42 shows the wind tunnel results for one output point for the three averaging times with both averaging methods plotted for the longer averaging times. We can see from this that as the averaging time increases the high percentiles decrease whereas the lower percentiles increase. We can also see from this graph that in order to capture the behaviour well at the highest percentiles a hundred measurements is insufficient in this case.

These results can also be compared to the ADMS fluctuations module using averaging times of 2.5 s and 25 s for the 0.025 s and 0.25 s cases respectively. As we can see from the plots in Figure 43 and Figure 44 there is again good agreement between ADMS and the wind tunnel measurements.

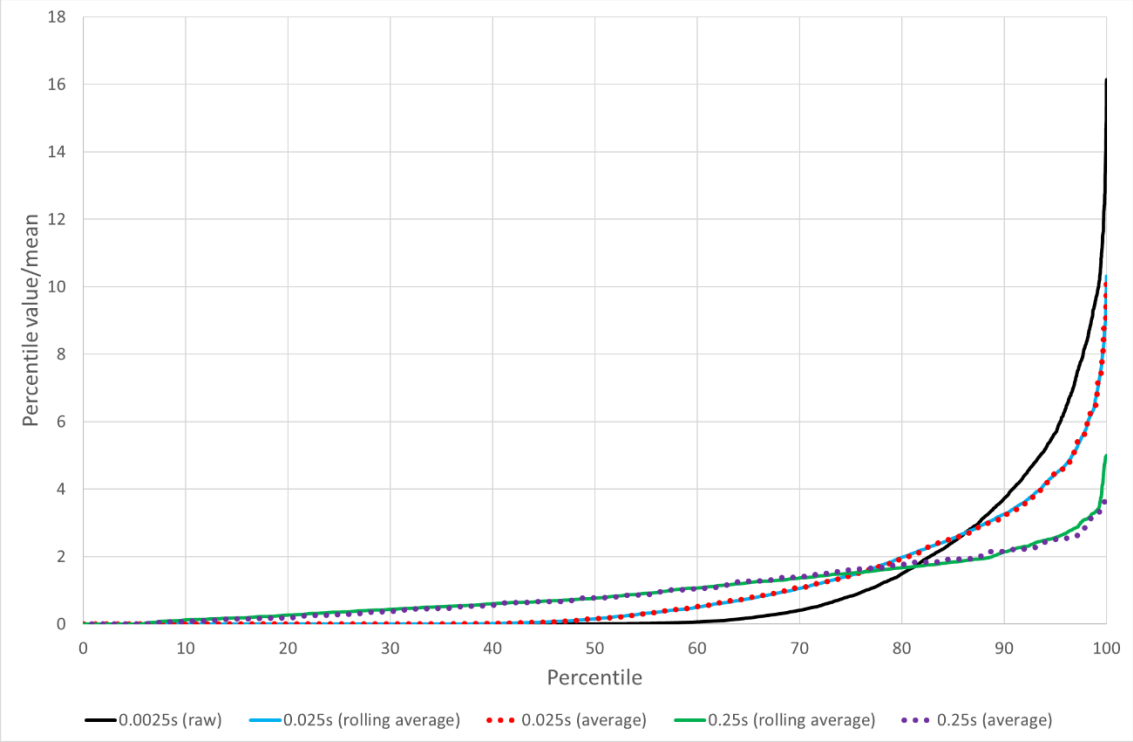

Figure 42: Comparison of wind tunnel values at -1H location for different averaging times.

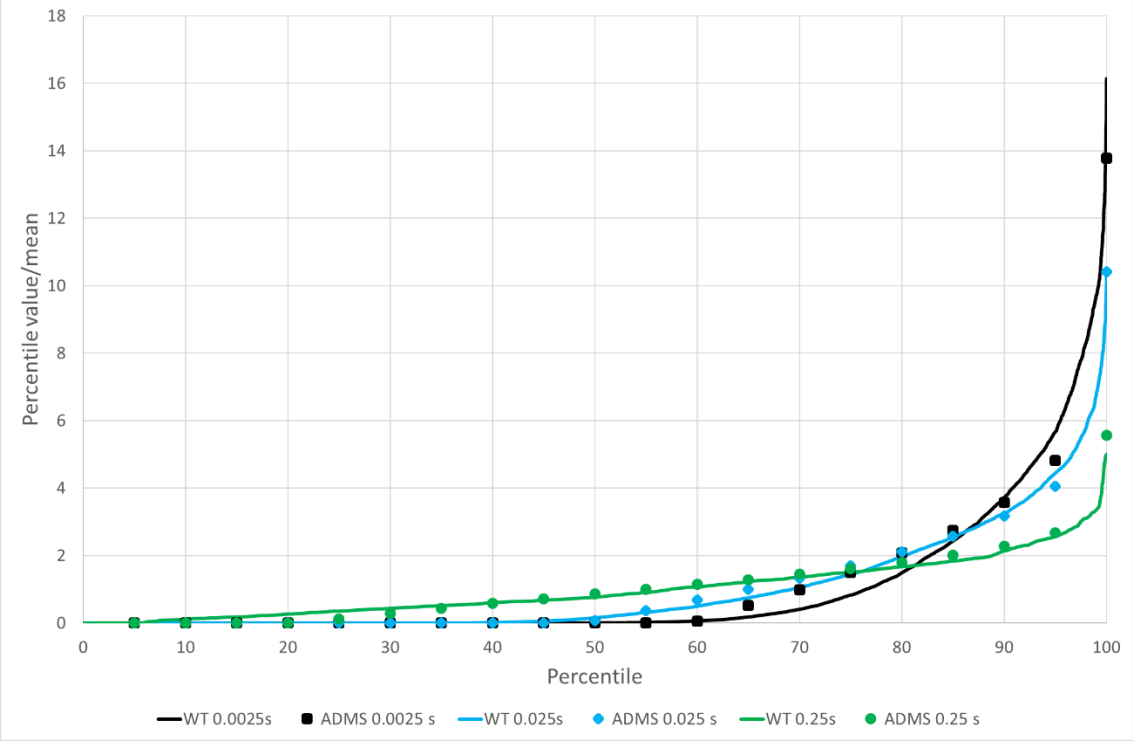

Figure 43: Comparison of ADMS and wind tunnel results at -1H location

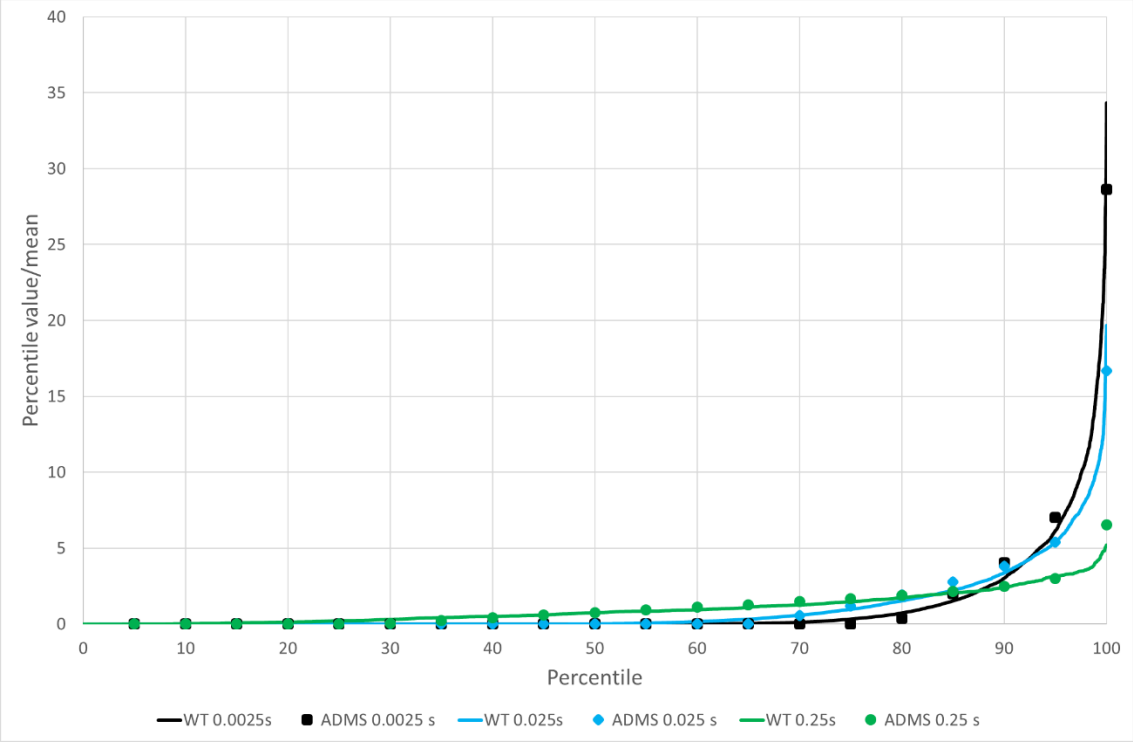

Figure 44: Comparison of ADMS and wind tunnel results at 1H location

6.6.2. Puff releases

For puff releases the variation in dose can be compared between the wind tunnel measurements and the ADMS fluctuations module. In the wind tunnel a series of experiments were carried out for a range of release times for the puff. For each release time around 100 experiments were carried out. For ADMS both the fluctuations and the puff dose modules were used. As the variation in total puff dose is being calculated no additional averaging time is required for the fluctuations module.

The figures show a comparison between ADMS and the wind tunnel data at the different downstream locations for the different puff release times. When comparing the results it is important to remember that there are only around 100 puff releases in the wind tunnel cases so the highest percentile values will be under predicted. Comparing the results we can see that we get good agreement between ADMS and the wind tunnel and that the results show that as expected the variation reduces the longer the release time of the puff.

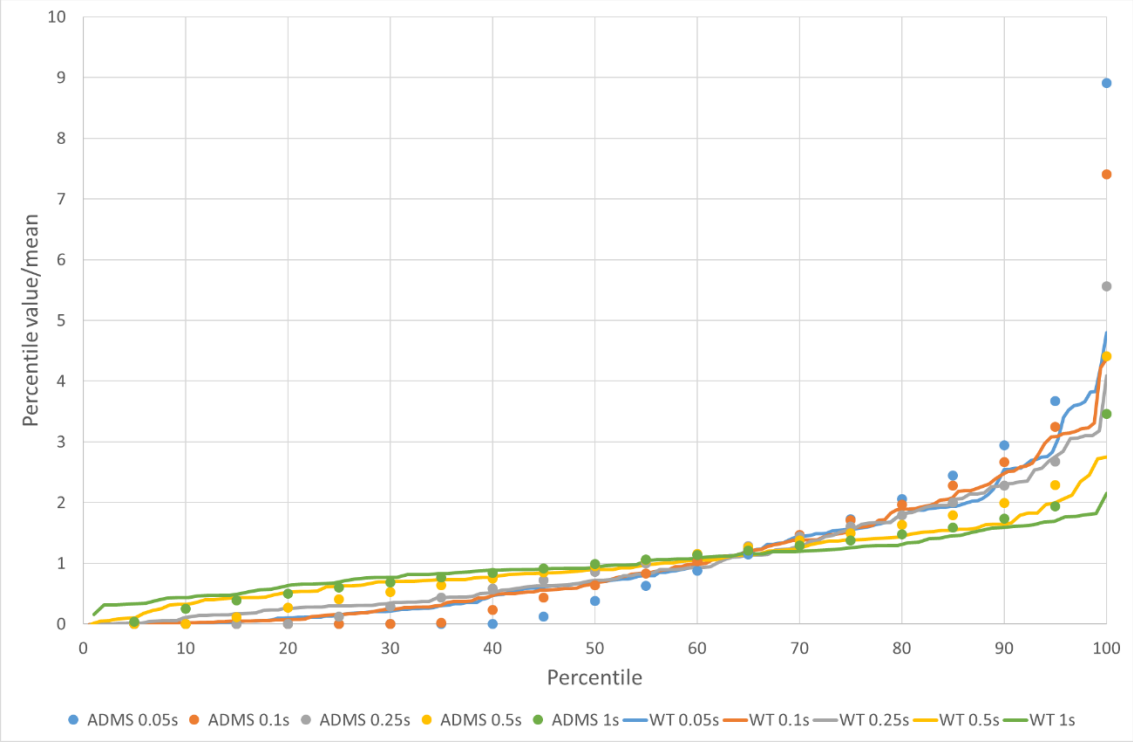

Figure 45: Comparison of ADMS and wind tunnel results for normalised puff dose at -1H location.

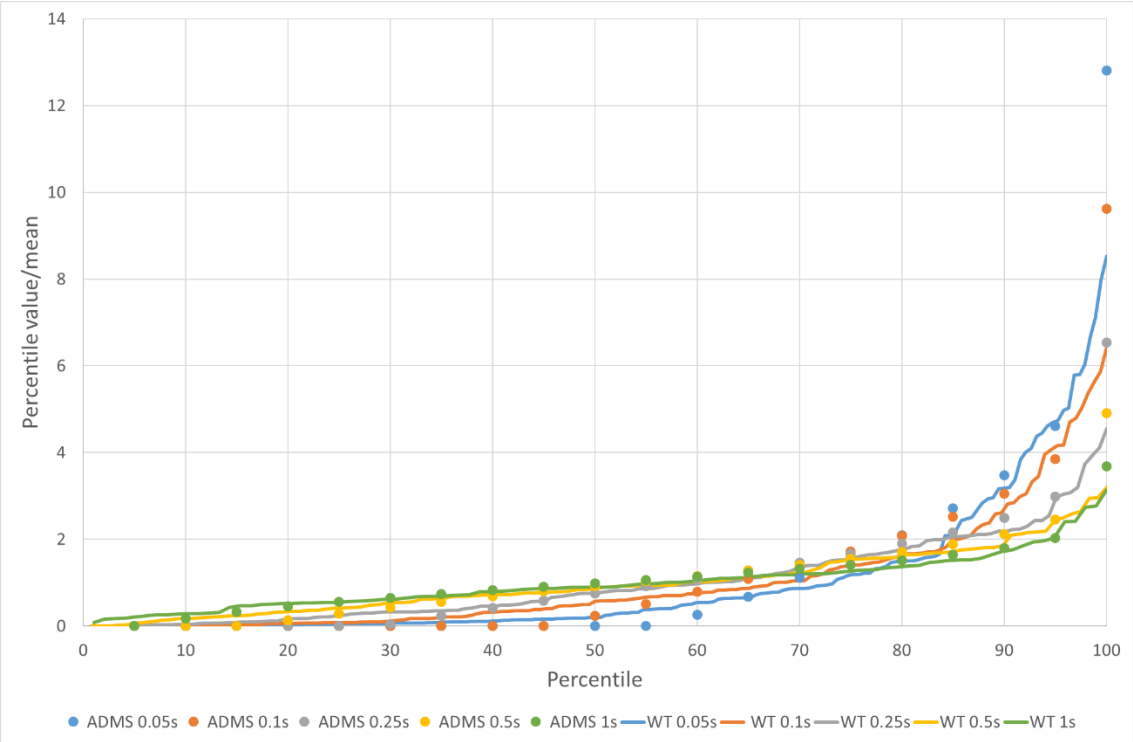

Figure 46: Comparison of ADMS and wind tunnel results for normalised puff dose at 1H location.

7. Discussion

7.1. Mean concentrations

The mean plume derived by ADMS tended to be wider than that seen in the wind tunnel (Figure 12 (a)). That is the Gaussian plume concentrations are lower at the plume centreline relative to those of the wind tunnel, while being higher after a certain distance away from the centreline. This was seen to be true both when flow profiles derived by the ADMS meteorology module were used, and when the wind tunnel flow profiles were specified directly. This is perhaps unsurprising as the Gaussian plume model is derived empirically from tracer releases in the "real world" atmosphere. In the real atmosphere, changes in the wind speed and direction, large scale atmospheric eddies and heterogeneous surface roughness can all play a part in increasing the plume spread – although a term accounting for additional plume spread due to large scale changes in wind direction was turned off for these ADMS simulations. These aspects are not accounted for within the wind tunnel, which is necessarily a more controlled environment with a fixed wind direction and the larger scale eddies are limited by the dimensions of the tunnel. However, the differences in concentration levels between the two are typical of those seen in previous comparisons (e.g. Robins 1978, Higson and Griffiths 1994). Were the additional plume spread due to large scale variations in wind direction included in the ADMS calculations, the plume would be even wider and therefore the effect of the building would be less significant.

It is evident from the comparisons in this report that the ADMS building module does not capture some important dispersion features for low releases upwind of a building. This includes the widening of the plume, both in the horizontal and vertical directions, by the building as seen in Figure 13 and Figure 14. This is relevant for emergency response as often identifying where any level of exposure is likely is as important as estimating the degree of exposure. This is also relevant within the context of building ventilation and assessing the susceptibility of building occupants to outdoor releases. The model is currently not able to capture the distribution of concentrations across the upwind building façade.

The effect of the horseshoe vortex at the base of the building is seen from both the wind tunnel and LES simulations to be important for both the near-field and far-field dispersion of the lower release plume, R2. For a low release, the vortex entrains the plume in front of the building, which is then dispersed within the vortex around both sides of the base of the building. This means that the plume splits, forming a two-plume dispersion pattern around and downwind of the building. At large distances downwind these two plumes will again resemble a single plume as they continue to widen, however for the distances considered in this report (up to 120m, 5H, downwind), two distinct plume centrelines were evident in all cases other than the unstable boundary layer case simulated using LES (Figure 31). This plume splitting and two-plume structure is not explicitly considered by the ADMS building module. Upwind and to the sides of the building, ADMS considers the plume to be equivalent to an undisturbed plume (i.e. with no building effects). Once downwind, this undisturbed plume continues, while a well-mixed model is used to represent the near-wake and a second plume is formed from this region. This can lead to a large underestimation of the concentrations at ground level near the building, both within and either side of the recirculation region, and further downwind of the building. At 0H, at the equivalent location of the maximum mean concentrations in the wind tunnel, the ADMS concentrations are lower by a factor of 10. Taking the maximum mean concentrations for ADMS at 0H, which occur at either side of

the building (at Y=$\pm H/2$), the ADMS concentrations are a factor of 2 lower than the maximum mean concentrations in the wind tunnel. For the lower release, R2, a close agreement was found between the wind tunnel maximum mean concentrations in the presence of a building and the ADMS maximum mean concentrations with no building at any given downwind distance. For the lower release the undisturbed plume may give a better estimate of the maximum ground level concentrations at any given downwind distance in the presence of a building when the source is upstream of the building.

The significance of the horseshoe vortex and its distance downwind is heavily dependent on the atmospheric stability. For stable and neutral boundary layers where there is no buoyancy enhanced vertical mixing, these distances are large, >5*H*. For the unstable case these distances are smaller due to increased vertical mixing. Large scale vertical motions within the atmosphere seen during unstable conditions are also likely to disturb the building flow features. Despite this, the effect of the horseshoe vortex was still visible for the unstable LES simulations of the lower release.

Gaussian plume models, such as ADMS and other Gaussian plume building modules such as AERMOD-PRIME, which are similar in concept using a two-plume approach, could be modified to follow a four-plume approach for low sources upwind of a building. A single plume would be used initially, and this would then split into 3 plumes as it approached the building, representing the flow over and around the building. Downwind of the building these plumes would be joined by a fourth component representing the dispersion from the near-wake. The weighting between the plumes going around and over the building could depend on the atmospheric stability as well as the relative plume/building locations and building shape. The empirical information needed to optimise such a development is, however, rather scarce.

ADMS's method of representing oblique buildings and buildings with complex geometries as a normal facing building with an equivalent frontal area and enhanced downwash seems appropriate. For the higher release location, this method successfully accounted for the increased downwash of the plume into the wake region of the building for building orientations with a larger frontal area, such as the 45 degree case. For the different building geometries considered in this report using LES modelling (45 degree building, 30 degree building, pitched roof), a maximum difference of up to 60% was seen in the mean concentrations downwind of the building. The largest difference was seen for the lower release between the normal facing building and the 30 degree building and was primarily due to the asymmetry of the 30 degree building about the *X*-*Z* plane. This asymmetry meant that the source lay to one side of the stagnation streamline, leading to the plume passing around one side of the building more frequently than the other and therefore resulting in higher time averaged concentrations to one side of the building. Any asymmetry in the building configuration relative to the approach flow is likely to cause similar underestimations of maximum mean concentrations. However, within the context of all other uncertainties involved for these problems this is likely an acceptable level of uncertainty.

Multiple downwind buildings were not considered in this report. However, the approximation made by the ADMS building module of multiple buildings as a single, effective block is likely to be problematic at the small scales considered here. Firstly, this approach will not provide an estimate of the concentrations between the buildings. Secondly, a complex array of buildings may lead to areas of recirculating or even stagnant air where plume material could remain for some

time after an emission has ceased. The possibility of such occurrences should be noted. However, identifying them is likely to require more expensive modelling methods such as CFD or wind tunnel experiments. Over larger scales, Gaussian plume models are routinely used to estimate concentrations within urban areas without considering the dispersion around individual buildings in any detail. Over the short distances considered in this report (<100m), it is likely that the undisturbed plume (i.e. no building case) can provide sufficiently accurate estimates of the maximum mean concentration expected at any given downwind distance, as was found for the lower release upwind of a single building. However, the undisturbed plume cannot be relied upon to provide accurate estimates of plume spread, or the locations of the plume maxima, in the presence of buildings.

A case was considered where an additional building was placed at a distance of 5*H* upwind of the main building using LES. The concentrations downwind of the main building were significantly lower than for the other cases with no building upwind of the source. Generally both mean and 95th percentile concentrations were a factor of two lower (Table 3 and Table 4). This was due to the additional mixing caused by the turbulence generated by the upwind building. This highlights the sensitivity of the concentrations to the approach flow statistics. Large uncertainties lie within the approximation of the boundary layer profiles given by the ADMS meteorology module, derived from Monin-Obukhov similarity theory. These flow profiles represent the flow above the surface roughness of the ground. In the case of urban areas, this "roughness" consists of the buildings and flow conditions which are likely to be highly variable both in space and time over the scales considered (<100m, <1h). At these scales, for cases where buildings lie upwind of the release, their impact on the flow profiles, and therefore dispersion, is likely to be as important as that of the downwind (main) building.

It is important to stress that due to their relative simplicity, Gaussian plume models cannot be expected to provide highly accurate estimates of concentrations or dose for sources close to buildings, regardless of the time and length scales involved. Rather, what is required from the model is reasonably representative estimates (typically within a factor of 2) which can be calculated quickly and inexpensively. While ADMS generally gave lower maximum mean concentrations to those measured in the wind tunnel or calculated using LES, the factor of underestimation was usually small and may in part be due to the ADMS parameterisations being applicable to the real atmosphere where larger scales are important. When using Gaussian plume models an underestimation of up to a factor two is within the expected level of uncertainty and should be accounted for appropriately.

7.2. Fluctuations and puff releases

Puff release experiments in the wind tunnel demonstrated both the complexity of dispersion within atmospheric flows, which is enhanced by the presence of a building, and the challenge involved in modelling a sufficiently large ensemble of releases with sufficient time resolution. The number of puffs considered within the wind tunnel varied from 90 to 190, depending on the puff release duration. Even these numbers were not sufficient to provide a well-converged probability distribution of puff dose, although the parameters that can be used to describe the distribution, namely the CV and 95th percentile, were relatively robust. Due to the long run times of LES simulations the number of puffs simulated numerically was around 30. This proved an insufficient number to provide suitably robust estimates of dose statistics and are therefore not presented in

this report. This highlights an inherent difficulty in modelling such release ensembles using deterministic models, as simulating a sufficient number of releases is always likely to be very resource intensive. The Gaussian plume model holds an advantage in this respect, being a statistical model. However, the accuracy of the Gaussian plume model in estimating the distribution in dose and peak dose, or peak concentration, will depend on the same assumptions and approximations as used to estimate mean concentrations for a continuous release. Some of the limitations of these assumptions have already been discussed.

The concentration and dose from a puff are both proportional to the total amount released, Q_s. If the release derives from a steady emission, q_s, over a period Δt, then $Q_s = q_s \Delta t$ and mean concentrations and doses are proportional to Δt. The normalised mean dose, using the release duration as the time scale, for an ensemble of puff releases can be shown to be the same as the normalised mean concentration in a continuous release (see Appendix 5). Therefore, a Gaussian plume calculation of mean concentrations in a continuous plume can be used to estimate the mean dose for an ensemble of puff releases. Further, a comparison of peak-to-mean ratios of concentrations for continuous releases, using an averaging time equal to the puff release duration, and those of puff dose for release ensembles showed that ratios derived for the continuous release concentrations could be used to provide a reasonable estimate of peak dose, represented in this case by the 95th percentile.

For the open terrain case, it is possible to use the ADMS Fluctuations module to estimate the distribution of puff dose expected from an ensemble of puff releases. Comparisons between the wind tunnel and the Fluctuations module confirmed its good performance at these scales. The Fluctuations module can be used for all boundary layer stabilities.

It was observed that as the building led to increased mixing and spreading of the plume or puff, peak-to-mean ratios in the presence of the building tended to be lower than those for an undisturbed release. Therefore, estimating peak concentrations or dose assuming an undisturbed flow (i.e. no buildings) is likely to provide conservative estimates of those in the presence of a building.

“Rule of thumb” peak-to-mean ratios were estimated for the release ensembles simulated in the wind tunnel; releases upwind of a normal building and an oblique building. These could be used to provide a quick estimate of peak dose for neutral boundary layer scenarios. However, it should be noted that these ratios may differ depending on factors not considered in this report such as source size, or release density and temperature. Further, for stable or unstable boundary layers, the peak-to-mean ratios are likely to be different from those for the neutral case.

7.3. Relevance of results to simpler Gaussian plume models

For a near-ground release upwind of a building, the R91 model (Clarke, 1979), which does not have a building model, could be used to give reasonable estimates of the maximum concentrations at any given downwind location. However, the model will not provide an accurate estimate of the plume dimensions which may be significantly increased by the presence of the building, or the location of the two plume centrelines formed as the plume splits at the building face. In the case of an elevated release upwind of a building, the R91 model is likely to significantly underestimate ground-level concentrations as it does not account for the downwash effect.

For the elevated release case, the R157 model (Jones, 1983) is likely to be more appropriate. The R157 model attempts to account for the presence of a building. For elevated emissions the model is based on similar assumptions to those behind the ADMS building module; mainly concerned with stack downwash effect and a two-plume model downwind of the building. As the ADMS building model was found to be effective at representing the elevated release in this study, the R157 model is likely to provide reasonable ground-level estimates in this case.

However, beyond stating that the maximum concentration at the upwind face of the building can be taken to be equal to the maximum concentration for an undisturbed flow, the R157 model does not provide a method to simulate the dispersion of upwind releases near the ground. While the horseshoe vortex is described in the R157 document, its effect on downwind dispersion is not described. As seen from the wind tunnel and LES simulations in this study, the use of a two-plume model downwind of the building is likely to lead to a significant underestimation of concentrations (see Table 2). For lower releases it is therefore more appropriate to assume the no building case to approximate the maximum concentrations at any given downwind distance. Allowances should be made for the likely widening of the plume due to the presence of a building in addition to the two plume centrelines that are likely to form, however these effects are not accounted for by the R157 model, nor the ADMS building model or AERMOD-PRIME for that matter.

Virtual source models have been used to treat low-level emissions near buildings by providing increased plume spread, either by moving the source upwind or by adding a term to represent additional spread. Such models need to be carefully tuned for any particular application, but were found to be acceptably accurate for estimating mean concentrations (e.g. see Foster and Robins, 1985).

It should also be noted that the concentrations estimated by the R91 and R157 models are representative of converged time-averaged concentrations. When considering time periods shorter than the time required to reach convergence, the concentrations will vary about the converged mean. In Section 6.2 the time required to reach a steady average for concentrations near a building in the wind tunnel was 15 seconds, which is equivalent to 25 minutes at full scale. For the unstable case simulated using LES, convergence was still not reached after 1 hour 30 minutes.

7.4. Discussion on methods

The focus of this study was to establish the limitations of Gaussian plume models at short length and time scales. However, the suitability of any model depends to some extent on the available alternatives. While there are alternatives beyond LES and wind tunnel modelling, such as Lagrangian models, a discussion of the methods used for this study is given here.

7.4.1. Wind tunnel

Wind tunnel modelling is a well-established method for simulating atmospheric flows and dispersion under neutral boundary conditions. It is possible to achieve high frequency sampled measurements within the wind tunnel. This is particularly important when studying fluctuations in concentrations about the mean as short measurement times are required to resolve the peak concentrations. For the experiments performed in this report the FFID response time was 0.0025s at wind tunnel scale, which equates to 0.25s at full scale (1:100 scale, 2ms^{-1} reference wind speed

at both scales). A disadvantage of wind tunnel modelling is the scaling required between the model in the wind tunnel and the full scale. This is not a big problem for neutral boundary layers with sufficiently high wind speeds, however modelling stable and unstable boundary layers is a challenge at the wind tunnel scale. Regardless of the boundary layer stability, only statistically steady meteorological conditions are usually simulated.

Within the context of this study the wind tunnel results proved to be highly valuable. The automation of the experimental method allowed a large number of puffs to be simulated with fast time response measurements. While smooth distributions of puff dose were not achieved, sufficient numbers of puffs were simulated to provide robust estimates of the Coefficient of Variation and the 95th percentile dose leading to meaningful insights into the behaviour of puff release ensembles around buildings.

7.4.2. LES modelling

Some features of LES modelling proved particularly problematic in modelling puff releases. The long run times required and high resolution output desired for the LES simulations limited the number of puffs that could be modelled. Typically up to around 30 puffs were achieved for each simulation, which did not provide sufficiently converged statistics. Further, the variation in dose, particularly peak dose, for the elevated release, R4 ($Z_s/H = 4/3$), was seen to be significantly underestimated by the LES simulations relative to those in the wind tunnel. It is thought that this was partly due to an insufficiently fine mesh at this height. This issue can be addressed if more time and computational resources are made available.

Despite these issues the LES proved a highly valuable tool for the analysis within this report. The ability to easily run different configurations allowed a sensitivity analysis of various building geometries and orientations. The LES also provided the means to simulate stable and unstable boundary layers, providing valuable insight into the validity of the assumptions made for the neutral case for varying boundary layer stabilities.

8. Conclusions

The conclusions from this study are as follows:

- For the lower release R2, $Z_s/H = 1/4$ and $X_s/H = -2.5, Y_s/H = 0$, the ADMS Building module was found to give normalised mean concentrations at the plume centreline a factor two lower than those seen in the wind tunnel and LES simulations. When values were compared at the location of the plume centreline as measured in the wind tunnel the factor was significantly larger (a factor of 10) at locations near the building.
- Closer estimates of the plume centreline concentrations both upwind and downwind of a building for this upwind release could be achieved by assuming the centreline concentrations given by ADMS for an undisturbed plume, i.e. with no building. At short range, an undisturbed plume is likely to provide working estimates of the plume centreline concentrations in the presence of a building. However, the undisturbed plume will not

provide a suitable estimate of enhanced plume spread due to the presence of buildings or the location of the plume maxima.

- Much closer agreement was seen for the elevated release case for which the impact of the building on the plume is accounted for within the original design of the ADMS building module, e.g. the downwash of the plume into the building wake.
- The short duration puff releases were found to show that the dose received was proportional to release time: when normalised for release time a dimensionless dose value was obtained which could be readily compared between the different cases investigated. The mean value of normalised dose, χ, conforms to the time averaged concentration obtained from the Gaussian plume model.
- Presented as normalised values, the CV and 95th percentile of dose could be readily applied in order to produce simple estimates of the likely value for source conditions similar to those tested. The formulation of χ, and associated statistical descriptors, in terms of a non-dimensional concentration also enables the ready generalisation of the results in this report to different scenarios involving different wind speed, building heights and pollutant release rates. However, it should be noted that the puff statistics derived in this report from wind tunnel experiments do not account for the effect of some important factors such as release size, boundary layer stability and release density and temperature. These are not unimportant matters.
- The ADMS Fluctuations module was found to compare well with the wind tunnel data when modelling concentration percentiles for a continuous release in an undisturbed flow. Good agreement was also seen between the Fluctuations module and the puff ensembles, although the wind tunnel gave lower values for the highest percentiles due to the use of an insufficient number of puffs. The ADMS Fluctuations module cannot be used in conjunction with the ADMS Building module. However, the wind tunnel experiments showed that the presence of the building leads to lower peak concentrations due to an increased mixing of the plume or puff. Therefore, the Fluctuations module could be used to derive conservative estimates of the maximum likely peak concentration and peak dose in the presence of a building by assuming the peak values given by the Fluctuations module along the plume centreline for an undisturbed plume (i.e. no building). The degree of over-prediction could, however, be substantial.
- Finally, the work undertaken as part of this project highlights the challenge involved in modelling puff ensembles using deterministic models. A high number of releases are required in order to obtain robust estimates of the variation in dose. For the shortest release time considered here of 0.05s, roughly 190 releases were considered in the wind tunnel. This proved enough to provide meaningful estimates of the Coefficient of Variation and 95% percentiles of puff dose. However, a smooth probability distribution of puff dose was not achieved. Within the time constraints of the project the LES simulations achieved only 30 puff releases. This was not considered a sufficient number to provide an entirely meaningful analysis. In this regard, Gaussian plume models are naturally well suited for such problems, as statistical estimates of the variation in dose can be calculated very quickly, even if less precisely.

References

Apsley DD, 1988. A model for dispersion in the wake of large buildings, CEGB Report RD/L/3359/R88.

Aristodemou E, Bentham T, Pain C, Robins A, 2009. A comparison of mesh-adaptive LES with wind tunnel data for flow past buildings: mean flows and velocity fluctuations. Atmos. Environ. 43, 6238–6253.

Aristodemou E, Boganegra LM, Mottet L, Pavlidis D, Constantinou A, Pain C, Robins A, ApSimon H, 2018. How tall buildings affect turbulent air flows and dispersion of pollution within a neighbourhood. Environmental Pollution, 233, 782-796.

Bentham JHT, 2003. Microscale Modelling of Air Flow and Pollutant Dispersion in the Urban Environment. Ph.D. Thesis. Imperial College London.

Blocken B, Stathopoulos T, Carmeliet J, Hensen JLM, 2011. Application of computational fluid dynamics in building performance simulation for the outdoor environment: an overview, Journal of Building Performance Simulation, 4:2, 157-184, DOI: 10.1080/19401493.2010.513740

Castro IP, Robins AG, 1977. The flow around a surface-mounted cube in uniform and turbulent streams, J. Fluid Mechanics, 79(2), 305-335.

CERC, 2016, ADMS 5 User Guide, Version 5.2.

Clarke RH, 1979. The first report of a Working Group on Atmospheric Dispersion: a model for short and medium dispersion of radionuclides released to the atmosphere. NRPB-R91, Chilton, UK.

COST Action 732 – Best practice guideline for the CFD simulation of flows in the urban environment, May 2007.

EnFlo, 2020, Meteorological Wind Tunnel, www.surrey.ac.uk/mes/research/fluids/enflo

Foster PM, Robins AG, 1985. The effects of buildings on low-level atmospheric discharges. CEC Report EUR 9980 EN, 1985.

Griffiths RF, Megson LC, 1984. The effect of uncertainties in human toxic response on hazard range estimation for ammonia and chlorine, Atmospheric Environment, 18 (6), 1195-1206.

Griffiths RF, 1990. The use of probit expressions in the assessment of acute population impact of toxic releases. Journal of Loss Prevention in the Process Industries, 4, 49-57

Higson HL, Griffiths RF, 1994. Concentration measurements around an isolated building: A comparison between wind tunnel and field data. Atmospheric Environment, 28(11), 1827-1836.

Health Protection Agency, Smith JG, Simmonds, JR (eds), The Methodology for Assessing the Radiological Consequences of Routine Releases of Radionuclides to the Environment, Report HPA-RPD-058, Chilton, Didcot, Oxon, 2009 (ISBN 978-0-85951-651-8)

Hosker RP, 1984. Flow and diffusion near obstacles. In: D. Randerson, ed. Atmospheric Science and Power Production. Office of Scientific and Technical Information, United States Department of Energy

Hunt JCR, Kaimal JC, Gaynor JE, 1988. Eddy structure in the convective boundary layer – new measurements and new concepts. Q.J.R. Meteorol. Soc., 114: 827-858. doi:10.1002/qj.49711448202

Hunt JCR, Robins AG, 1982. A model for assessing dispersion of plumes from sources in the vicinity of cuboid shaped buildings. Proc. EUROMECH conference on surface mounted bluff bodies in turbulent boundary layers, Lisbon.

Jones JA, 1983. The fifth report of a Working Group on Atmospheric Dispersion: Models to Allow for the Effects of Coastal Sites, Plume Rise and Buildings on Dispersion of Radionuclides and Guidance on the Value of Deposition Velocity and Washout Coefficients. NRPB-R157, Chilton, UK.

Lilley DG, 1997. Fuel Release and Ignition Calculations. American Institute of Aeronautics and Astronautics.

Lilley DG, 2011. Explosions, Expulsion rate, Dispersion and Ignition of Released Fuels: A Review. 49th AIAA Aerospace Sciences Meeting including the New Horizons Forum and Aerospace Exposition.

Pavlidis D, Gorman G, Gomes J, Pain C, ApSimon H, 2010. Synthetic-Eddy Method for Urban Atmospheric Flow Modelling, Boundary-Layer Meteorology, 136, 285–299.

Robins AG, 1978. Plume dispersion from ground level sources in simulated atmospheric boundary layers. Atmospheric Environment, 12, 1033-1044.

Robins AG, McHugh CA, Carruthers DJ, 1997. Testing and evaluating the ADMS building effects module. International Journal of Environment and Pollution, 8, 708-717.

Santos JM, Griffiths RF, Reis NC, Mavroidis I, 2009. Experimental investigation of averaging time effects on building influenced atmospheric dispersion under different meteorology stability conditions. Building and Environment, 44, 1295-1305.

Singer IA, 1961. The relationship between peak and mean concentrations. Journal of Air Pollution Control Association, 11:7, 336-341.

Stathopoulos T, Hajra B, Bahloul A, 2008. Analytical Evaluation of Dispersion of Exhaust from Rooftop Stacks and Buildings, IRSST Report R-576.

Stocker J, Ellis A, Smith S, Carruthers D, Venkatram A, Dale W, Attree M, 2017. A review of dispersion modelling of agricultural emissions with non-point sources. International Journal of Environment and Pollution, 62(2-4) 247-263. DOI: 10.1504/IJEP.2017.089410.

Xie ZT, Hayden P, Wood CR, 2013. Large-eddy simulation of approaching-flow stratification on dispersion over arrays of buildings. Atmospheric Environment, 71, 64-74.

Appendix 1 – Neutral and stable dispersion parameters

The ADMS user guide (CERC, 2016) gives the vertical dispersion parameter, σ_z, for neutral or stable boundary layer stabilities as:

$$\sigma_z = \sigma_w t \left\{ \frac{1}{b^2} + \frac{N^2 t^2}{1+2Nt} \right\}^{-1/2},$$

where σ_w is the vertical component of turbulence and N is the buoyancy frequency and are calculated by ADMS' boundary layer parameterisation. t is the travel time from the source and b is a parameter given by:

$$b = \begin{cases} \dfrac{1 + 0.4u_* t/z_s}{1 + u_* t/z_s}, & \text{if } z_s/h \leq 0.05, \\ \left(1 - \dfrac{z_s/h - 0.05}{0.1}\right)\left(\dfrac{1 + (0.4u_*\, t)/z_s}{1 + (u_*\, t)/z_s}\right) + (z_s/h - 0.05)/0.1 & \text{if } 0.05 < z_s/h < 0.15, \\ 1, & \text{if } z_s/h > 0.15. \end{cases}$$

Here z_s is the height of the release, h is the boundary layer height and u_* is the friction velocity. The transverse dispersion parameter, σ_y, is given by:

$$\sigma_y^2 = {\sigma_y}_t^2 + \sigma_{y_w}^2,$$

where σ_{y_t} accounts for transverse spreading due to turbulence and is given by $\sigma_{y_t} = \sigma_v t(1 + (2.5u_*\, t)/h)^{-1/2}$. σ_{y_w} represents transverse spreading due to large scale variations, σ_θ, in the wind direction. For the short length and time scales considered in this report we assume that σ_θ (and therefore σ_{y_w}) is equal to zero.

Appendix 2 – ADMS Building model

Building properties

For each source and wind direction the building effects module determines equivalent idealised building parameters: building height, crosswind width, along-wind length and orientation. The idealised building that is created is orthogonal to the flow, the 'orientation' is a parameter used to define some aspects of roof flow and near-wake behaviour. For a single building the crosswind width, W_B, is calculated as the projected crosswind width of the actual building. The along-wind length, L_B, is the along-wind projection from the furthest upwind mid-face to the furthest downwind mid-face. Figure 47 shows the effective buildings calculated for a cube at a variety of orientations.

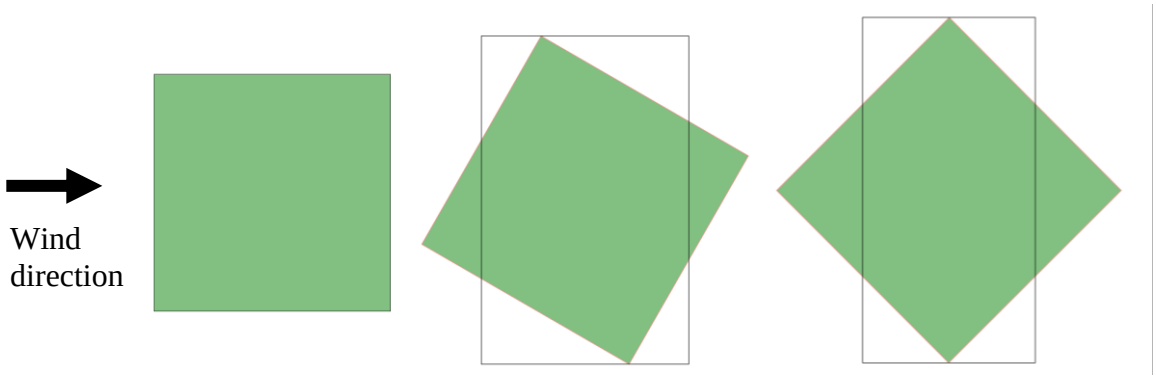

Figure 47: Input building (green square) and calculated effective building (black rectangle) for 3 different orientations of building (0º, 30º and 45º) to the wind (left to right).

In the case of multiple buildings, similar limits are applied using a subset of the input buildings which satisfy height and position criteria.

Flow field

The building-affected dispersion model is only used if the source lies within a 'buildings-affected' region, the size of which is calculated from the dimensions of the effective building. This region is subdivided, as shown in Figure 48, into the recirculating flow region **R**, wake **W**, and three 'external' sub-regions: **U** directly upwind, **A** the remainder of the perturbed flow around the building and **E** the region external to the wake. For convenience, **U**, **A** and **R** are lumped together as the 'near wake' and **W, E** as the 'main wake'.

The upwind boundary of the region is set on the assumption that building effects can be ignored if a plume's dimensions (evaluated at the upwind face) are significantly larger than the building dimensions. The vertical and crosswind limits are given by a modified '3 times rule' determined from wind tunnel studies.

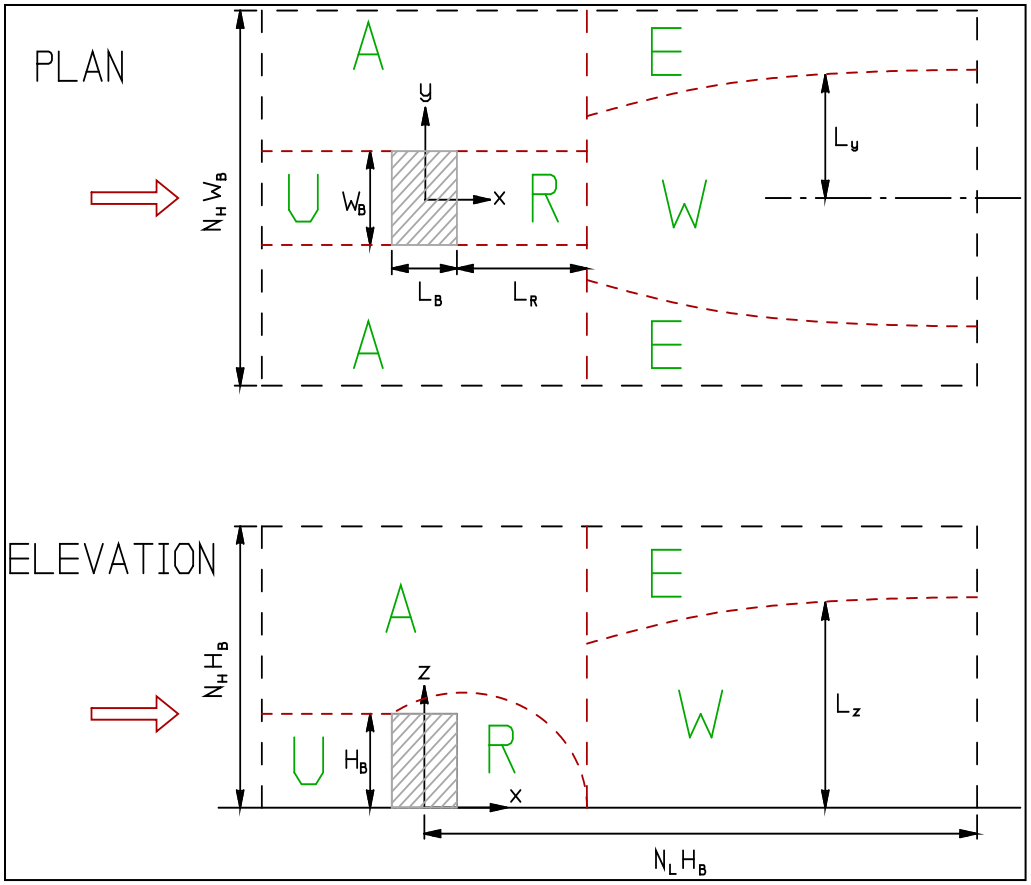

Figure 48: Regions of flow in the ADMS buildings module (CERC, 2016).

Recirculation region

The recirculating flow region **R** is modelled as a volume of uniform cross-section across the width of the building, as illustrated in Figure 49. It is formed from the shear layers separating from the leading or trailing edge of the roof and side walls, depending on whether the former reattach. Whether the flow reattaches depends on the relative length of the along-wind length of the effective building to its height and crosswind width.

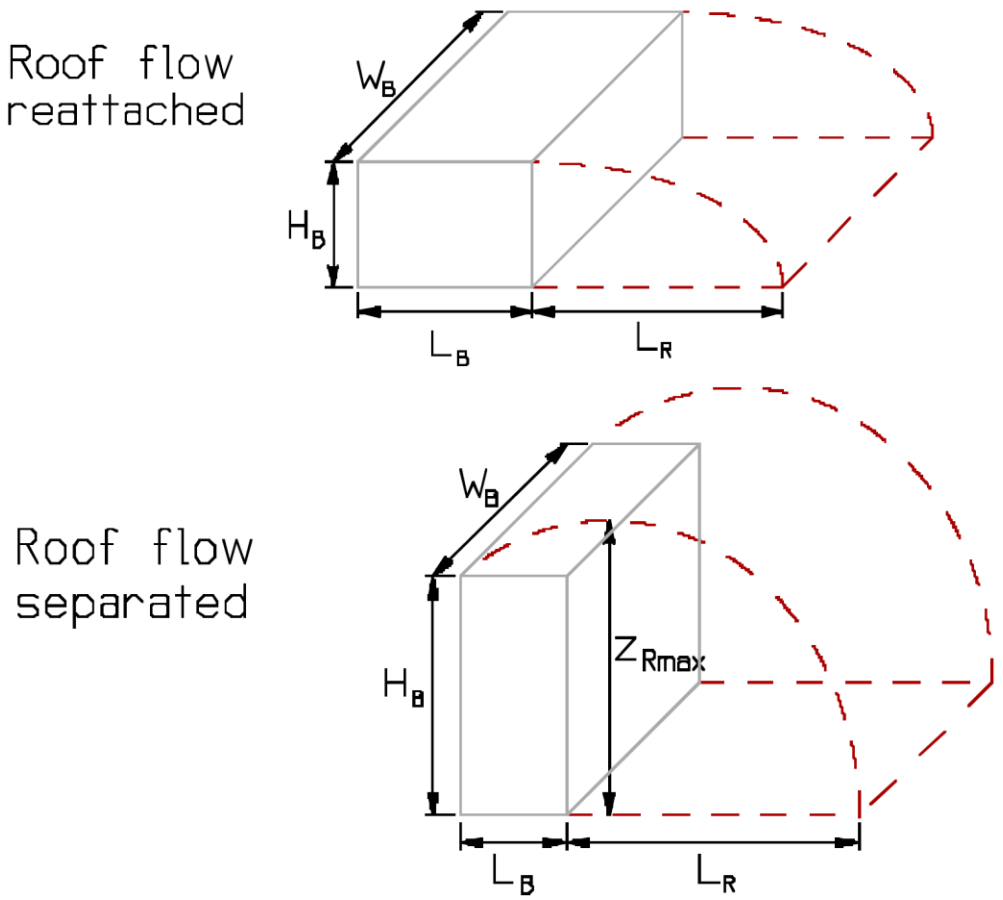

Figure 49: Recirculating flow region (CERC, 2016).

Near wake

Within the near wake a passive plume trajectory is horizontal for buildings normal to the flow. Otherwise the plume trajectory follows the boundary to **R** to an extent depending on source height and the orientation of the building.

This formulation is based on wind tunnel studies showing how plume heights and concentration fields just downwind of the recirculating region behind a block-shaped obstacle respond to changes in building orientation. These showed that the weakest effects arise when the building is normally aligned to the approach flow, and the strongest when 'diagonally' aligned.

Main wake

Downstream of the recirculating flow, in regions **W** and **E**, a small-deficit wake model is used to describe the perturbed mean flow. The model assumes self-preserving profiles, a uniform approach flow, and constant eddy-viscosities. While an analytical expression is used for the mean velocity field throughout regions **W** and **E**, turbulence levels are only enhanced by a bulk measure of the excess turbulence within the central wake region **W**. The limits of **W**, and the mean velocity deficit, which is required for the calculation of the excess turbulence, are derived by a process of *wake-averaging* which requires that these simplified conditions produce the same mean and mean-square velocity deficits as the analytical velocity profile.

Dispersion

The velocity field information described above is used as the basis for dispersion calculations. Plume trajectories are defined by the full velocity solution and the wake-averaged model is used for calculating the turbulence levels and associated rates of plume spread.
The main features are:

- uniform concentrations within the well-mixed recirculating flow region;
- a double plume concentration profile in the main wake;
- modified plume spread coefficients in the main wake regions **W** and **E**.

Sources releasing directly into the recirculating flow are regarded as fully entrained. In all other cases a release may be partially entrained as it is swept around the building and the recirculating flow downwind, and its dispersion may still be significantly affected by the distorted flow field. The model estimates the fraction of the released material entrained into the recirculating flow and subsequently re-emitted as a ground-level plume, and the remainder behaving as an elevated release. A two-plume concentration distribution is then seen in the main wake.

For sources outside the recirculating flow region, the concentration within **R** is taken to be the average of that which would arise from the non-entrained plume on the boundary of **R**. The rate of incorporation of material into **R**, which, in the steady state, is equal to the effective source strength from this region, is then determined from the mean volume of **R** and the residence time.
For passive plumes outside the recirculating flow, the plume centreline is a streamline of the idealised mean flow field. Cross-streamline transport occurs when the plume possesses excess momentum or buoyancy. The longitudinal rate of change of dispersion parameters σ_y and σ_z is governed by the local turbulence levels and, in the wake, by the convergence or divergence of mean streamlines. Undisturbed flow values are used for σ_y and σ_z in the near wake, region **A**, but in the main wake region there are two sets $\left({\sigma_y}^{(\mathrm{W})},\ {\sigma_z}^{(\mathrm{W})}\right)$ and $\left({\sigma_y}^{(\mathrm{E})},\ {\sigma_z}^{(\mathrm{E})}\right)$ for dispersion inside and outside **W**. A summary of the dispersion model for different source locations is set out in Table 9.

*Table 9: Dispersion model features according to location and source. The term 'elevated plume' is used to describe any plume that is not fully entrained into the recirculation region, which includes ground level emissions in regions **U**, **A** and **W**.*

Source region	Dispersion region			
	Upwind	Recirculation region, **R**	Around **R**	Main wake
U	Undisturbed	Uniform concentration	Elevated plume	Elevated + ground-level plumes
A	Undisturbed	Uniform concentration	Elevated plume	Elevated + ground-level plumes
R	---	Uniform concentration	Ground-level plume	Ground-level plume
E, **W**	---	---	---	Elevated plume

Appendix 3 – Flow profiles

Open terrain

Roughness elements were used within the wind tunnel upwind of the release location in order to generate a fully developed turbulent flow representative of a neutral atmospheric boundary layer with a surface roughness equivalent to 0.3m at full-scale. Scaling the wind tunnel boundary layer to full scale, results in a boundary layer height of 100m. A much deeper boundary layer height would usually be expected for neutral boundary conditions however as the extent of the processes studied occur within the log law region this was judged to be an acceptable scaling.

Figure 50 shows the average velocity, Reynolds stress and turbulent length scale profiles of the approaching flow in the wind tunnel. The wind tunnel mean velocity, *U*, and vertical turbulence, $(\sigma_w/U_{ref})\text{^}2$, profiles are comparable to those obtained from the ADMS meteorology module using a surface roughness of $z_0 = 0.3m$ (Figure 51). The turbulence parameters are defined as $\sigma_u = \sqrt{uu}$, $\sigma_v = \sqrt{vv}$, $\sigma_w = \sqrt{ww}$. The horizontal turbulence components, which are influenced by non-boundary layer processes, in the wind tunnel are lower than those given by ADMS. As always with wind tunnel experiments, the scaling factor used is arrived at through a compromise between an appropriate representation of the full-scale boundary layer and a sufficiently high Reynolds number, a large enough building to allow accurate measurements and an appropriate full scale-equivalent response time for the sensor. In this study the Reynolds number for the wind tunnel experiments calculated using U_{ref} and the building height was approximately 2.6×10^4. For a flow past a cube in a simulated atmospheric boundary layer, Castro and Robins (1977) found no Reynolds number dependence over 4×10^3. For the LES simulations the Reynolds number was approximately 2.6×10^6.

Empirical functions were fitted to the wind tunnel profiles and used as inputs to the LES simulations to define the flow at the domain inlet. These are shown in Figure 52. It was found that the turbulence statistics from the wind tunnel (seen in Figure 50 and denoted by the black line in Figure 52) that were applied at the inlet were not replicated along the domain length within the LES simulation. Generally, it was found that with this mesh configuration the turbulence intensity reached a stable state approximately 40% lower than that applied at the inlet. Despite this the profile shapes remained representative of those within the wind tunnel (Figure 52). This configuration was used for the majority of the simulations presented here, with the exception of the stable and unstable boundary layer simulations which are discussed in Section 5.4. A sensitivity study was implemented in which two additional simulations were run for the normal facing building case using an increase in the magnitude of the approach flow turbulence. As discussed in the next section it was found that the increased turbulence intensities did not have a significant impact on the flow structures around the building.

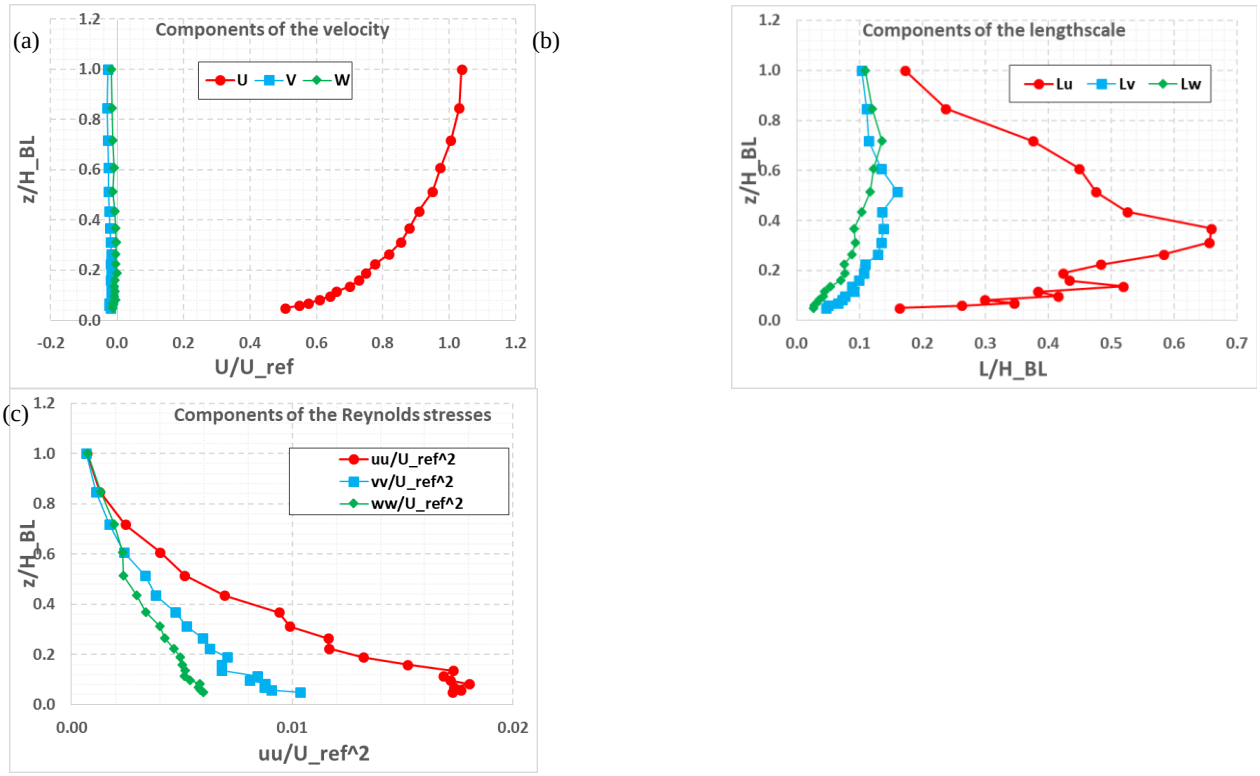

Figure 50: Wind tunnel flow profiles used as inlet boundary conditions for the LES simulations; a) the mean velocity components; b) turbulent length scales; c) Reynolds stresses.

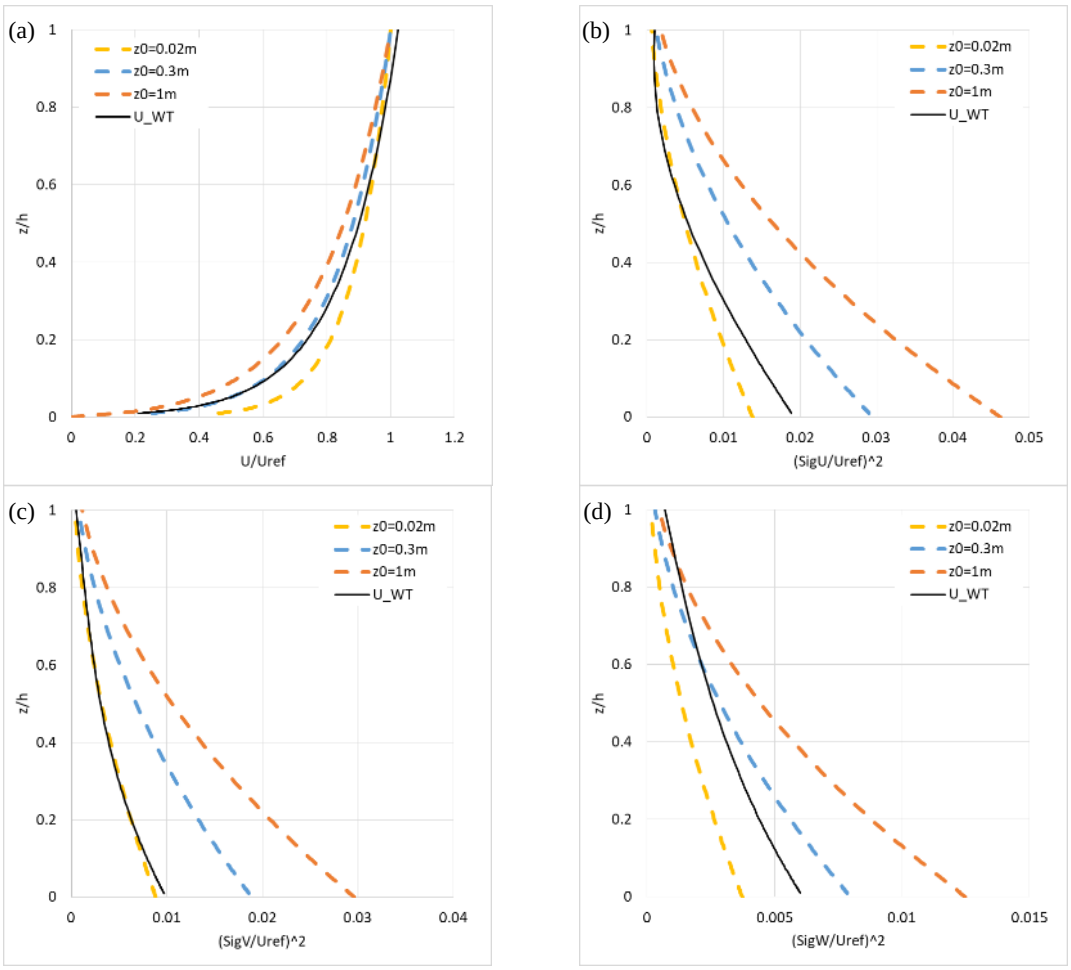

Figure 51: ADMS flow profiles for neutral boundary layer and different surface roughness lengths and LES inlet flow profiles (best fit functions to wind tunnel profiles).

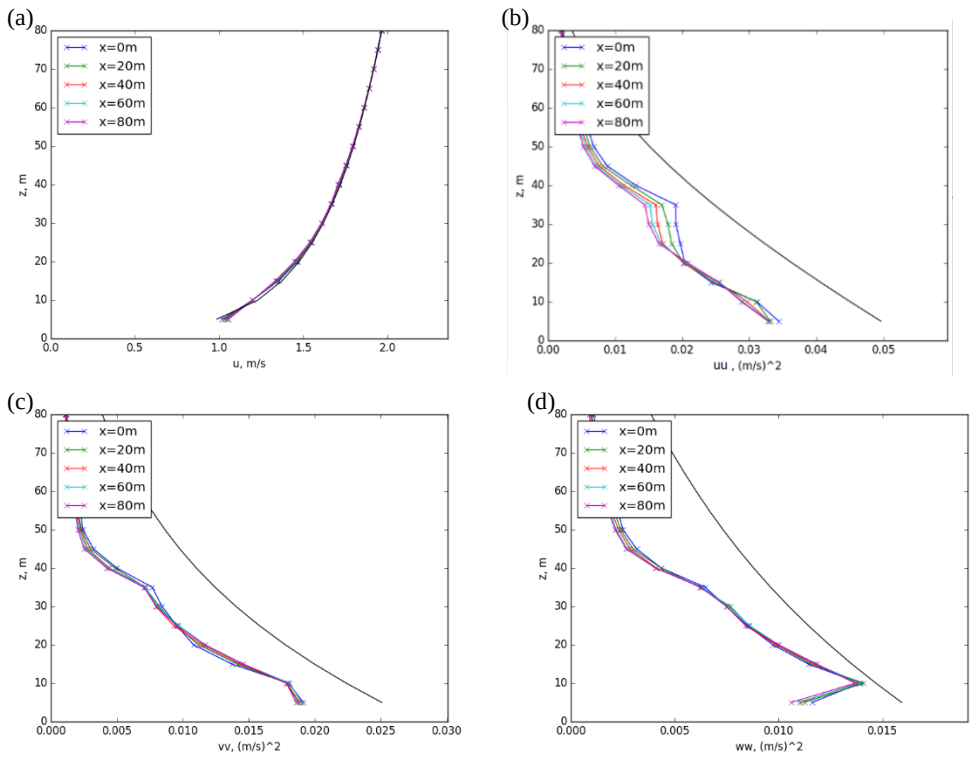

Figure 52: LES flow profiles at several stream wise locations. The black line indicates the LES inlet profiles.

Flow statistics around the building

Three different levels of turbulence were set at the inlet for the normal facing building LES simulations. These turbulence levels are representative of the range of values expected in a boundary layer passing over terrain types varying from rural to suburban. Figure 53 shows the flow profiles upwind of the building for the three simulations and the wind tunnel. The velocity profiles are unchanged between each simulation, however the turbulence levels increased from the low to high simulations.

The medium turbulence (blue circles) was intended to replicate the wind tunnel turbulence. While this is the LES simulation with the closest turbulence profiles to those of the wind tunnel, there are still differences, particularly for the u component of the Reynolds stress which is underestimated. The high turbulence case was intended to achieve turbulence representative of an urban boundary layer. Turbulent length scales were unchanged for each simulation.

Figure 54 shows the flow profiles for each model at 1H, i.e. a building length downwind of the building centre. Here it is seen that the building has a similar impact on each flow despite the varying turbulence intensities. This suggests that at these levels of turbulence and eddy length scales the building remains the dominant influence on the turbulence immediately downwind. The LES simulations compare reasonably well with the wind tunnel, capturing the features of the flow seen in the wind tunnel. The medium turbulence case gives the best agreement, which is expected as it has the closest matching approach flow. However, there are differences, mainly in the u component of both the velocity and the Reynolds stresses. The influence of the initial turbulence levels is still visible downwind of the building, but the differences are much reduced as the turbulence generated by the building tends to dominate.

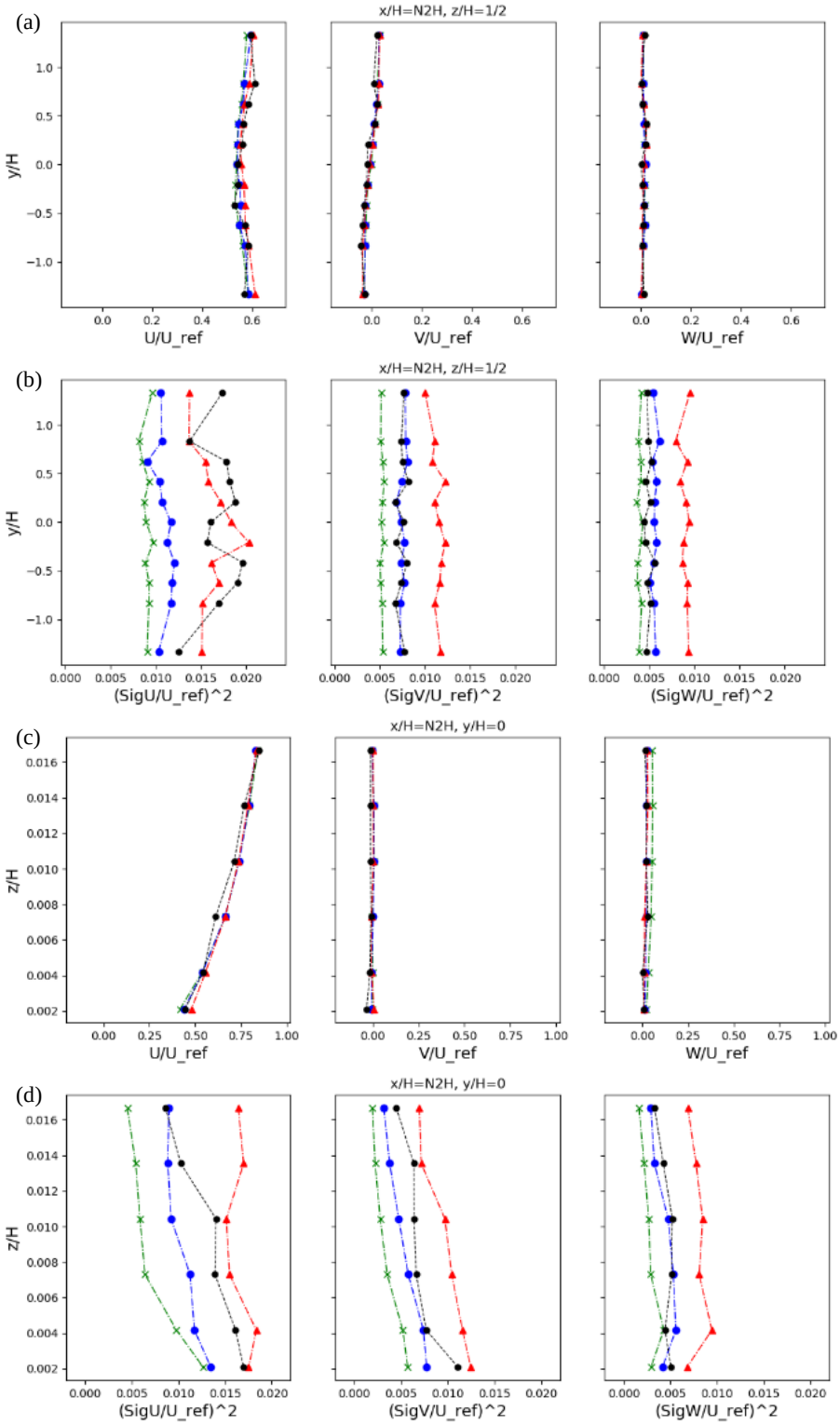

Figure 53: Velocity and Reynolds stresses along (a and b) horizontal line at Z/H=1/2 and (c and d) vertical line at Y/H=0 for the wind tunnel (black circles), low (green crosses), medium (blue circles) and high (red triangles) turbulence LES simulations at N2H.

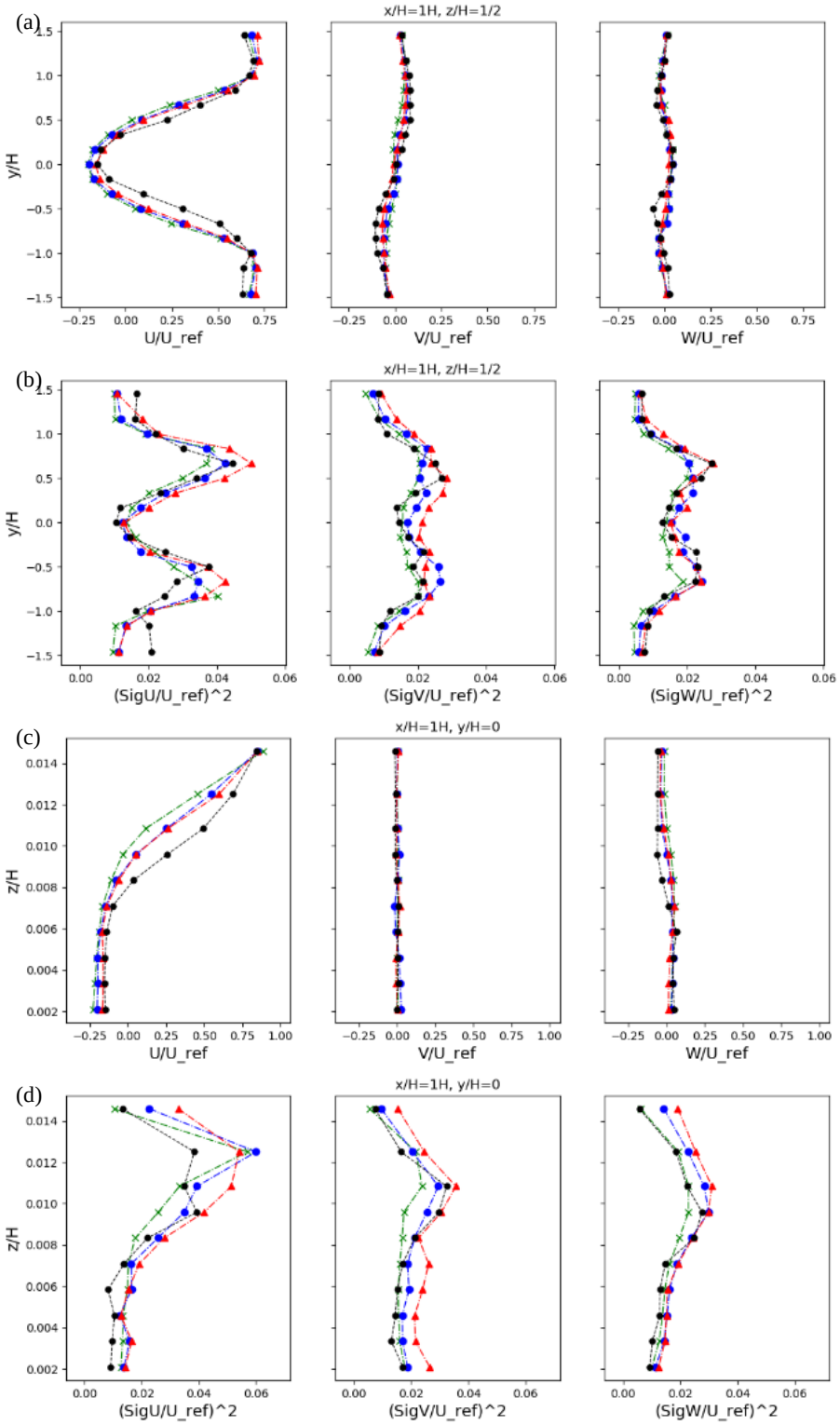

Figure 54: Velocity and Reynolds stresses along (a and b) horizontal line at Z/H≈1/2 and (c and d) vertical line at Y/H=0 for the wind tunnel (black circles), low (green crosses), medium (blue circles) and high (red triangles) turbulence LES simulations at 1H.

Appendix 4 – Unstable and stable boundary layer simulations

Both unstable and stable boundary layer LES simulations were considered. Flow profiles were output from the ADMS meteorology module and used as boundary conditions for these simulations. This included the average velocity, Reynolds stresses and average potential temperature. These were applied at the inlet using the synthetic eddy method. A heat flux was applied at the ground corresponding to that used to configure ADMS. An equivalent heat flux with the opposite sign was applied at the top of the boundary in order to simulate the entrainment of colder air from higher in the atmosphere. Zero heat flux was set at the building surfaces. The meteorology parameters supplied to the ADMS meteorology module are given in Table 10 along with the resulting stability class and h/L_{MO}.

Table 10: Meteorology parameters used for unstable and stable boundary layer simulations and corresponding stability class.

	z_0 (m)	Wind speed at 10m (m/s)	Surface heat flux (W/m^2)	Boundary layer height (m)	Pasquill-Gifford stability	h/L_{MO}
Unstable	0.3	1.25	5	800	B/C	-12
Stable	0.3	2	-6	120	F	1

Figure 55 shows a comparison of the lower 100m of the LES flow profiles at X=0m for an open terrain case (i.e. no building) for the unstable boundary layer. Differences exist between the turbulence profiles of the two models, with the LES giving higher vertical turbulence and lower horizontal turbulence components. Figure 55(e) shows the potential temperature gradients where good agreement is seen.

Figure 56 shows a comparison of the concentrations at 2H downwind of a release at height H/4. Good agreement is seen between the two models at this location, despite the LES predicting a higher degree of vertical mixing. The difference between the two models was seen to gradually increase with distance downwind due to the differences in turbulence. However, the results were deemed acceptable over the distances considered in this report.

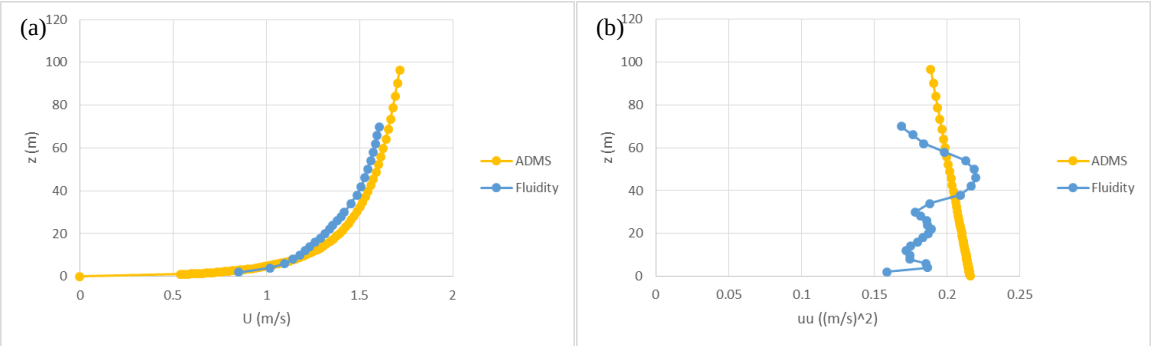

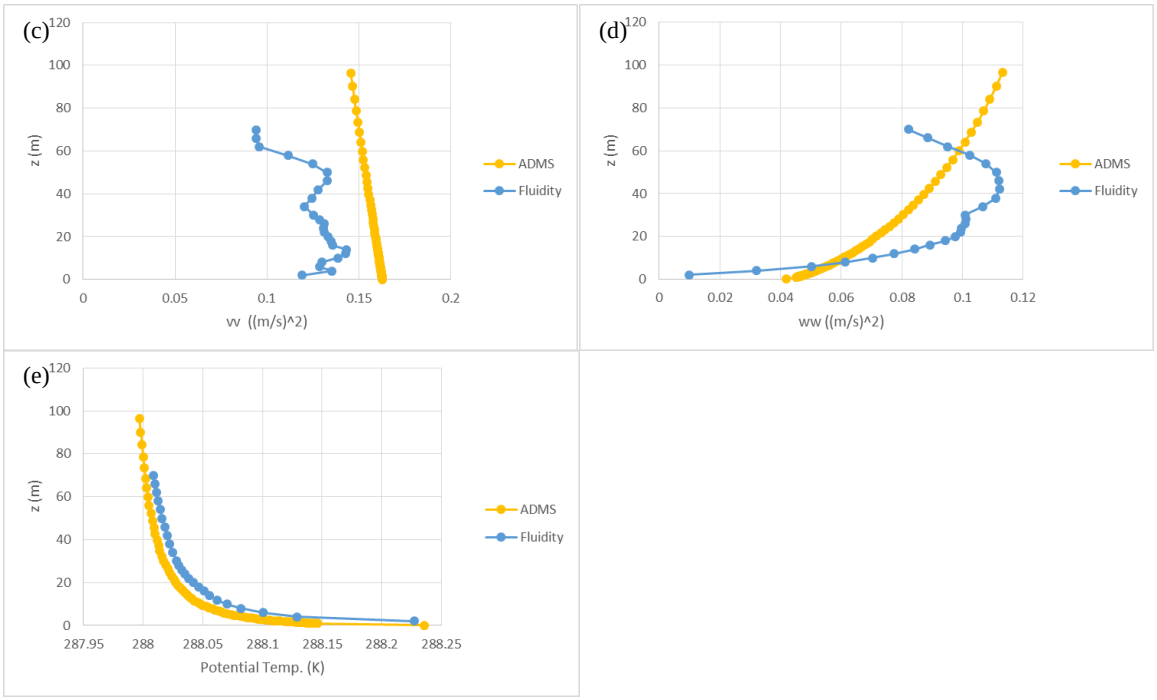

Figure 55: (a) Average velocity, (b-d) Reynolds stress and (e) potential temperature gradients for the unstable boundary layer simulations.

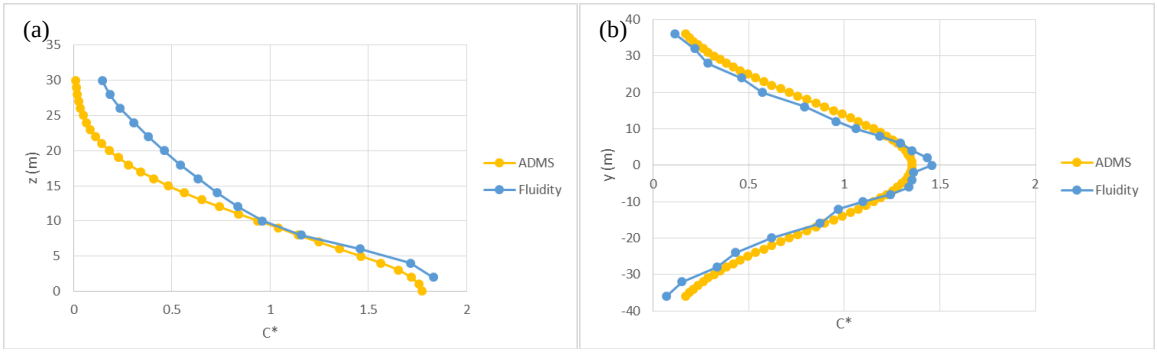

Figure 56: Concentrations 2H downwind of release at $Z_s = H/4$ along (a) vertical line and (b) horizontal line through plume centreline.

Figure 57 shows a comparison of the lower 80m of the LES flow profiles at *X*=0m for an open terrain case (i.e. no building) for the stable boundary layer. As for the unstable simulation, differences exist between the turbulence profiles of the two models, with the LES again giving higher vertical turbulence and lower horizontal turbulence components. The turbulence intensity falls significantly for the LES simulations above 40m. This is due to the coarser mesh used above this height. Figure 57(e) shows the potential temperature gradients for the two models.

Figure 58 shows a comparison of the concentrations at 2*H* downwind of a release at height *H*/4. Fluidity gives significantly higher concentrations at the plume centreline and a narrower plume, whilst also giving higher concentrations over the first 20 m above the ground. These differences are again likely due to the differences in the flow turbulence.

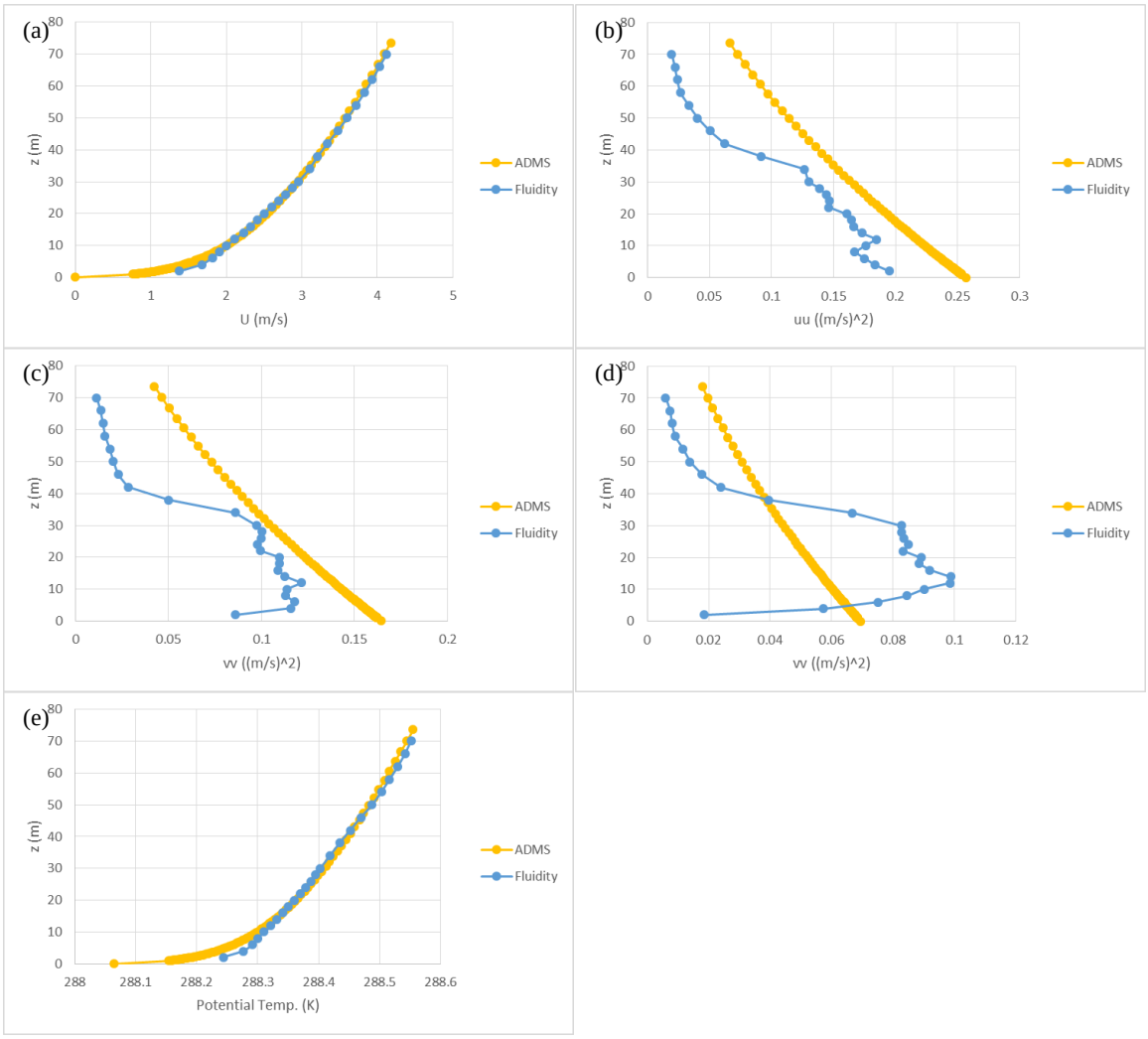

Figure 57: (a) Average velocity, (b-d) Reynolds stress and (e) potential temperature gradients for the stable boundary layer simulations.

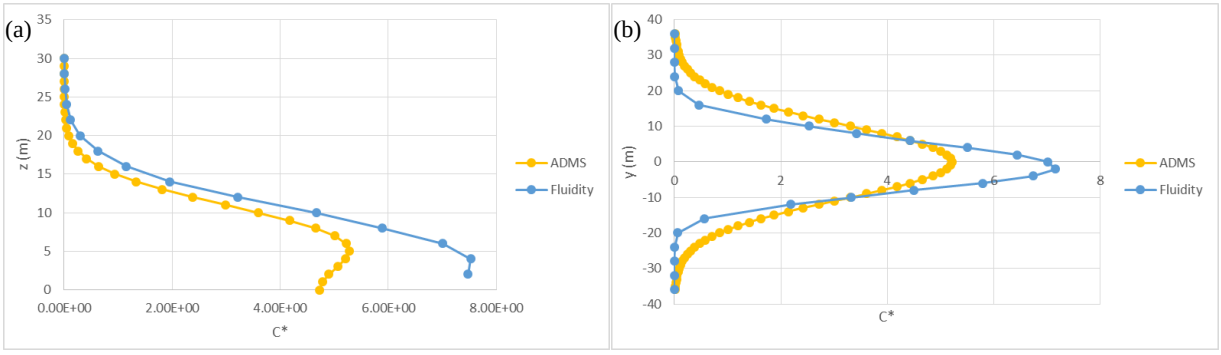

Figure 58: Concentrations 2H downwind of release at $Z_s = H/4$ along (a) vertical line and (b) horizontal line through plume centreline.

Figure 59 and Figure 60 show a comparison of the concentration distributions downwind of a building for the release at $Z_s/H = 4/3$ for the unstable and stable case, respectively.

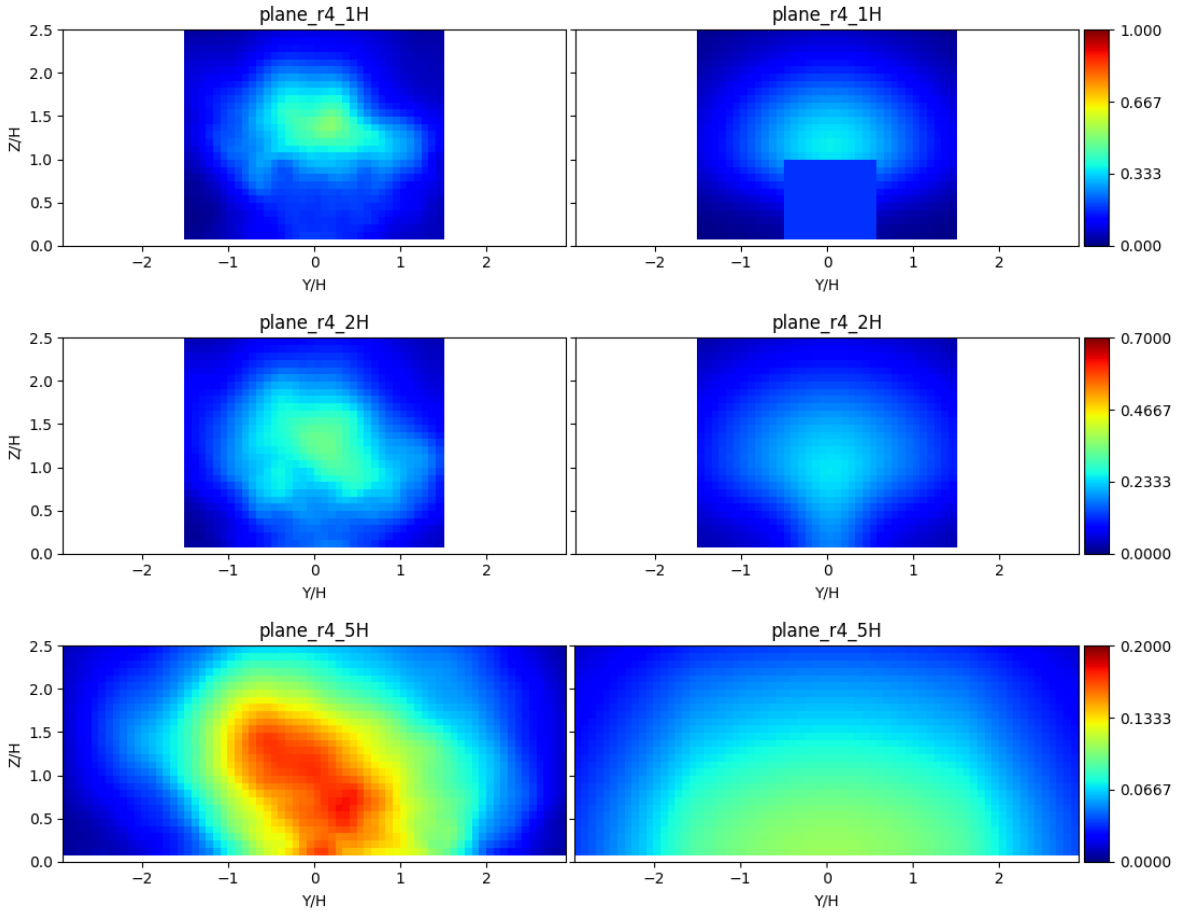

Figure 59: Unstable boundary layer normalised mean concentrations at location 1H, 2H and 5H for R4 (Z_s/H=4/3) upwind of a normal facing building. Figures on the left are LES and on the right are ADMS concentrations.

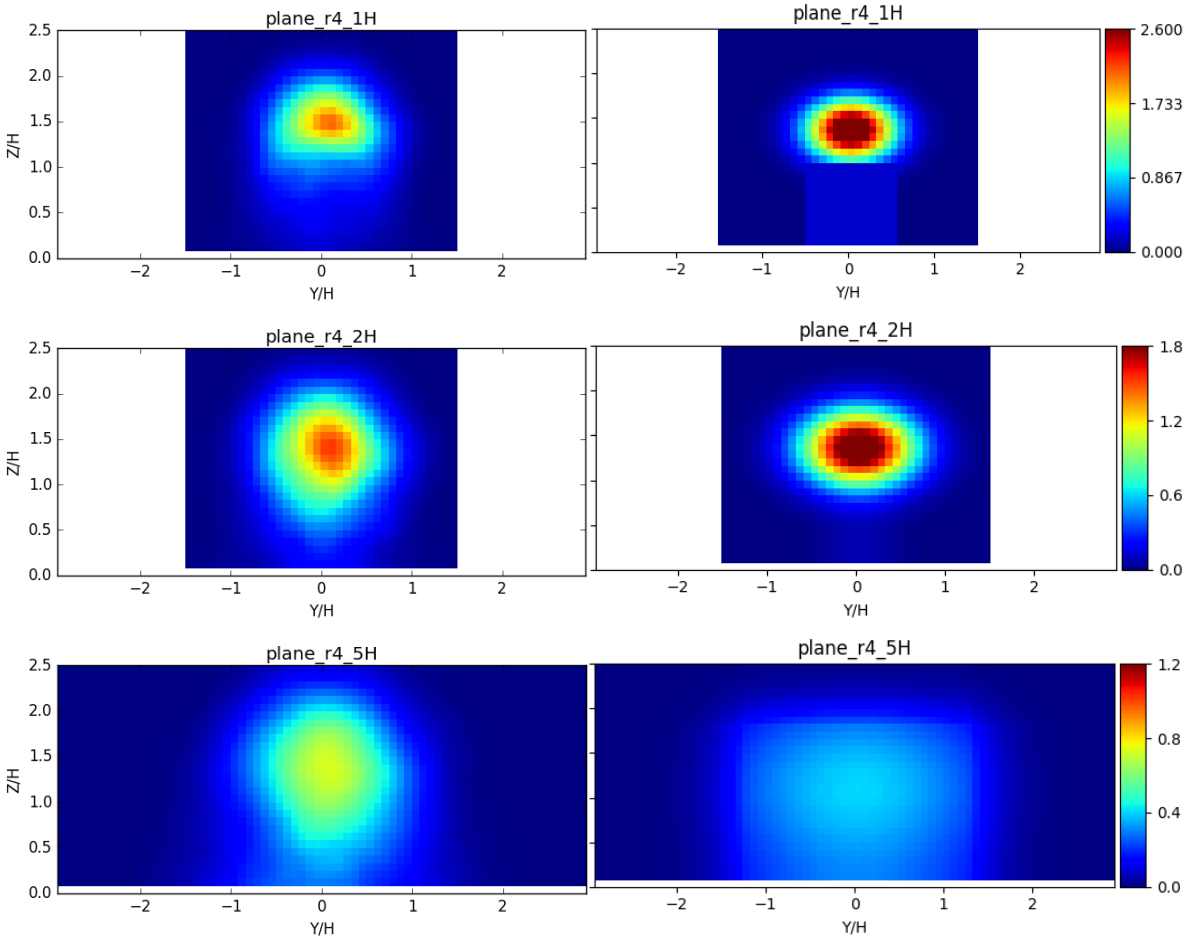

Figure 60: Stable boundary layer normalised mean concentrations at location 1H, 2H and 5H for release 4 (Z_s/H=4/3) upwind of a normal facing building. Figures on the left are LES and on the right are ADMS concentrations.

Appendix 5 - Puffs and plumes

Doses and release duration

In a pollutant cloud the ensemble averaged concentration, $\langle C \rangle$, is

$$\langle C \rangle \sim \frac{Q}{\sigma_x \sigma_y \sigma_z} f_c\left((x - Ut)/\sigma_x, y/\sigma_y, z/\sigma_z\right)$$

where Q is total amount released and f describes the distribution of concentration in the cloud. The mean dose, $\langle D \rangle$, is

$$\langle D \rangle = \int \langle C \rangle dt = \frac{Q}{\sigma_x \sigma_y \sigma_z} \frac{\sigma_x}{U} \int f_c\left((x - Ut)/\sigma_x, y/\sigma_y, z/\sigma_z\right) \frac{U dt}{\sigma_x}$$

that is $\Rightarrow \quad \langle D \rangle = \int \langle C \rangle dt = \frac{Q}{U \sigma_y \sigma_z} I_t f_d\left(y/\sigma_y, z/\sigma_z\right)$

The distribution is usually writen as

$$f_c = f_t\left((x - Ut)/\sigma_x\right) f_y\left(y/\sigma_y\right) f_x\left(z/\sigma_z\right)$$

in which case

$$I_t = \int f_c\left((x - Ut)/\sigma_x\right) \frac{U dt}{\sigma_x}$$

If $Q = qT_o$

where q is a (constant) emission rate, and

T_o the release duration, then

$$\frac{\langle D \rangle}{T_o} = \frac{q}{U \sigma_y \sigma_z} I f_d\left(y/\sigma_y, z/\sigma_z\right).$$

The statement that puff dose scales linearly with release duration comes about because we are taking $Q = qT_o$; if the amount released were fixed, then the dose would be independent of the release duration.

Mean puff dose and plume concentration

The mean concentration, $\overline{C}$, in a plume is

$$\overline{C} = \frac{q}{U\sigma_y\sigma_z} f_p\left(y/\sigma_y, z/\sigma_z\right)$$

we take f_d and f_p to be the same, so that

$$\frac{\langle D\rangle}{T_o} = I\overline{C}$$

Of acourse, the average dose, $\overline{D}$, over a period T_E, in a plume is

$$\overline{D} = \overline{C}T_E$$

where T_E is the exposure time.

Finally, the relationship between mean cloud dose and plume concentration emerges from the conservation condition for the cloud.

The conservation condition is

$$\int\langle C\rangle\, dx\, dy\, dz = Q$$

written as

$$\sigma_x I_x \sigma_y I_y \sigma_z I_z = Q$$

$$\langle C\rangle = \frac{Q}{\sigma_x I_x \sigma_y I_y \sigma_z I_z} f_c$$

The integral I is therefore equal to I_z and

$$\langle D\rangle = \frac{Q}{\sigma_y I_y \sigma_z I_z} f_d \quad \text{and} \quad \frac{\langle D\rangle}{T_o} = \overline{C}$$

Lastly, we note that these results still hold if *q*, the emission rate, is a function of time, providing that the emission remains passive. The variation with time is removed in the integration used to form the dose.